5-2013

# Spectral investigation of the conformation of primary and secondary micelles of sodium cholate and the impact of pH and salt concentration.

Sarah Elizabeth Milliner
*University of Louisville*

# SPECTRAL INVESTIGATION OF THE CONFORMATION OF PRIMARY AND SECONDARY MICELLES OF SODIUM CHOLATE AND THE IMPACT OF pH AND SALT CONCENTRATION

By

Sarah Elizabeth Milliner
B.S., Eastern Kentucky University, 2008
M.S., University of Louisville, 2011

A Dissertation
Submitted to the Faculty of the
College of Arts and Sciences of the University of Louisville
in Partial Fulfillment of the Requirements
for the Degree of

Doctor of Philosophy

Department of Chemistry
University of Louisville
Louisville, Kentucky

May, 2013

SPECTRAL INVESTIGATION OF THE CONFORMATION OF PRIMARY AND SECONDARY MICELLES OF SODIUM CHOLATE AND THE IMPACT OF pH AND SALT CONCENTRATION

By

Sarah Elizabeth Milliner
B.S., Eastern Kentucky University, 2008
M.S., University of Louisville, 2011

A Dissertation Approved on

April 26, 2013

By the Following Dissertation Committee:

_____

Dissertation Director
Professor M. Cecilia Yappert

_____

Professor Douglas Borchman

_____

Professor Muriel Maurer

_____

Professor Christine Rich

_____

Professor Francis Zamborini

DEDICATION

This dissertation is dedicated to my two beautiful daughters

Norah Renae Milliner

and

Isabel Reese Milliner

Always follow your dreams

Catch the star that holds your destiny-
The one that forever twinkles in your heart
Take advantage of precious opportunities while they still sparkle before you
Believe that your goal is attainable
Commit yourself to it
Though the barriers may stand in your way remember…
Your destiny is hiding behind them
Accept that not everyone will approve of your choices
Have faith in your judgments
Take pride in your accomplishments
Don't let your mistakes discourage you
Value your capabilities and talents for they are what make you truly unique
The greatest gifts in like are not purchased but acquired through hard work and determination
Find the star that twinkles in your heart
You are capable of making your dreams come true
Give your hopes everything you've got
You will catch the start that holds your destiny

-Shannon M. Lester

Arts, B. M., *Always Follow Your Dreams*.

ACKNOWLEDGMENTS

I owe my deepest gratitude to my mentor, Dr. M. Cecilia Yappert. Her guidance, support and friendship have been an instrumental part of my success throughout this journey. Her passion for research has been so inspiring to me and I sincerely have appreciated her dedication. I also wanted to extend a special thank you Kristen Magness and Bryan Wessel, my lab partners who's friendship, help during the final stages of this process, and insightful conversations have been unwavering.

I would like my committee members, Dr. Douglas Borchman, Dr. Muriel Maurer, Dr. Christine Rich and Dr. Francis Zamborini, for their insightful advice, guidance, support and helpful suggestions. I owe many thanks to Dr. Neal Stolowich for his training and support of the NMR instrumentation and to Dr. Donald DuPré for his contribution to the theoretical calculations of this work which aided in the experimental analysis.

I would like to thank Dr. Douglas Borchman for his time spent on collaboration of research, and for allowing me the opportunity to co-author on several of his research articles.

I would like to thank the Department of Defense for the award received by the Department of Chemistry. This funding allowed for the purchase of the 700 MHz NMR spectrometer which was vital to the research presented in this dissertation.

I would like to thank my undergraduate advisor Dr. Darrin Smith for inspiring me to pursue chemistry and to continue my education, his passion for chemistry and its inner workings was what inspired me to follow my dreams of obtaining my Ph.D. Dr. Smith was and remains my best role model for a scientist, mentor, and teacher. I still think fondly of my time as an undergraduate student.

I would like to express my deepest gratitude to the University of Louisville Chemistry Department for their financial support and oversight throughout my graduate studies. To the GEMS program for their funding, support, and guidance which continued throughout my graduate school experience. I would like to also personally thank my colleagues Govardhan Veerareddygari, Sébastien Laulhé, Mohamed Marei and Katherine Sellers for their friendship and support.

I would like to thank my wonderful husband Scott, without you none of this would have been possible. Your support, love, and encouragement were constant. You inspired me to keep going and were the encourager of my dreams. Thank you for everything throughout this process and for being so understanding during these long years of me obtaining my education.

I would like to thank my Parents and Family for inspiring me through the years and for you constant words of encouragement when I needed them. Thank you for being my biggest cheerleaders and fans during this process. Your help, patience, and love have been so instrumental in this endeavor.

I would like to thank my Friends for being guidance, help, and a listening ear

when needed. Thank you to each of you for everything. You all have inspired me to keep moving forward in reaching my goal.

ABSTRACT

SPECTRAL INVESITGATION OF THE CONFORMATION OF PRIMARY AND SECONDARY MICELLES OF SODIUM CHOLATE AND THE IMPACT OF pH AND SALT CONCENTRATION

Sarah Elizabeth Milliner

April 26, 2013

Bile salts are biosurfactants that aid in the digestion and absorption of lipids. Unlike most classical surfactants, they are facial amphiphiles with a rigid steroid backbone whose hydrophobic and hydrophilic faces are on opposite sides. As the concentration of bile salts increases, primary micelles are formed. Despite decades of studies of the molecular organization of these micelles, there is no agreement on their arrangement. To bridge this gap, one- and two-dimensional NMR studies of sodium cholate (NaCho) monomers and primary micelles were carried out. The experimental changes in chemical shift were interpreted with the aid of theoretical predictions. The observed trends and the presence of new through-space interactions observed upon micellization indicate that four (or six) monomers are arranged in an anti-parallel fashion. The top and bottom of the barrel-like micelles are held by ionic interactions and water-mediated hydrogen bonds. A cooperative hydrogen-bond 'belt' is formed with the hydroxyl groups in the central region of NaCho and surrounds the micelle. Our results point to the importance of both hydrophobic interactions and hydrogen bonding in the formation of micelles.

Larger aggregates (secondary micelles) form at higher concentrations (> 50 mM). Little is known about their molecular arrangement. Our NMR studies enabled the postulation and partial validation of a model for these aggregates in which primary micelles are stacked together via ion-dipole and H-bonding interactions. The stacks interact with each other in a staggered fashion where the top/bottom of a primary micelle is in the vicinity of the central H-bond belt of its neighboring micelle.

Both pH and salt concentration affect primary and secondary micelles of bile salts. We investigated the effect of increasing concentrations of NaCl, $NH_4Cl$, $CaCl_2$ and $MgCl_2$ on both primary and secondary NaCho micelles. Due to its smaller charge density, $NH_4^+$ had the least impact because of its interactions with hydroxyl and carboxylate groups are weaker relative to those of the other cations. On the other hand, the higher charge density of $Ca^{2+}$ and $Mg^{2+}$ caused the greatest tightening ($Mg^{2+}$) and even aggregation ($Ca^{2+}$) as these cations interact with the electronegative moieties of NaCho more effectively.

TABLE OF CONTENTS

LIST OF FIGURES

FIGURE PAGE

LIST OF TABLES

TABLE PAGE

# CHAPTER 1

# INTRODUCTION AND BACKGROUND

This chapter provides background information on the classification of bile salts and our current knowledge of the molecular conformation/structure of their micelles. In addition, the effects of salt concentration, pH and temperature on micelle formation will be addressed. The various bile salt micellar arrangements that have been proposed in the past will be discussed. Since there is no agreement on the structures of bile salt micelles, the main goal in this dissertation is to understand the forces and interactions that lead to the formation of these nanostructures and to propose models for both primary and secondary micelles of sodium cholate, one of the most abundant primary bile salts. These studies mainly focus on the use of one- and two-dimensional nuclear magnetic resonance (NMR) spectroscopy to elucidate molecular structures.

## BILE SALTS: CLASSIFICATION AND CHEMICAL STRUCTURE

Surfactant molecules self-aggregate spontaneously into micelles when dissolved in aqueous media at concentrations above their critical micelle concentration (*cmc*).[1-4] According to their chemical make-up, surfactants can be classified as ionic, non-ionic, or zwitterionic detergents.[5] A classical ionic surfactant such as sodium dodecyl sulfate (SDS), consists of a polar head group and a non-polar hydrocarbon tail. SDS self-associates in organized spherical structures where the polar head groups interact with the aqueous phase and the hydrocarbon chain form the core of the micelle.[6] Triton X-100 is a

non-ionic surfactant with a hydrophilic polyethylene oxide chain and a hydrophobic aromatic hydrocarbon group.[7] Zwitterionic detergents contain both positively and negatively charged groups with an overall net charge of zero. CHAPS, 3-[(3-cholamidopropyl)dimethylammonio]-1-propanesulfonate, a derivative of cholic acid, is an example of this class of detergents with a zwitterionic head group and a steroidal tail.[8] Above the concentration where surfactant molecules associate to form micelles (critical micelle concentration, *cmc),* surfactants act as emulsifiers, dissolving compounds that are normally insoluble in the solvent being used. For example, CHAPS is used as a detergent to solubilize membrane proteins.[9]

Bile salts are considered detergents but are significantly different from classical amphiphiles.[10] In classical amphiphiles, the polar and non-polar regions are clearly separated; there is a polar head group and a hydrophobic tail comprised of hydrocarbon chains. The separation of hydrophobic and hydrophilic regions in bile salts is quite different. Bile salts have a rigid steroid framework and exhibit facial polarity.[11, 12] The hydrophilic face, also considered the concave side of the molecule, is polar due to the presence of two or three hydroxyl groups.[10, 13-15] Conversely, the hydrophobic face is the convex side of the steroid backbone where methyl groups are located. Bile salts have an acidic moiety in their tails. At pH values above their pKa, these sites become deprotonated and these anionic amphiphiles form anionic micelles that are thermodynamically stable. Figure 1-1 shows the structure of different bile salts that are produced in our body. Naturally occurring bile salts are conjugated with glycine or taurine.[10, 16] This dissertation focuses on sodium cholate (NaCho) which is a trihydroxy bile salt with alpha hydroxyl groups at positions C3, C7 and C12. The tail is composed of

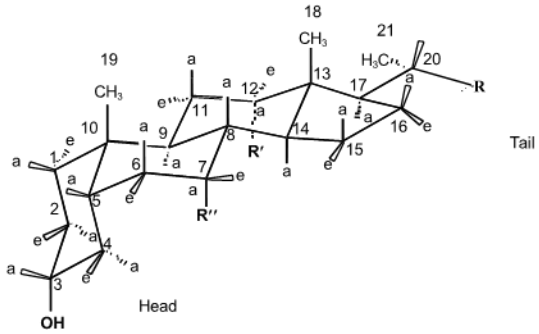


| | | |
|---|---|---|
| Sodium Cholate | **- R = $(CH_2)_2COO^-$**<br>**- R′ = OH**<br>**- R″ = OH** | **$Na^+$** |
| Deoxycholate | **- R = $(CH_2)_2COO^-$**<br>**- R′ = OH**<br>**- R″ = H** | **$Na^+$** |
| Chenodeoxycholate | **- R = $(CH_2)_2COO^-$**<br>**- R′ = H**<br>**- R″ = OH** | **$Na^+$** |
| Glycocholate | **- R = $CH_2(CO)NHCH_2COO^-$**<br>**- R′ = OH**<br>**- R″ = OH** | **$Na^+$** |
| Taurocholate | **- R = $CH_2(CO)NH(CH_2)_2SO_3$**<br>**- R′ = OH**<br>**- R″ = OH** | **$Na^+$** |
| Taurodeoxycholate | **- R = $CH_2(CO)NH(CH_2)_2SO_3$**<br>**- R′ = OH**<br>**- R″ = H** | **$Na^+$** |

**Figure 1-1:** General structure of bile salts and their conjugates.

a carboxylate group which is at the opposite end from OH-3 (head) of the monomer. Methyl groups are located on the hydrophobic face at positions C18, C19 and C21.

**BILE SALT FUNCTIONS**

Bile salts are synthesized in the liver and are byproducts of the catabolic pathway of cholesterol in mammals.[17] Through modification and hydroxylation of cholesterol, the bile salt end products have a rigid steroid backbone with a hydrophobic and hydrophilic face.[17] They are present in the bile along with cholesterol, derivatives of cholesterol and lipids. Bile salts are stored in the gall bladder and emptied into the intestine by passive diffusion during the digestion of a meal.[18] Bile salts are then reabsorbed from the ileum and returned to the liver by the portal blood. The enterohepatic circulation of bile salts occurs 4 – 12 times a day. The concentration of bile salts varies depending on the different body compartment. In the gall bladder, the concentration is between 10 and 50 mM, in the liver it is lower, between 4 and 20 mM and in the liver *Cancliculi* it is around 5 mM. The concentration decreases in the portal vein blood (0.1 mM) and in the peripheral blood (5 – 20 μM).[18]

Bile salts aid in the excretion of insoluble lipids including lecithin and cholesterol and promote absorption of insoluble dietary lipids in the intestine.[19, 20] Bile salts form mixed micelles with cholesterol, lecithin, monoglycerides and fatty acids so that they can be transported in aqueous biological fluids.[17, 19, 21] About 80 % of the bile salts in the bile are primary bile salts synthesized from cholesterol and include cholate and chenodeoxycholate. Secondary bile salts such as deoxycholate are derived from primary ones. These are produced in the colon by bacterial 7α-dehydroxylation (removal of the

hydroxyl group at C-7) and make up the remainder (about 20 %) of bile salts present in the bile.[21]

**MICELLE FORMATION**

At low concentrations, bile salts are present in their monomeric form. As the concentration increases, a transition occurs where monomers begin to associate forming micelles.[22-24] The concentration at which this transition takes place is called the critical micelle concentration (*cmc*); this value varies for individual bile salts due to differences in their chemical makeup.[25] At the *cmc*, half of the bile salts are in their monomeric form and half associate to form primary micelles. As the bile salt concentration continues to increase past the *cmc*, a second micellization step is reached[26, 27] and primary micelles begin to associate to form larger aggregates. The first *cmc*'s of dihydroxy bile salts are below 5 mM and trihydroxy bile salts have higher *cmc*'s ranging between 10-20 mM. The increase in *cmc* values is attributed to their increased solubility in water.[16]

The *cmc* values for the various bile salts have been determined using techniques such as light scattering[28], isothermal titration calorimetry[29] and fluorescence spectroscopy[30]. Solution parameters such as ionic strength, pH and temperature can alter the *cmc* values for bile salts. A lower *cmc* can be achieved by increasing the ionic strength of the solution. This reduces electrostatic repulsions between the charged groups and allows for the formation of micelles at lower bile salt concentrations.[11, 25, 27, 29] Altering the pH can also affect the *cmc* of bile salts. Bile salt molecules are ionized well above their pKa values. At pH values around the pKa, bile salt molecules become partially protonated and anionic repulsions that keep the micelles from aggregating are reduced.[21, 25] This leads to micelle precipitation. Temperature-dependent studies of *cmc* values for bile salts showed the minimum *cmc* to be around room temperature and these

values increase with increasing temperature.[23, 24] However, the temperature dependence of *cmc* is not as pronounced as that observed with salt concentration.

The number of bile salt monomers that associate to form primary micelles (aggregation number, *n*) has been evaluated by ultracentrifugation and quasielastic light scattering.[28] The aggregation number of bile salts ranges from 2 to 10 for primary micelles, an order of magnitude smaller than for classical amphiphiles. Similar to the *cmc*, the aggregation number is also dependent on the structure of the bile salt and solution parameters. Increased bile salt concentration and ionic strength lead to an increase in aggregation number.[21, 28, 29] On the other hand, decreasing pH causes an increase in aggregation number. For dihydroxy bile salts, a decrease in pH leads to a thickened and more gel-like aqueous solution.[31]

In addition to determining the aggregation numbers of bile salts, quasielastic light scattering was used by Mazer *et al.* to determine the size of bile salt micelles.[28] In this study, aqueous bile salt solutions in the presence of 0.15 and 0.6 M NaCl were examined. Results showed that trihydroxyl taurocholate (TC) forms much smaller micelles with a mean hydrodynamic radius ($\overline{R}_h$) between 10-15 Å and dihydroxy bile salts have $\overline{R}_h$ values of 15 – 60 Å.[28] The sizes of the three trihydroxy bile salts examined varied in size with the following order: taurodeoxycholate (TDC) > taurochenodeoxycholate (TCDC) > tauroursodeoxycholate (TUDC). The difference in hydrodynamic radii for the bile salts examined is due to the number and positioning of hydroxyl groups on their hydrophilic surface.[28] Increases in NaCl concentration resulted in micellar growth. For example, TC micelles hydrodynamic radius increased to 38.5 Å at high NaCl concentrations.[28] This group also carried out concentration-dependent studies on NaTDC at a higher salt concentration (0.8 M NaCl).[32] The hydrodynamic radius was found to be between 11 to

16 Å, in good agreement with previous results. Bile salt aggregates form small globular primary micelles with aggregation numbers around 10 or less. At the second micellization step, as the concentration of the bile salt increases, primary micelles polymerize to form rodlike secondary micelles with quasielastic light scattering the hydrodynamic radii were found to be greater than 90 Å.[32]

**Postulated Models on the Formation of Bile Salt Micelles**

Several models have been proposed for the formation of primary micelles of bile salts. The first bile salt micelle model was reported by Small *et al.* who proposed a two-step process for the formation of primary and secondary micelles.[10] As mentioned previously, the formation of primary micelles is the first step and occurs around the *cmc*.[14] Bile salt monomers associate due to the hydrophobic effect where the hydrophobic faces of the monomers orient themselves toward each other and away from the solvent; this creates the non-polar interior of the primary micelle. This leaves the hydrophilic face with the hydroxyl and the deprotonated acidic groups in contact with the solvent.[10] Depending on the type of bile salt, the number of monomers and the structure of the primary micelles varies. However, Small *et al.* suggested that up to ten bile salt monomers can associate to form primary micelles.[10] Aggregation numbers above ten would leave space in the center of the primary micelles thus exposing the hydrophobic faces to water. The second step in this process is the formation of secondary micelles and occurs at higher bile salt concentrations. Although there was no experimental evidence, hydrogen bonding between the hydroxyl groups of neighboring primary micelles was proposed to result in elongated secondary micelles. (see Figure 1-2).[10, 14]

A second model was proposed by Kawamura *et al.*, who investigated the structure of di- and tri-hydroxy bile salt micelles using spin-labeled probes and Electron Spin

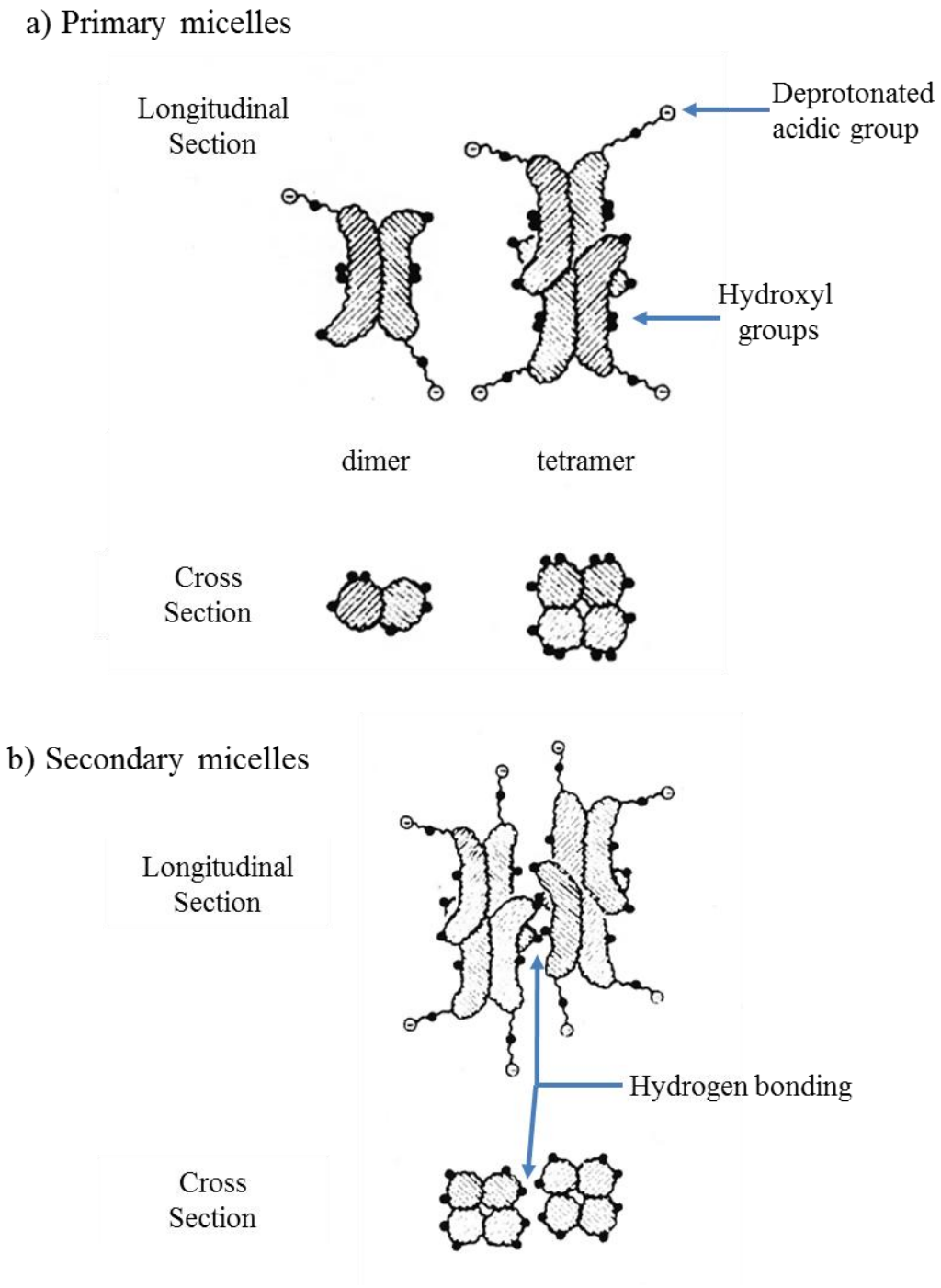


**Figure 1-2:** Primary model proposed by Small *et al.* a) Proposed primary micelle model for bile salt dimer and tetramer and b) Proposed secondary micelles of bile salts (hydrogen bonding interactions are shown with blue arrows Adapted from Small *et al.*[10]

Resonance (ESR) techniques.[33] Stearic acid labeled with a methyl ester nitroxide probe at various sites within the fatty acid were solubilized by the bile salt and used to examine the interior of bile salt micelles. The rotational correlation time ($\tau_1$) of the spin probes was examined above and below the *cmc* to determine if the spin probes had been solubilized by the bile salt micelles. $\tau_1$ was also used to measure the degree of immobilization of the spin probe as the position of the nitroxide group was changed along the stearic acid for all bile salts examined.[33] These results suggest that bile salts have similar shape regardless of the differences in molecular structure. In this study, bile salt concentrations were well beyond the *cmc* (100 mM) and a fixed spin probe concentration of 0.1 mM was used. Based on the conditions used in this study, a disklike model was proposed as a common model for micellar structures (See Figure 1-3). In this model, hydrophobic faces are oriented toward the interior of the micelle and hydrophilic faces are oriented toward the solvent. This model can be applied to bile salts with low aggregation numbers and loose structures (trihydroxy) and to dihydroxy bile salts that form larger micelles.[33] The solubilized spin probes experienced similar environments when placed on carbon-5 (head) or carbon-16 (tail) suggesting monomers in the micelles orient in an anti-parallel arrangement (See Figure 1-3).[33] If the monomers associated in a parallel fashion, the top of the micelles will be composed of all the deprotonated acidic groups and the bottom would only have hydroxyl groups at the C3 position. Therefore, the environment that the spin probe (measured by rotational correlation time $\tau_1$) sensed at the top and bottom of the primary micelles would be different.

An alternative arrangement was proposed by Giglio *et al.* based on the crystal structure of sodium glycodeoxycholate obtained by X-ray diffraction.[34, 35] The structure of the crystalline state suggests a helical arrangement for bile salt micelles. Association of

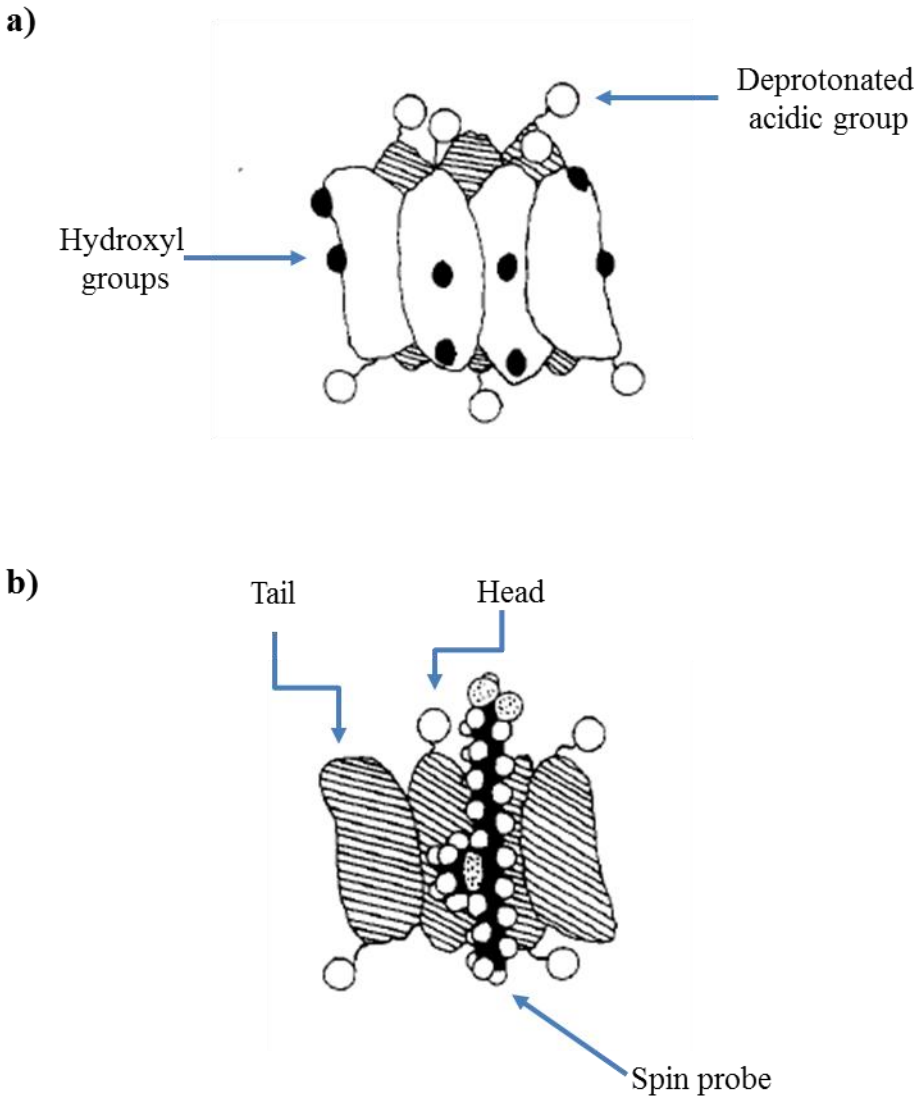


**Figure 1-3:** Disklike model proposed by Kawamura *et al.* a) Representation of the disklike bile salt micelle model (deprotonated acidic group and hydroxyl groups are shown in blue arrows. b) Representation of bile salt micelle with solubilized spin probe (shown with blue arrow). In this model, the head and tail of the bile salt are also labeled to show the anti-parallel arrangement. Adapted from Kawamura *et al.* [33]

monomers into micelles is driven by polar interactions. Similar to reversed micelles, the interior of the helix is filled with cations and surrounded by water and the hydrophobic surfaces are oriented outward. X-ray diffraction offers detailed structural information, However, for optimal results this method is restricted to molecules in crystalline form.

The ability to examine molecules in the aqueous phase is advantageous since the environment mimics physiological conditions more closely. In addition, experimental variables such as temperature, salt content and pH can be manipulated quite easily.[36] Nuclear magnetic resonance (NMR) spectroscopy is a powerful tool for the elucidation of the molecular structure and conformation of organic and inorganic species. The greatest advantage of the application of NMR to the study of biomolecules is that they can be investigated in solution and the effects of solution parameters (temperature, pH and salt concentration) can be explored. In addition, interactions with other biomolecules can also be examined.[36-38] NMR spectroscopy has already been used in our laboratory to explore the molecular arrangements of NaCho micelles. The details of those previous studies will be presented later in the section on NMR studies of bile salts.

## NMR SPECTROSCOPY

### 1D-NMR: Principles

NMR is based on the absorption of electromagnetic radiation in the radio-frequency (rf) region. This occurs in nuclei with a non-zero quantum spin number ($I \neq 0$). Proton ($^{1}H$), carbon ($^{13}C$) and phosphorus ($^{31}P$) nuclei have a spin quantum number of I = 1/2. Nuclei with spin quantum number I can adopt 2I + 1 orientations.[38] For the nuclei mentioned above, two spin states exist, m = +1/2 and m = -1/2. In the absence of a magnetic field, the energies of these quantum states are identical. When a magnetic field

is applied, the spin states are no longer degenerate and they separate into two energy levels. The more stable, lower energy state, m = +1/2 (α) is aligned with the magnetic field and m = -1/2 (β) is the higher energy state and opposes the magnetic field direction.[37] For any system at thermal equilibrium, the nuclei population will be in slight excess for the α state. When the nuclei are irradiated with rf radiation, a photon is absorbed by the nucleus in the lower spin state (α) and is flipped into the higher energy state (β). For resonance to occur, the energy gap between the two spin states must exactly match the energy of the absorbed photon.[36-38]

$$\Delta E = \frac{\gamma \hbar \mathbf{B}_0}{2\pi}$$

Where γ is the gyromagnetic ratio, a proportionally constant characteristic of the isotope being examined, *h* is Plank's constant and $\mathbf{B}_0$ is the magnetic field strength.

After irradiation ceases, the excited spins return to their equilibrium state (excess α spins) through relaxation processes. The rate of this relaxation process is governed by spin-lattice or longitudinal relaxation time constant, $T_1$. The larger the $T_1$ value, the longer it takes for the nuclei to return to equilibrium (Boltzmann distribution). The second type of relaxation process is called spin-spin or transverse relaxation, $T_2$.[36] After the nuclei are irradiated, individual magnetic moments begin to lose phase coherence. Typically, $T_2$ is much shorter than $T_1$. The values of $T_1$ and $T_2$ depend on the type of nucleus, the size of the molecule, the temperature and the tumbling or correlation time, ($\tau_c$).[37] Correlation time is defined as the time it takes for a spin to rotate one radian.[37] (Figure 1-4). Larger molecules have longer $\tau_c$ (tumble more slowly) and thus have small $T_2$ values (fast spin-spin relaxation). Spin-spin relaxation time can also provide information on molecular motion; this can be inferred by the resonance linewidths at half-height ($\Delta\nu_{1/2}$) defined as:

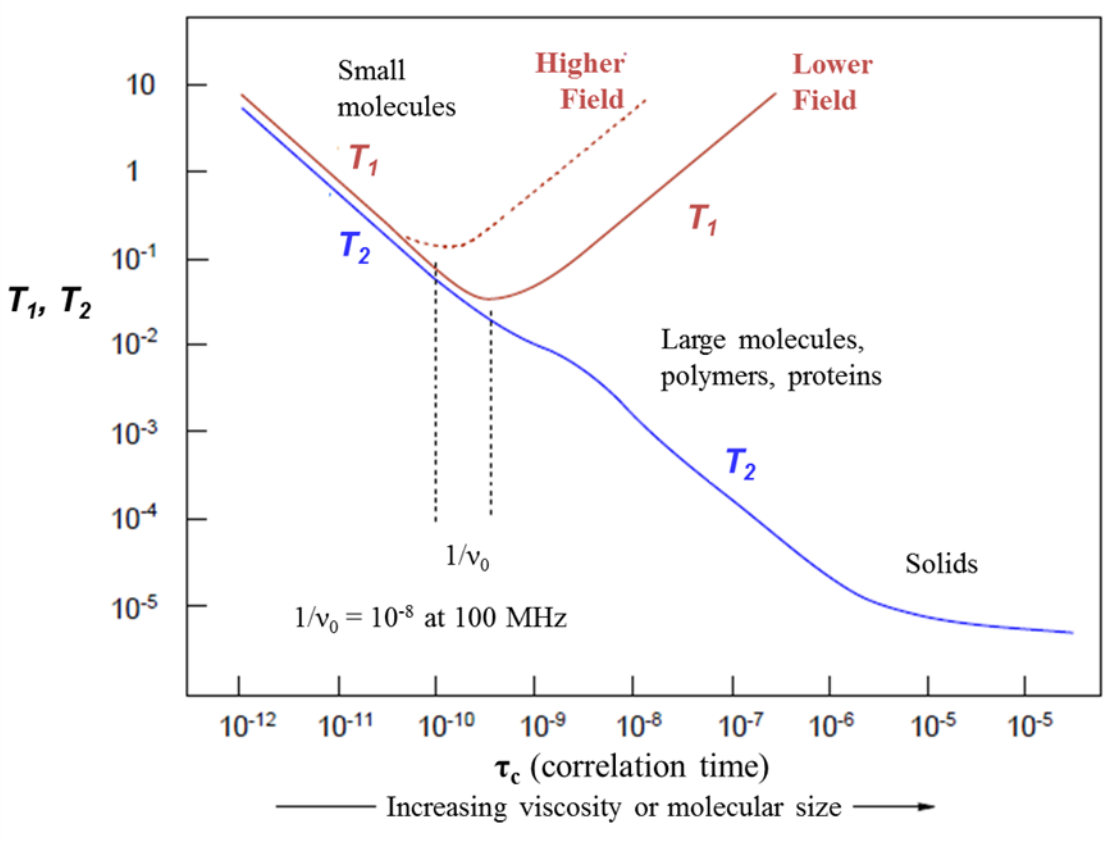


**Figure 1-4:** Relationship between the correlation time ($\tau_c$), and both spin-lattice ($T_1$) and spin-spin ($T_2$) relaxation times. (Source: http://www.chem.wisc.edu/areas/reich/nmr/08-tech-01-relax.htm)

$$\Delta\nu_{1/2} = \frac{1}{\pi T_2}$$

The linewidths of flexible and rigid molecules do show differences. When resonances are narrow this suggests a long $T_2$ and molecules are considered flexible. Line broadening is indicative of lower $T_2$ values and can be attributed to more rigid molecules. $T_2$ also depends on the size of the molecule, small organic molecules have small correlation times and long $T_2$ values; this is reflected in narrow linewidths.[37] However, larger molecules and molecules that form aggregates have longer correlations times and small $T_2$.[37] This causes the individual nuclear magnetic moments to lose phase coherence faster and leads to line broadening.

*Chemical Information Obtained:*

The return of the magnetization to equilibrium conditions is monitored and the time-dependent signal acquired is referred to as free induction decay (FID) signal. With the use of Fourier transform (FT), the FID is converted to a frequency-dependent signal or spectrum. Information on the molecular structure can be inferred from the chemical shift, number and area of NMR signals, and splitting patterns. The nuclei being examined in an NMR experiment precess at different frequencies due to differences in their molecular environment; this gives rise to separate NMR signals. Factors that influence chemical shift include electron density and the electronegativity of the neighboring groups. A nucleus in a molecule experiences a magnetic field (B) different from the applied magnetic field ($B_0$) due to additional magnetic fields caused by the motion of electrons. This is described as $B = B_0 (1-\sigma)$ where $\sigma$ is the shielding constant. There are two components to the shielding constant (diamagnetic and paramagnetic).[37] The diamagnetic component is due to circulation of electrons that generates a magnetic field that opposes the applied magnetic field, $B_0$. The paramagnetic component is due to the

circulation of electrons moving between their ground state and excited state orbitals. This generates an induced magnetic field parallel to $B_0$ and enhances the magnetic field experienced by the nucleus (deshields the nucleus).[37] Typically, the greater the electron density around the nucleus the more it is shielded from the effects of the applied magnetic field and the signal will appear in the lower chemical shift region. A nucleus in the proximity of an electronegative group experiences a decrease in electron density and becomes deshielded. This nucleus senses more of the external magnetic field and this is reflected in higher precession frequencies (higher chemical shift values). Therefore, the chemical shift provides information of the electronic and magnetic environment in a molecule. The number of NMR signals allows one to determine how many nonequivalent nuclei (protons, carbons or phosphorus) are present in the molecule.

Structural information also can be obtained from the splitting patterns or coupling constants J (measured in Hertz). When two nuclei in a molecule are nonequivalent and are within one to three bonds from each other, multiplicity (number of lines) in a given NMR signal can be observed. If a nucleus is coupled to *n* other I = ½ nuclei the signal for the nucleus will be split into $n + 1$ lines.[37, 38] The spacing between the lines within each multiplet is referred to as the coupling constant, J. Depending on how strongly the nuclear spins influence each other will affect the distance between two peaks in the resonance. The mechanism in which two nuclei can couple occurs when spin information is transferred through bond. It is dependent on the nuclear properties and independent of the magnetic field strength.[38] Coupling constants provide information on bond distance and angles.[38]

**2D-NMR: Principles**

In addition to the power of 1D-NMR analysis, 2D-NMR techniques can provide valuable information on through-bonds or through space interactions between two or more nuclei. In 2D-NMR, there are two frequency scales; Fourier transformation of the FID on the horizontal scale is the direct measurement. The second frequency on the vertical scale is the indirect measurement. There are four steps to any 2D NMR experiment: preparation (excite nucleus A), evolution (indirectly measure the chemical shift of nucleus A), mixing (transfer magnetization from nucleus A to B through bond or through space) and detection (measure the chemical shift of nucleus B).[36] The resulting 2D NMR data can be plotted as a contour plot. Correlations between two nuclei will be observed by the presence of off-diagonal cross-peaks. 2D NMR experiments provide information on the connectivity and proximity of the nuclei of interest for structural elucidation.[36]

*Chemical Information Obtained:*

Conventional 2D-NMR experiments that provide information about through-bond connections include $^{1}$H-$^{1}$H Correlation SpectroscopY (COSY), $^{1}$H-$^{1}$H TOtal Correlation SpectroscopY (TOCSY) and HETeronuclear CORrelation Spectroscopy (HETCOR). COSY can be used to determine $^{1}$H-$^{1}$H that are coupled through one (geminal) or two (geminal) bonds. Longer-range couplings (three to four bonds) can be observed using TOCSY.[36] HETCOR provides correlations between $^{1}$H and $^{13}$C resonances when nuclei are directly bonded to each other. In this experiment, the chemical shift of the $^{1}$H is measured indirectly, as its magnetization is transferred to the $^{13}$C and its chemical shift is measured directly.[37, 39] However, it should be noted that the sensitivity of this type of experiment is not very high due the low abundance of $^{13}$C (1.1 %) and its nearly four

times smaller gyromagnetic ratio $\gamma$ relative to $\gamma_H$.[36] To improve the sensitivity on 2D experiments, new techniques have been developed and will be presented in more detail below.

The second type of interactions that can be detected using 2D NMR is through space interactions. Interactions between protons separated by < 5 Å can be observed through Nuclear Overhauser Effect SpectroscopY (NOESY) and Rotating frame Overhauser Effect SpectroscopY (ROESY) (see Figure 1-5).[36, 39] The volumes of the observed NOESY and ROESY cross-peaks reveal the internuclear distances between protons in a molecule. Spatial relations between protons and other heteroatoms can be observed with hetero-nuclear NOESY.[36] Analysis of the data acquired in these 2D experiments can be used to obtain structural and conformational details on the molecular structure.

Inverse 2D- NMR experiments such as Heteronuclear Single Quantum Correlation (HSQC) and Heteronuclear Multiple Quantum Correlation (HMBC) provide enhanced sensitivity compared to conventional experiments such as HETCOR. In these experiments, the $^1$H nuclei is detected directly and heteroatoms ($^{13}$C or $^{15}$N) are indirectly detected.[36] The signal intensity of the NMR increases proportionally with $\gamma^2$ of the detected nuclei. By directly detecting $^1$H in inverse 2D experiments ($\gamma_H$ is four times larger than $\gamma_C$) results in a 16-fold increase in the NMR signal. In addition, the intensity of the noise is proportional to the square root of the frequency being detected and this reduces the signal-to-noise by a factor of $\sqrt{\gamma B_0}$.[36] For $^1$H-$^{13}$C 2D NMR inverse detection, the signal-to-noise ratio increases by a factor of eight. Another advantage of directly detecting $^1$H is that a proton can only be attached to one $^{13}$C. This eliminates the complexities of refocusing $^{13}$C antiphase coherence. Different optimal times are required

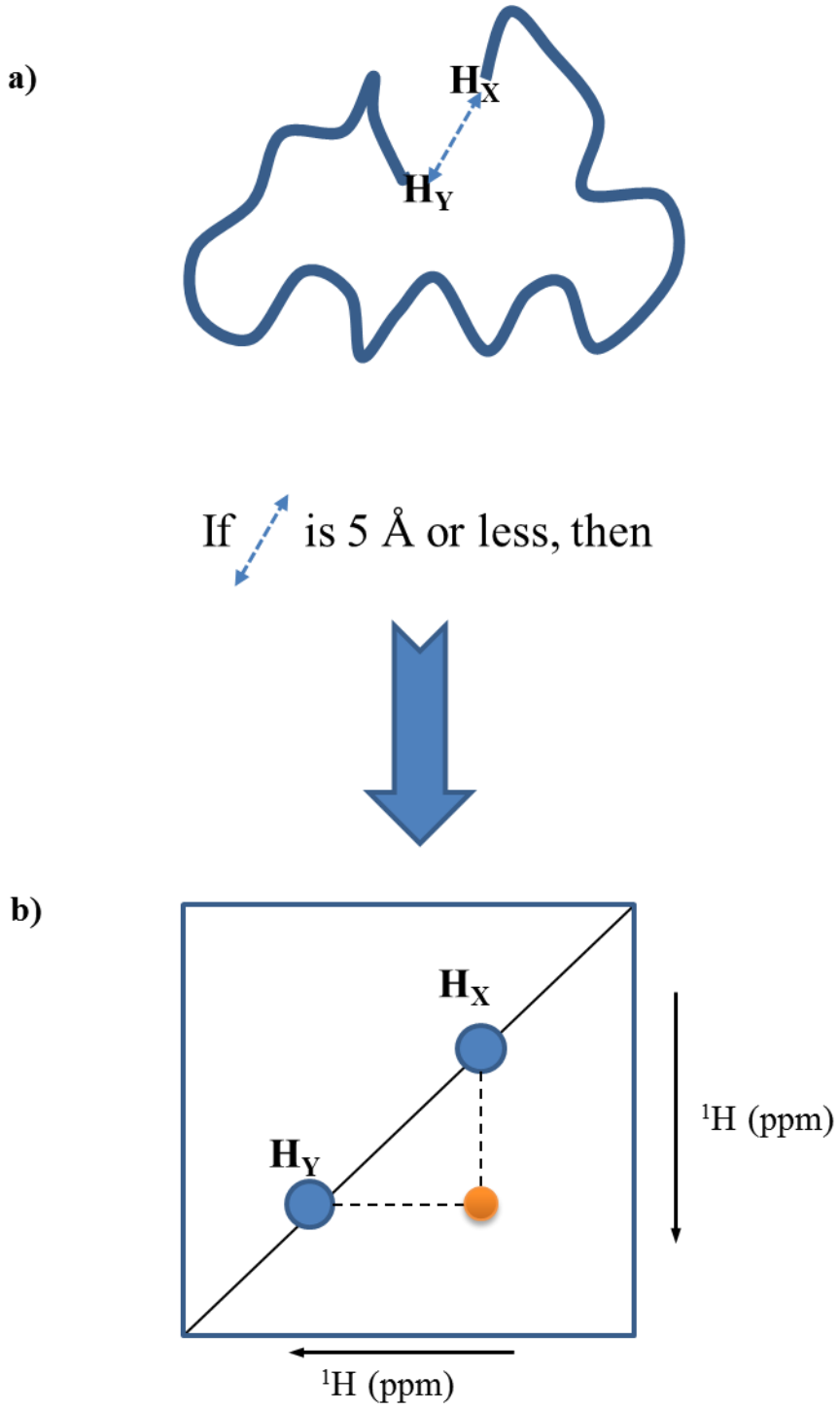


**Figure 1-5:** Schematic diagram explaining ROESY NMR. a) Schematic diagram of a biomolecule illustrating through-space interactions between $H_Y$ and $H_X$ (less than 5Å away from each other) and b) Representation of a $^1$H-$^1$H ROESY (or NOESY) spectrum obtained from this type of NMR experiment.

to refocus CH, $CH_2$ and $CH_3$ groups. Since protons are attached to only one $^{13}C$, the protons will always be a doublet and will refocus in the same time.[36]

The one disadvantage of detecting directly $^{1}H$ in heteronuclear 2D-NMR experiments is the low abundance of $^{13}C$. In addition, if one is trying to observe protons associated with $^{13}C$ in the presence of 98.9% of protons that are associated with $^{12}C$, both associations give rise to the $^{1}H$ signal.[36] The signals corresponding to $^{12}C$-$^{1}H$ are 100 times larger than $^{13}C$-$^{1}H$ (appear as tiny satellite peaks) and will have much smaller J-values ($^{1}J_{CH}$ for $^{13}C$-$^{1}H$ is around 150 Hz).[36] Special techniques (isotope filtering) are used to eliminate $^{12}C$-$^{1}H$ artifacts and, therefore, only $^{13}C$-$^{1}H$ correlations are observed.[36] Despite this limitation, the signal-to-noise advantages mentioned above make indirect 2D-NMR methods more effective than direct ones.

HSQC experiments correlate two different types of nuclei ($^{1}H$ and $^{13}C$) through evolution and transfer of single-quantum coherence. In the presence of a magnetic field, a nucleus with spin ½ has two energy levels, α and β. Single quantum transitions occur when a spin is promoted from the lower energy level to the higher energy and vice versa ($\alpha \rightarrow \beta$ or $\beta \rightarrow \alpha$).[36, 39] In HSQC, the sign of the cross-peak provides information on the number of protons attached to the carbon. This technique also allows for differentiation between CH/$CH_3$ (positive) and $CH_2$ (negative) peaks (see Figure 1-6) Heteronuclear multiple quantum correlation (HMQC) is similar to HSQC but uses double-quantum and zero-quantum coherence during the evolution period. When two spins are J-coupled they have four energy levels available, double-quantum transitions ($\alpha\alpha \rightarrow \beta\beta$ or $\beta\beta \rightarrow \alpha\alpha$) and zero-quantum transitions ($\alpha\beta \rightarrow \beta\alpha$ or $\beta\alpha \rightarrow \alpha\beta$).[36] These transitions cannot be observed directly but are allowed to evolve and are converted back to observable single-quantum coherence for detection.[36]

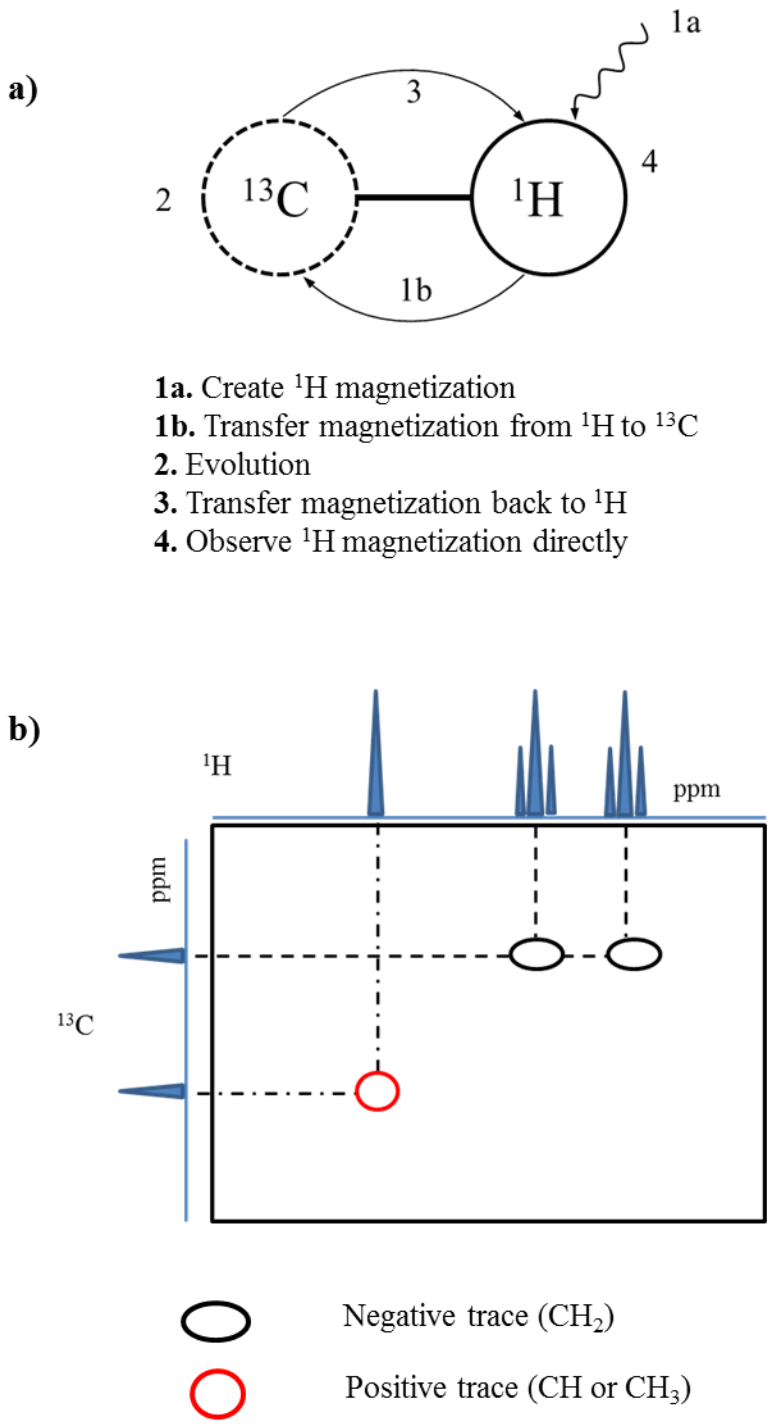


**Figure 1-6:** Schematic diagram explaining HSQC NMR. a) Diagram representing the transfer of magnetization from $^{1}H$ to $^{13}C$ and back to $^{1}H$ in indirect HSQC NMR experiments and b) schematic diagram of the HSQC spectrum obtained correlating $^{1}H$ to $^{13}C$. This diagram also shows how differentiation between $CH/CH_3$ and $CH_2$ can be observed.

In addition to the enhanced sensitivity provided by inverse experiments, the ability to see long-range $^{13}C$ and $^{1}H$ (two to three bonds) interactions is extremely helpful for molecular characterization.[36] HMBC is similar to HMQC in that they both use multiple quantum transitions. However, HMBC detects connections up to three bonds by selecting J-values around 10 Hz ($^{2,3}J_{CH}$) for coherence transfer and rejecting one-bond relationships ~ 150 Hz ($^{1}J_{CH}$) (used in HMQC).[36] Both HSQC and HMBC are powerful methods with means of providing valuable information on $^{13}C$-$^{1}H$ connectives that lead to tracing out the carbon skeleton of molecules.

**NMR STUDIES OF BILE SALTS**

$^{1}H$ and $^{13}C$ NMR studies have been used to elucidate the correct proton and carbon assignments for bile salts. Barnes and Geckle used a 400 MHz NMR to resolve the proton assignments of sodium cholate.[40] Before this study, resolution was an issue for the complex region of the spectrum. Therefore, the assignments reported corresponded only to the methyl protons and protons attached to carbons with adjacent hydroxyl groups whose resonances can be easily identified. $^{1}H$ NMR studies have also been used to quantify taurine-conjugated and other bile acids present in bile.[41] In addition, concentration dependence studies were completed to examine effects of aggregation by altering the side chain and taurine moiety on taurine-conjugated bile salts.[42] The results showed micelle aggregation to be most affected by the steroid side-chain due to their involvement in the hydrophobic interactions bringing monomers together to form micelles. However, this study did not address the intermolecular interactions involved in the micellization process.[42]

2D-NMR spectroscopy was used to elucidate proton resonance assignments for common bile acids. The first of these studies used homonuclear-decoupled-heternuclear-correlated two-dimensional NMR (HETCOR) experiments to assign proton resonances. This 2D-NMR experiment gave the advantage of identifying the protons connected to the same carbon.[43] Additional 2D- COSY (COrrelated SpectroscopY) NMR studies were completed for sodium cholate and deoxycholate to complete proton and carbon resonance assignments.[44] $^{13}$C assignments for NaCho's C3-C7 and C19-C21 and NaDC's C3-C12 that were inverted in previous studies were corrected.[44]

Funasaki *et al.* has reported multiple studies on bile salt aggregation numbers and critical micelle concentrations for sodium taurocholate (TC) and taurodeoxycholate (TDC).[45, 46] With the use of frontal derivative chromatography and a step-wise aggregation model, results support the formation of TC and TDC dimers at low bile salt concentrations and larger multimers as the bile salt concentration increases.[46]

In addition, Funasaki *et al.* studied the NaTC micelle formation and structure using two-dimensional NMR techniques.[47] $^{1}$H and $^{13}$C resonances were assigned based on the literature and carbon-hydrogen correlation spectroscopy (C, H COSY) experiments. Critical micelle concentrations were determined by monitoring the changes in chemical shift for H12. Results showed a large range for the transition from monomers to primary micelles to take place suggestive of a stepwise self-association. ROESY and NOESY experiments were used to examine the micelle structure for 1 mM (monomer), 8 mM and 30 mM NaTC (micelles). The volumes of these cross-peaks were evaluated by integration and used to determine the effective distance between protons. 2D spectra for 1 mM and 8 mM naTC were compared and additional cross-peaks were observed suggesting the dimerization of TC.[47] Increasing the concentration to 30 mM showed new cross-peaks

that were not observed at 8 mM, at this higher concentration these new contacts were due to the presence of primary micelles.[47]

Similar studies were conducted for sodium taurodeoxycholate (NaTDC) using one- and two-dimensional NMR.[8] NaTDC and NaTC are bile salts that differ only in the number of hydroxyl groups. NaTDC contains two hydroxyl groups at positions 3 and 12 and NaTC has three hydroxyl groups at positions 3, 7 and 12. The loss of the hydroxyl group at position 7 makes NaTDC more hydrophobic compared to NaTC. The *cmc* values for NaTDC were found to be 3.5 and 4.0 mM and form micelles at lower concentrations than NaTC.[8] ROESY spectra were collected for 0.5, 3, 8 and 15 mM NaTDC and the volume of the cross-peaks were determined as discussed above for NaTC. At concentrations below 3 mM, NaTDC does not self-associate, however; at 8 mM additional cross-peaks were observed suggestive of the formation of dimers. Six possible dimeric fragments of NaTC and NaTDC micelles were considered for dimerization shown in Figure 1-7.[8, 47] There are three types of interactions that stabilize these dimers. The first is the hydrophobic interactions between the non-polar steroid nucleus, this type of interaction is shown in ABB (antiparallel back-to-back) and PBB (parallel back-to-back). Secondly, stabilization due to the reduction of electrostatic repulsion between sulfonate ions is seen in ABB, AFF (antiparallel face-to-face) and ABF (antiparallel back-to-face). However, strong repulsions due to sulfonate ions are present in PBB, PFF (parallel face-to-face) and PBF (parallel back-to-face). Another interaction that promotes stable dimers through hydrogen bonding between hydroxyl groups; this is present in AFF and PFF. Of these six dimer structures, ABF and PBF are considered unstable due to the hydrophobic back of one monomer being in contact with the hydrophilic face of the neighbor. [8]

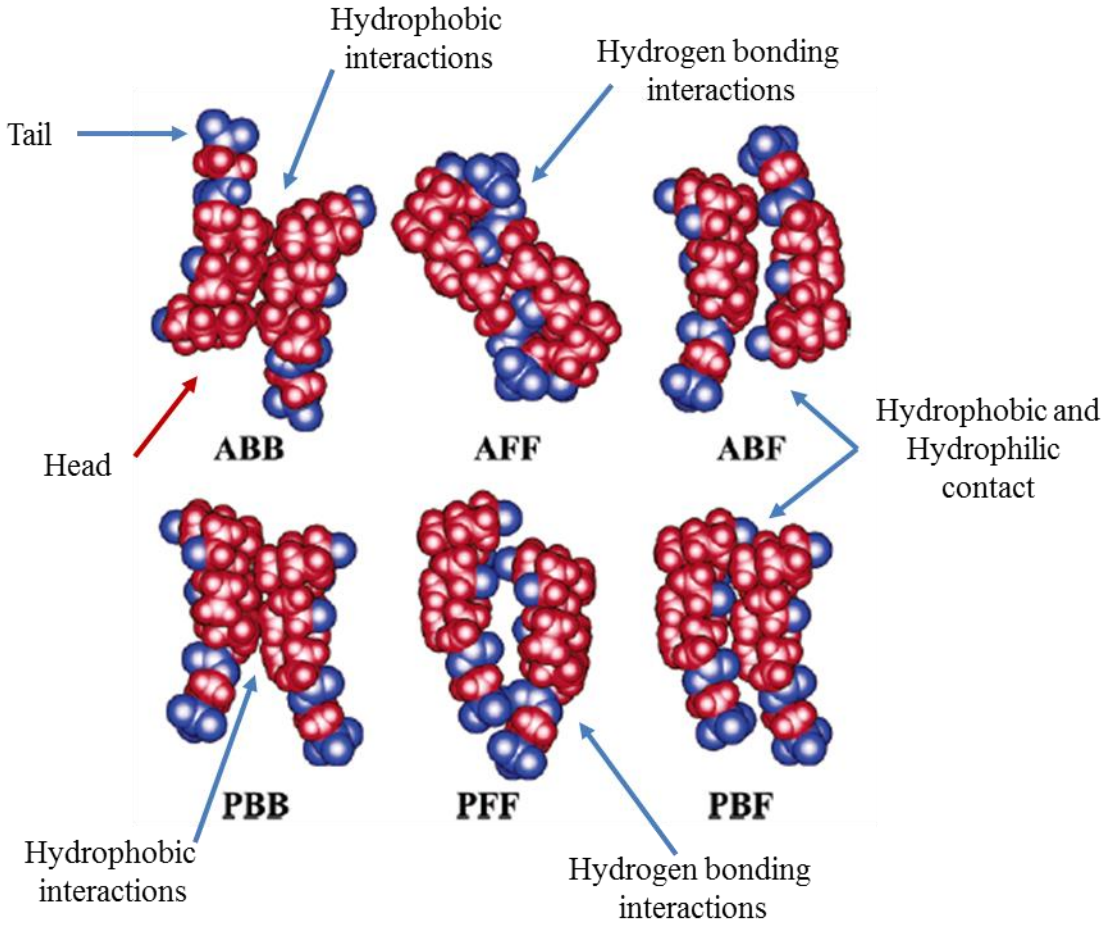


**Figure 1-7:** Dimeric fragments of NaTC and NaTDC micelles. Antiparallel back-to-back (ABB), antiparallel face-to-face (AFF), antiparallel back-to-face (ABF), parallel back-to-back (PBB), parallel face-to-face (PFF) and parallel back-to-face (PBF). Types of interactions present in each dimer are shown with blue arrows. Adapted from Funasaki *et al.*[8, 47]

Based on the ROESY results from this study, at 8 mM NaTC, monomers form a dimer and these micelles are composed of the ABB and PBB fragments. The major dimer fragments of NaTDC are AFF and PFF due to the missing hydroxyl at position 7, this face of the molecule has more hydrophobic character. This leads to hydrophobic interactions between the less hydrophilic face and the hydrophobic face of the monomers. Stabilization of these structures comes from the close contact between the concave (hydrophilic) and convex (hydrophobic) planes of the molecules involved in the dimer.[8]

It is the shape of these micelles that leads NaTDC to have smaller *cmc* values and the ability to form larger micelles compared to NaTC.[8] The structures of dimers and small micelles have been resolved. However; the structures of larger micelles (above 30 mM TC) formed by dihydroxy bile salts have not been elucidated.

Previous studies from our laboratory investigated the molecular arrangement of primary and secondary micelles of NaCho using a 500 MHz NMR spectrometer. Changes in chemical shifts were examined for the protons on NaCho as the bile salt concentration increased. From these results it was postulated that primary micelles are composed of four (or six) monomers arranged in an antiparallel fashion and the hydrophobic faces are oriented toward the core of the micelle. The primary micelles were proposed to be held together at the top and bottom by water-mediated interactions between the $COO^-$ group of the tail and the hydroxyl groups at position C3. It was also postulated that a hydrogen-bond network surrounding the hydroxyl groups at position C7 and C12 is formed as monomers associate to form primary micelles.[48] This proposed model is shown in Figure 1-8. This study was also extended to the micellar organization of secondary micelles. It was postulated that the secondary micelles formation involves the stacking of primary micelles through ion-dipole and H-bonding interactions connecting the ends of the

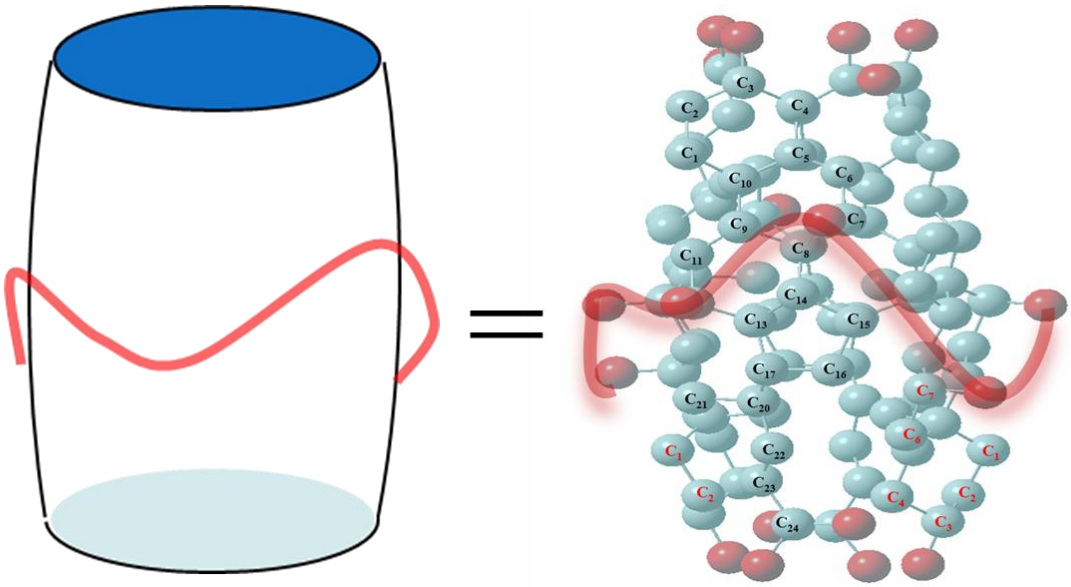

**Figure 1-8.** Primary micelle model proposed by our group. In this 'barrel' model four (or six) monomers arranged in an antiparallel fashion. A hydrogen-bond network surrounding the hydroxyl groups at position C7 and C12 is formed as monomers associate to form primary micelles (shown in red).[48]

primary micelles together. In addition, an extended H-bonding network surrounds the secondary micelles (see Figure 1-9). Chapter 2 of this dissertation will focus on the validation of the molecular arrangements for primary micelles using one- and two-dimensional NMR experiments that were carried out in the 700 MHz NMR spectrometer. Chapter 3 will examine the molecular arrangements of secondary micelles.

Additional studies in our laboratory examined the interactions between NaCho primary micelles and adenosine triphosphate (ATP) using 1D- $^{1}$H and $^{31}$P NMR on a 500 MHz NMR spectrometer. In that work, changes in chemical shifts were monitored for both NaCho and ATP. From these results, key interactions between NaCho primary micelles and ATP involved hydrogen bonding with the hydroxyl groups of NaCho (OH-7 and OH-12) and the adenosyl group of ATP.[49] From the chemical shifts for H5′A and H5′B in the presence of NaCho primary micelles indicates that ATP is in a self-stacked arrangement. Figure 1-10 shows the proposed interaction of ATP with the hydrophilic surface of the NaCho monomers.[49]

## GOALS OF THIS WORK

The studies in this dissertation will focus on micelles of sodium cholate, a naturally occurring primary bile salt present in the body. In the past, there have been various studies on bile salts, their critical micelles concentrations and aggregation numbers. There have been few studies on the molecular arrangement of these bile salt micelles and models have been proposed. Since there are contradicting models, the first goal in this dissertation is to revisit and test the models for NaCho primary and secondary micelles proposed by our group.

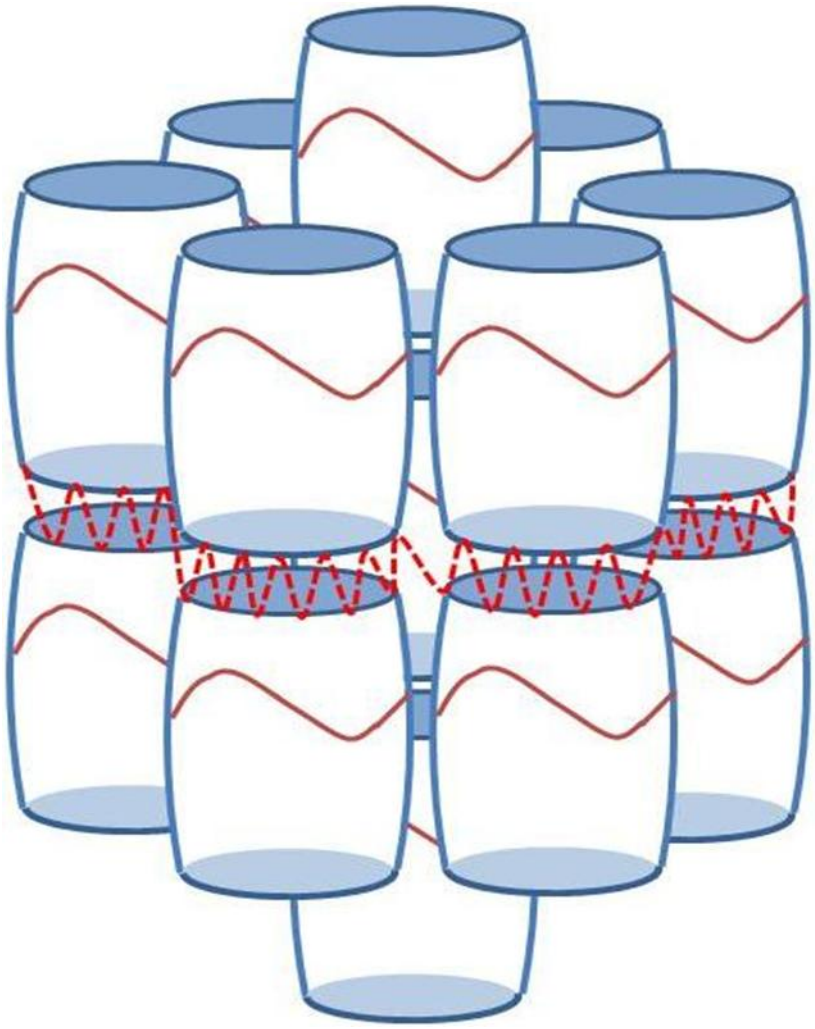

**Figure 1-9.** Secondary micelle model proposed by our group. In this model primary micelles stack together to form secondary ones. The tops and bottoms are held together by ion-dipole and water mediated interactions (shown in a dotted red line).[48]

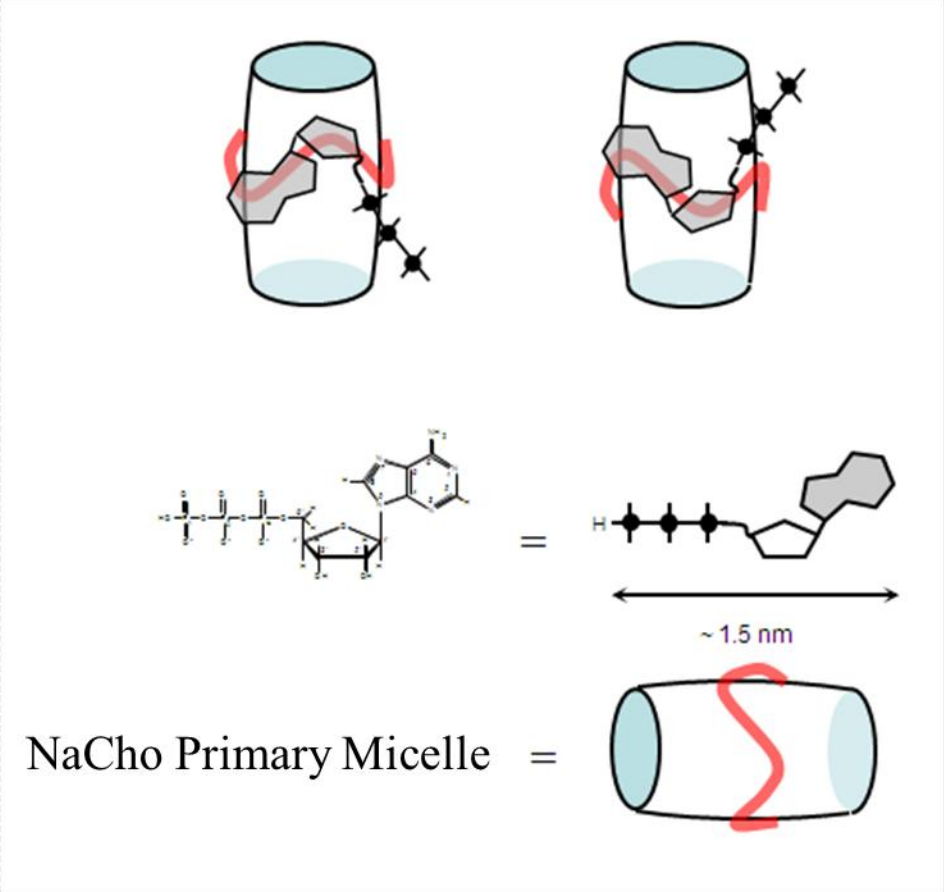


**Figure 1-10.** Proposed interactions between NaCho primary micelles and ATP. The adenosyl group of ATP is involved in hydrogen bonding with the hydroxyl groups of NaCho (OH-7 and OH-12).[49]

In addition, it is important to determine how salt concentration and pH affect micelle formation. Understanding the interactions and forces involved in bile salt micelle formation can then be used to make modifications (using different bile salts or altering solution parameters) to apply these nanostructures for other applications such as understanding the structure of mixed micelles, transportation of hydrophobic molecules and for drug delivery.

# CHAPTER 2

## NMR CHARACTERIZATION OF PRIMARY MICELLES OF SODIUM CHOLATE

### INTRODUCTION

Bile acids (BA) and salts (BS) are important biosurfactants for digestion and absorption of fats in the small intestine of mammals.[11, 12, 17] These biosurfactants are able to solubilize and transport lipids by forming mixed-micelles aggregates of lipids such as fatty acids, PLs, cholesterol and monoglycerides.[50] Bile acids are facial amphiphiles, as they have a hydrophobic (non-polar) and a hydrophilic (polar) face. In the presence of water, very small micelles are formed in which the nonpolar sides are believed to face each other toward the interior of the micelle and the polar faces with the hydroxyl groups interact with the aqueous surroundings.[10, 19]

Several techniques such as potentiometry[25], light scattering[28], fluorescence[30], small neutron scattering[4, 51], chromatography, micro-calorimetric titration[22] and isothermal titration calorimetry (ITC)[3, 52, 53] measurements have been used to determine the aggregation number, critical micellar concentration (*cmc*) and in some cases the apparent pKa values of sodium cholate (NaCho) and other bile salts.[54] These reports showed that the *cmc* value for NaCho at normal conditions is about 16 mM. In addition, the aggregation number was determined to be 4 to 5 at low temperatures but showed a pronounced increase (from 5 to 13) when the temperature was increased. Depending on the concentration of the bile salts, the formation of micelles occurs in two different stages. The first stage leads to primary micelle formation and occurs when the

concentration of the bile salts solution reaches its *cmc* (NaCho ~16 mM). The second stage is the formation of secondary micelles that result from the aggregation of the primary micelles.

One- and two dimensional NMR spectroscopy has been applied in the characterization of natural and synthetic bile acids. The assignments of $^{1}H$ and $^{13}C$ NMR resonances have been previously reported for NaCho and other conjugated bile salts.[40, 44, 55] 2D-NMR studies have also been used to study the structure of the micelles formed, their influence and binding with aromatic molecules, phospholipids and other compounds.[56, 57] With the use of Nuclear Overhauser Effect Spectroscopy (NOESY), Rotating frame Overhauser Effect Spectroscopy (ROESY) and Coherent Overhauser Spectroscopy (COSY) possible intra- and inter-molecular interactions between these macromolecules and bile salts micelles were investigated. These studies were useful to determine the intensities of intermolecular cross-peaks in the nuclear spectra of sodium taurodeoxycholate (NaTDC) in $D_2O$ and the possible structures of the micelles were postulated.[8] In addition, the inter-proton distance was estimated based on the intensity of cross-peaks observed in NOE and ROE spectra.[47, 58] From these results, several models of possible dimer arrangements between bile salts monomers were proposed.[8, 47] However, these proposed arrangements are limited to dimer fragments (see Chapter 1). As discussed in Chapter 1, previous studies from our laboratory investigated the molecular arrangement of NaCho primary micelles by monitoring the changes in chemical shifts for NaCho protons as the bile salt concentration increased. From the results of those studies, the 'barrel' model was proposed. However, the resonances in the complex region of the spectrum (1.0 – 2.3 ppm) could not be followed accurately using the 500 MHz NMR spectrometer. In this chapter, the micellar organization of NaCho will be revisited using

one- and two-dimensional NMR techniques on a 700 MHz NMR spectrometer to test the accuracy of the 'barrel' model. This information could then be used to understand how lipids and/or drug molecules may be incorporated within the micellar arrangement.

## MATERIALS AND METHODS

**Chemicals.** $D_2O$, NaOD, NaCho and 4,4-dimethyl-4-silapentane-1-sulfonic acid **(**DSS) were purchased from Sigma Chemical Co, St. Louis, MO.

**Preparation of NaCho micelles** The concentrations used were 0.2, 2, 4, 10, 15, 20, 30 mM in $D_2O$. The solutions were sonicated in a bath sonicator (Cole-Parmer 8890) for about 15 minutes and the pH was adjusted with 1 M NaOD at physiological pH (7.4). No buffers were used in the initial studies to reduce possible spectral interferences and prevent buffer-related effects on the formation of the micelles.

**Spectral Acquisition.** $^{1}H$ and $^{13}C$ and 2D-NMR spectra were acquired with a Varian INOVA 500 and 700 MHz NMR spectrometers, Palo Alto, CA. A coaxial insert containing 1.0 mM 4,4-dimethyl-4-silapentane-1-sulfonic acid (DSS) dissolved in $D_2O$ was inserted in the NMR tube and used for signal locking and referencing of NMR spectra. The following acquisition parameters were used for $^{1}H$: a minimum of 16 scans, relaxation delay of 1.000 second, 45º pulse width, and 25 ºC. For gHSQC spectra, 4 scans per increment and 128 increments were used. For ROESY experiments, relaxation delay of 1.000 sec, mixing time of 300 ms, 8 scans acquired per FID and 2 x 256 increments, the spectral width was between -1 and 9.5 ppm.

**Data Analysis.**All spectra were analyzed using MestReC software, version 4.7.0 or the newer MestReNova, version 7.1.2 (Santiago de Compostela, Spain). The resonance

associated with the methyl groups in 4,4-dimethyl-4-silapentane-1-sulfonate, sodium salt (DSS) was used as for referencing of NMR spectra.

**Theoretical Calculations.** The integral equation formalism (IEF) method of the polarizable continuum solvation model (PCM) of Tomasi and coworkers was used to investigate the simulation of the environmental effects on the NMR properties of the cholate molecule.[59] The single point wave function for these models was calculated at the HF/6-31+G(d,p) level of theory using Gaussion03.[60] NMR shielding tensors and chemical shifts were then obtained with the gauge including atomic orbital (GIAO) method at the same level of theory. To coordinates of the cholate atoms were obtained from published X-ray work.[61] The electronically unperturbed molecule and three solvents which varied in dielectric constants were considered. These solvents included chloroform, methanol and water which have dielectric constants (ε) of 4.9, 32.63, and 78.39, respectively.

## RESULTS AND DISCUSSION

### Confirmation of previous assignments of $^{1}$H and $^{13}$C NMR resonances

Initial studies were conducted to confirm the assignments of $^{1}$H and $^{13}$C resonances. Figure 2-1 shows the HSQC NMR spectrum for 20 mM NaCho. HMQC data were acquired to corroborate/correct assignments of proton resonances in NaCho, especially those between 0.6 and 2.2 ppm, where there is significant spectral overlap. The observed correlations enabled the confirmation of all proton resonance assignments reported earlier.[62] In addition, the $^{13}$C resonance assignments reported by Muccio were also confirmed and indicated that earlier assignments for C19 and C21 were reversed.[43]

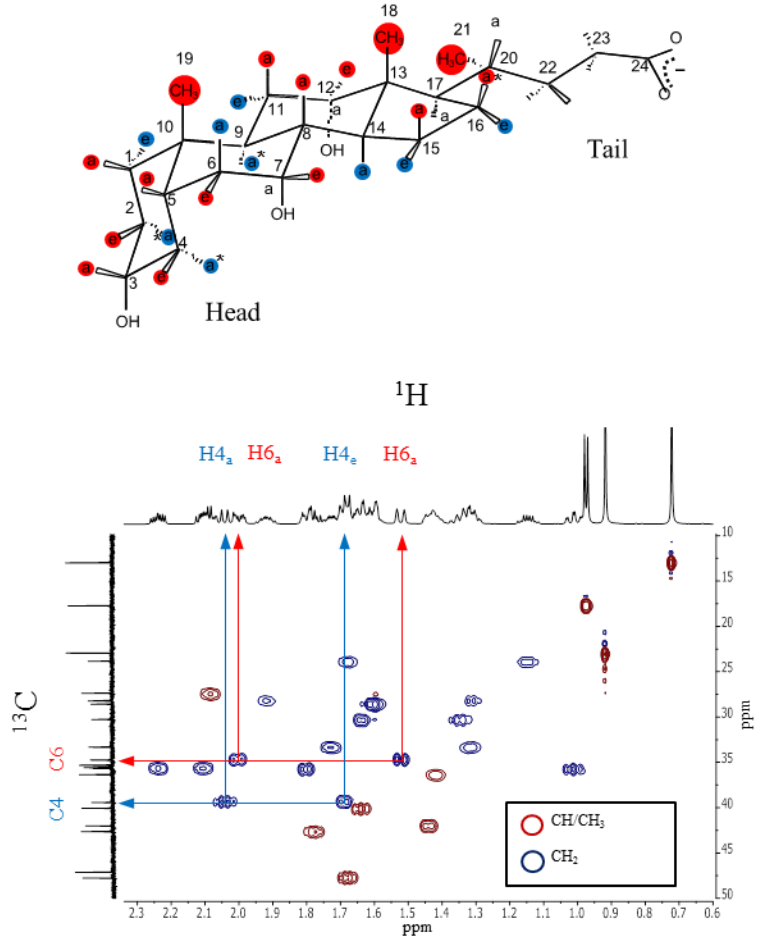


**Figure 2-1:** HSQC spectrum for 20 mM NaCho. $^{1}$H and $^{13}$C assignments for H4$_a$ and H4$_e$ are shown in blue and H6$_a$ and H6$_e$ are shown in red.

Table 1 in the Supplementary information lists the assignments for all resonances for the monomer (2 mM) and the primary micelles (20 and 30 mM). These chemical shift values were obtained from two-dimensional HSQC experiments acquired for all NaCho concentrations in this study.

**Concentration-dependent changes in chemical shifts**

At a 2 mM concentration, only NaCho monomers are present. At 20 mM, comparable numbers of primary micelles and monomers co-exist. At 30 mM, there are more micelles than monomers. As shown in Figure 2-2, one-dimensional $^{1}$H NMR spectra showed changes in chemical shifts upon formation of micelles (*cmc* ~ 16 mM). For example, $H15_a$ showed slight shielding with increasing concentration, as highlighted by the black arrow. Other resonances, such as 6e and 16e, showed the opposite trend (deshielded). There were slight changes (increase) in linewidth as primary micelles formed. However, changes in splitting patterns for some resonances and spectral overlap made it difficult to evaluate the degree of broadening.

For the interpretation of the trends observed in chemical shifts, we divided the protons of NaCho into two categories: hydrophobic and hydrophilic. Figure 2-3 shows the changes in $^{1}$H chemical shifts for the resonances that revealed critical information for the postulation of the arrangement of the monomers in primary micelles. These changes are relative to the chemical shifts measured for the monomers (2 mM). The relative changes in other $^{1}$H resonances are graphed in the Supplemental Information.

Among the protons in the hydrophobic region, those corresponding to the methyl groups at C18 and C19 become more shielded, as evidenced by the decrease in their chemical shifts with increasing concentrations (see Figure 2-3A). The resonances for the

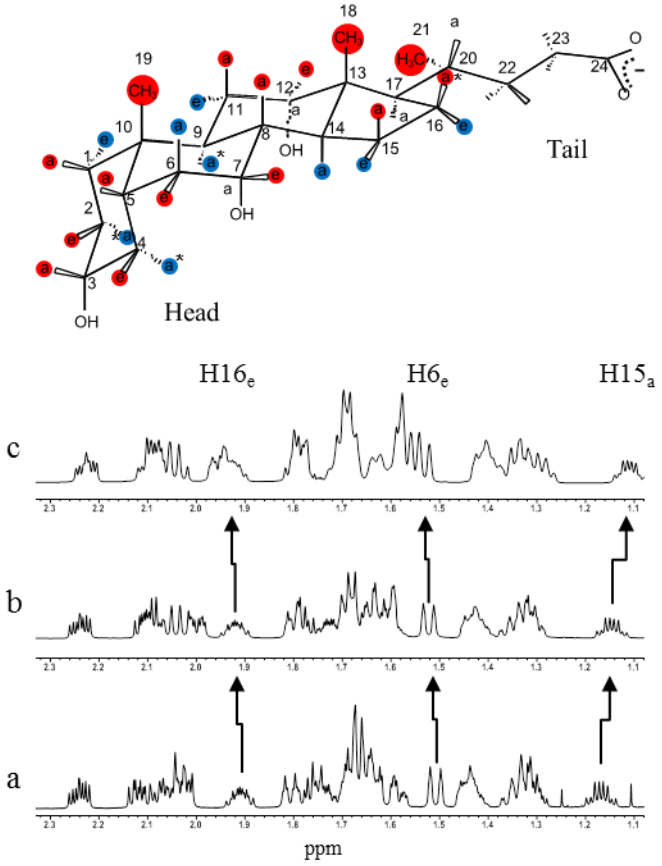


**Figure 2-2:** Labeled NaCho monomer and $^{1}$H NMR spectra for 2, 20 and 30 mM NaCho. Protons on the hydrophilic and hydrophobic face are shown in blue and red respectively. The chemical shifts of protons with an asterisk did not follow the expected trends. $^{1}$H NMR spectra for a) 2 mM b) 20 mM and c) 30 mM NaCho. Concentration-dependent changes in chemical shift are highlighted for $H6_e$, $H16_e$ (deshielded) and $H15_e$ (shielded).

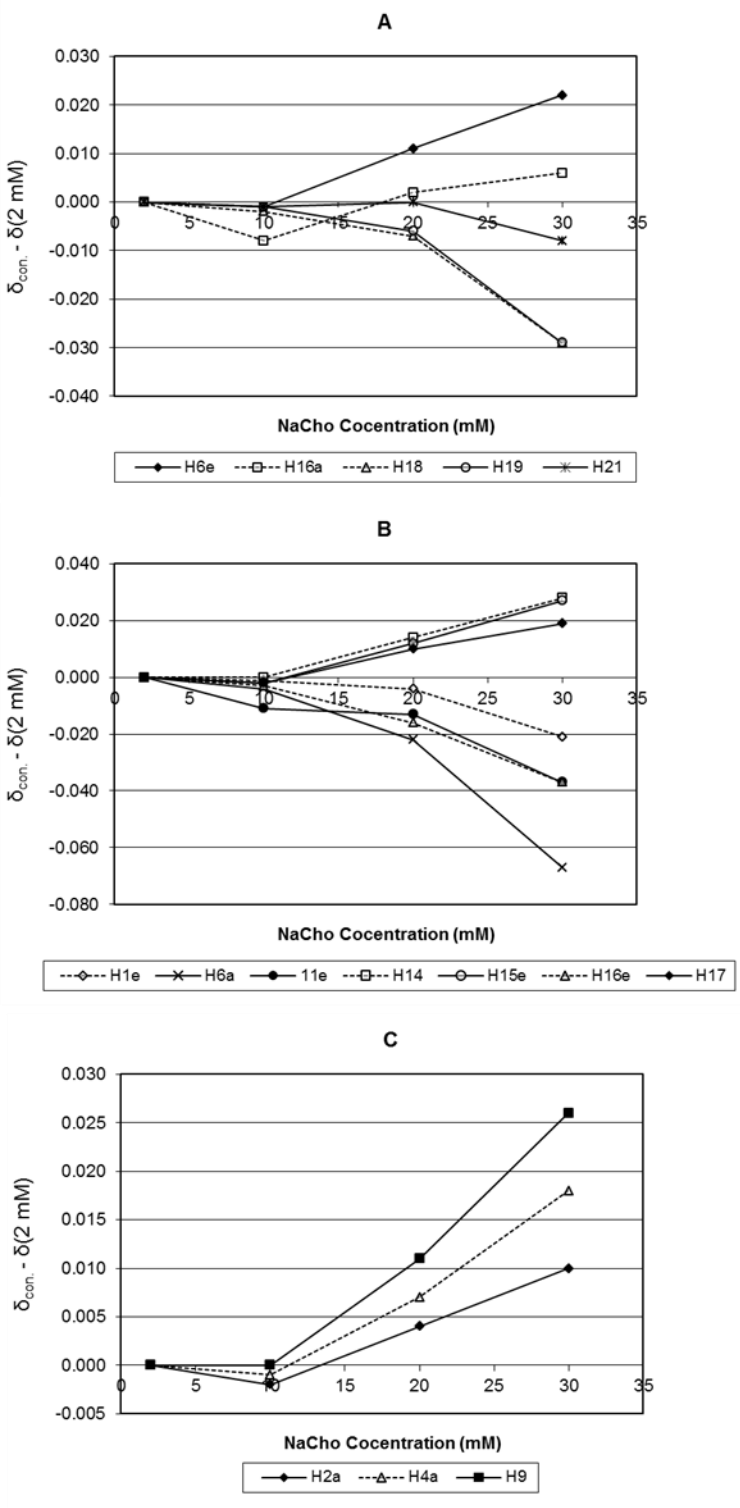


**Figure 2-3:** Changes in chemical shift for A) hydrophobic protons, B) hydrophilic protons and C) protons that did not follow the expected trends.

methyl group at C21 and for H6a and H6e, on the other hand, increased their chemical shift with concentration.

Although little change was expected for the resonances corresponding to protons in the hydrophilic face of NaCho, both increases and decreases in $\delta$ were observed (see Figures 2-3b and c). The interpretation of these changes is presented later in this report.

**Theoretical Calculations**

To interpret the experimental trends, theoretical calculations were performed using the polarizable continuum medium (PCM). Chemical shift calculations were obtained as the dielectric constant was changed from that of a non-polar solvent, chloroform ($\varepsilon = 4.9$), to that of a polar one, water ($\varepsilon = 78.39$). The theoretical analysis is presented in Table 2-2. As the polarity of the solvent increased most of the protons became deshielded. However, there were some notable exceptions: resonances for protons $2_a$ ($\Delta\delta$ = -0.13 ppm), $4_a$ ($\Delta\delta$ = -0.14 ppm), and 9 ($\Delta\delta$ = -0.08 ppm) decreased their chemical shifts (or these protons became significantly more shielded) as the polarity increased. Protons whose chemical shifts also decreased but to a lesser extent include 1e ($\Delta\delta$ = -0.02 ppm), 6a ($\Delta\delta$ = -0.02 ppm), 16e ($\Delta\delta$ = -0.02 ppm) and the smallest decrease was observed for 11e ($\Delta\delta$ = -0.014 ppm). This is a consequence of the greater deshielding effect of the oxygen lone pairs in the hydroxyl groups on neighboring protons when the solvent is non-polar (chloroform). In the presence of methanol and water, this deshielding is reduced and leads to a decrease in chemical shift (greater shielding). Indeed, protons $2_a$ and $4_a$ are in close proximity to OH-3, and the oxygen lone pairs cause the deshielding of its neighboring protons. As the dielectric constant of the solvent increases to $\varepsilon = 78.39$ (water), the lone pairs interact with the surrounding water molecules and their

| Label Proton | Chloroform δ (ppm) $CHCl_3$ ε = 4.9 | Methanol δ (ppm) $CH_3OH$ ε = 32.63 | Water δ (ppm) $H_2O$ ε = 78.39 |
|---|---|---|---|
| H1E | 2.0031 | 1.9883 | 1.9848 |
| H1A | 0.7317 | 0.8098 | 0.8216 |
| H2A | 1.2097 | 1.0935 | 1.0828 |
| H2E | 1.1693 | 1.1729 | 1.1693 |
| H3 | 2.9908 | 3.0905 | 3.1036 |
| H4A | 2.2817 | 2.156 | 2.1399 |
| H4E | 1.0065 | 1.097 | 1.1074 |
| H5 | 0.6887 | 0.7952 | 0.8096 |
| H6E | 1.3496 | 1.4021 | 1.4147 |
| H6A | 1.2011 | 1.1894 | 1.1808 |
| H7 | 3.5509 | 3.5928 | 3.5968 |
| H8 | 1.0374 | 1.1058 | 1.132 |
| H9 | 2.3563 | 2.2899 | 2.2731 |
| H11A | 1.439 | 1.4818 | 1.4942 |
| H11E | 1.7014 | 1.6961 | 1.6876 |
| H12 | 3.7849 | 3.8036 | 3.8123 |
| H14 | 1.873 | 1.9098 | 1.9302 |
| H15A | 0.8542 | 0.9156 | 0.9176 |
| H15E | 1.1594 | 1.239 | 1.2553 |
| H16A | 1.387 | 1.4146 | 1.4161 |
| H16E | 2.1044 | 2.0861 | 2.0821 |
| H17 | 0.9032 | 0.9607 | 0.9746 |
| H18 | 0.1243 | 0.1727 | 0.1751 |
| H18 | -0.0175 | -0.035 | -0.0374 |
| H18 | 0.6 | 0.6536 | 0.6664 |
| H19 | 0.7319 | 0.7245 | 0.7307 |
| H19 | 0.2577 | 0.314 | 0.3231 |
| H19 | -0.0107 | 0.0032 | 0.0002 |
| H20 | 0.5202 | 0.6455 | 0.6495 |
| H21 | 0.5966 | 0.4281 | 0.3933 |
| H21 | 0.46 | 0.6056 | 0.6329 |
| H21 | -0.4796 | -0.5341 | -0.5367 |
| H22A | 0.9843 | 1.124 | 1.1497 |
| H23E | 1.6644 | 1.4936 | 1.4629 |
| H23A | 1.5779 | 1.6491 | 1.6657 |
| H23A | 1.7207 | 1.7111 | 1.714 |

**Table 2-1:** Theoretical calculations of chemical shifts (δ) for the NaCho molecule using the polarizable continuum medium (PCM)

deshielding effect on $2_a$ and $4_a$ diminishes (these proton resonances become shielded). A similar effect takes place with proton 9 which is located close to OH-7 and OH-12.

Another proton whose average chemical shift decreased by $\Delta\delta$ = -0.09 ppm correspond to the methyl group at C21. It is proposed that the deshielding effect exerted on these protons by the nearby $COO^-$ group diminishes in the presence of water.

These predicted changes in chemical shifts were used as a guideline to estimate if a given proton entered a more or less polar environment as the transition from monomer to primary micelle took place.

**Interpretation of Experimental Trends**

We have calculated the difference between chemical shifts for each proton at different concentrations with respect to those at 2 mM to extract trends that could aid us to understand the organization of NaCho micelles at the molecular level (see Figure 2-3). Figure 2-2 shows the NaCho monomer protons that are located on the hydrophobic face in red and hydrophilic face in blue. Protons in the tail were not colored because due to the flexibility of this region of NaCho, it can adopt many orientations. Therefore, it is more difficult to classify the hydrophobic/hydrophilic protons.

We expected the protons on the hydrophobic face of the monomer to sense a more hydrophobic environment as the micelles formed, and the protons in the hydrophilic face would not be affected significantly. However, several resonances did not follow the expected trends and they are denoted with an asterisk (see Fig. 2-2). The following discussion focuses on the significant changes in chemical shift that were observed.

**Hydrophobic Face**

Protons in the hydrophobic face of the monomer (shown in red in Fig. 2-2) are expected to enter a less polar environment as the micellization process occurs. At a 2 mM

NaCho concentration, monomers are present in solution and both the hydrophobic and hydrophilic faces are exposed to water. As primary micelles are formed, the hydrophobic faces of the monomers are expected to be near each other and away from the aqueous solvent. For example, methyl protons on C18 and C19 enter a less polar environment as the concentration of NaCho is increased, and this effect leads to a decrease in δ for their resonances. However, the theoretical trends were not observed in protons $6_e$, $16_a$ and 21. $H6_e$ increased its chemical shift by 0.02 ppm, suggesting that it is in a more polar environment in the micelle. $H16_a$ is located at the interface between the hydrophobic and hydrophilic side. $H16_a$ increased its δ by only 0.005 ppm (not statistically significant). H21 decreased its δ by 0.008 ppm and, according to theoretical predictions, this indicates a more polar environment. This change can be attributed to H21 being in closer proximity to $COO^-$ in the primary micelles than in the monomer.

**Hydrophilic Face**

Protons on the hydrophilic face of NaCho are highlighted in blue in Figure 2-2. Logically, one would not expect the hydrophilic face to experience a more polar environment as micellization occurs because it is already exposed to water in the monomeric form. However, changes in chemicals shifts for protons around the hydroxyl groups (OH-3, OH-7 and OH-12) suggest that they experience a more polar environment upon micellization. A noteworthy change in chemical shift was observed with proton $1_e$ ($\Delta\delta$ = -0.02 ppm) (see Fig. 2-3B) that is located near the hydroxyl group (OH-3). Interestingly, and according to the theoretical predictions of chemical shifts, proton $1_e$ appears to sense a more polar environment as micelles begin to form. To explain this trend, $H1_e$ would need to be in the proximity of a moiety more polar than water when the micelle is formed. It is proposed that in the micelle, $H1_e$ is near the carboxylate group of

the neighboring monomer. This suggests that monomers adopt an anti-parallel arrangement as micellization occurs. As a result, the tail of one monomer is in the vicinity of the head of the neighboring monomer. Other protons that experience a more polar environment upon micellization include $H6_a$ ($\Delta\delta$ = -0.07 ppm), $H11_e$ ($\Delta\delta$ = -0.04 ppm), H14 ($\Delta\delta$ = 0.03 ppm), $H15_e$ ($\Delta\delta$ = 0.03 ppm), $H16_e$ ($\Delta\delta$ = -0.04 ppm), and H17 ($\Delta\delta$ = 0.02 ppm) (see Fig. 2-3B); these protons are in the vicinity of OH-7 and OH-12. The greatest change in $\delta$ for $H6_a$ and could be attributed to its proximity to OH-7 and the $COO^-$ group in the neighboring monomer. Hydrophilic proton $H16_e$ also had a considerable decrease in chemical shift. It is possible that the NaCho tail in the primary micelle may place the $COO^-$ group closer to $16_e$ causing a more polar surrounding when compared to the monomer.

Protons $11_e$, 14, $15_e$ and 17 are not expected to be in the vicinity of $COO^-$ groups in the monomer or primary micelles. However, it is possible that a network of hydrogen bonding involving these hydroxyl groups (OH-7 and OH-12) with surrounding water molecules may be formed. This hydrogen-bond belt network could affect the orientation of the hydroxyl groups so that a set of lone pairs on both OH-7 and OH-12 become closer to neighboring protons. This in turn could create a more polar environment surrounding these protons.

Interestingly, some protons on the hydrophilic face of the monomer sensed a less polar environment upon micellization. These exceptions to the expected trend include protons H2a, H4a, and H9a (see Fig. 2-3C) for which an increase in chemical shift was observed. Based on the theoretical predictions, this trend indicates that these protons enter into a less polar environment as primary micelles are formed. Protons $H2_a$ and $H4_a$ are in the vicinity of the OH-3 group. If the monomers are oriented in a head-to-tail

arrangement, primary micelles could be stabilized through ion-dipole and hydrogen bonding interactions around the top and bottom of the micelle. The interactions between OH-3 and neighboring $COO^-$ groups could diminish the deshielding effect of the lone pairs in OH-3 on neighboring protons and lead to the shielding of protons $2_a$ and $4_a$. Proton H9, located in the vicinity of OH-7 and OH-12, increases its chemical shift (see Fig. 2-3C). In the monomer, this proton is proposed to be more deshielded by the lone electron pairs OH-7 and OH-12 due to a change in the orientation of hydroxyl groups as they form a hydrogen-bond belt network. This may cause the delocalization of electron density around this network resulting in a decrease of polarity around H9.

**Proposed Primary Micelle Model**

From the analysis of the experimental $^1H$ NMR data with the aid of chemical shift predictions, the model presented in Figure 2-4 is proposed. The first model (Fig. 2-4a) represents four monomers associating to form a primary micelle where monomers are arranged in an anti-parallel arrangement. Hydroxyl groups around the central hydrogen-bond belt network (OH-7 and OH-12) are highlighted with red circles. The network of hydrogen bonds is shown as a red line connecting hydroxyl groups. In this model the top and bottom of the 'barrel' micelle is held together by water-mediated hydrogen bonds between the hydroxyl (OH-3) and carboxylate groups (water molecules are not shown). Figure 2-4b shows a simpler model demonstrating the anti-parallel arrangement, hydroxyl and carboxylate groups are shown to be involved in hydrogen-bonding. Figure 2-4c shows an illustration of the barrel-shaped model proposed for NaCho primary micelles.

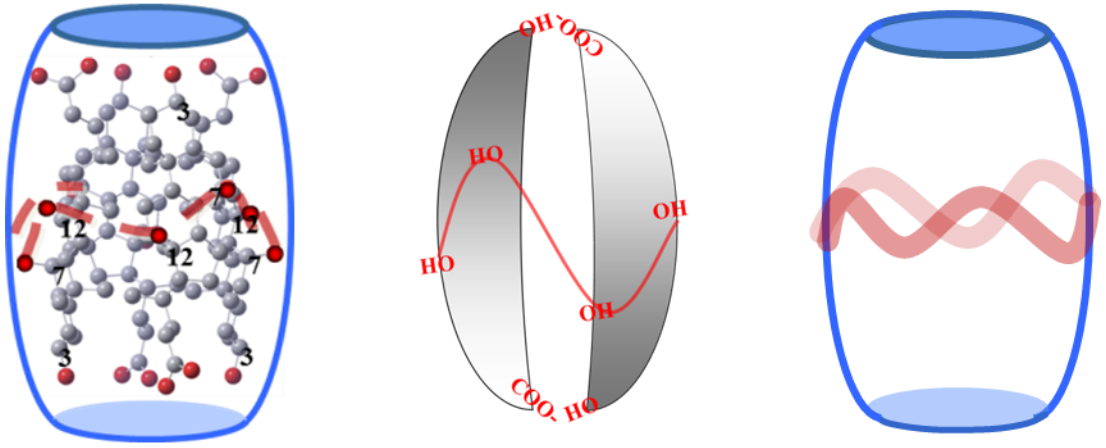


a b c

**Figure 2-4:** a) Proposed 'barrel' model for NaCho primary micelles. Four monomers associate in an anti-parallel arrangement forming a hydrophobic core. A central hydrogen-bond 'belt' (shown in red) involving OH-7 and OH-12 surrounds the barrel. b) Simplified model showing the anti-parallel arrangement. c) Cartoon representation of the barrel-shaped model.

**Confirmation of Anti-Parallel Arrangement by Two-dimensional NMR studies**

ROESY or NOESY experiments ($^1H$ –$^1H$ correlation data) can be used to probe internuclear distances of less than 5 Å. Figure 2-5 shows ROESY spectra obtained for NaCho at two concentrations, 2 mM and 30 mM, respectively. At 2 mM, cross peaks are observed between the resonances corresponding to H23 and H23' with H21 (methyl protons) as well as the resonances due to the H19 (methyl protons) and H6a. These cross peaks are expected due to the spatial proximity of these protons in the monomer. At 30 mM, four new off-diagonal peaks were observed in this region (see dotted lines). One of the new peaks connects H6a (second steroidal ring) with H21 (methyl protons); such a contact would not be possible in the monomer. The other cross peaks indicate that H19 (methyl protons) are within 5 Å of H23, H23' and H9 (Figure 2-5B). The presence of these new correlations confirms that monomers orient in an anti-parallel arrangement. Figure 2-5 shows NaCho monomers in anti-parallel arrangement and the new contacts observed at 30 mM NaCho are shown with grey arrows.

Therefore, the carboxylate group of one monomer is in close proximity to the hydroxyl (OH-3) group of its neighboring monomer. This arrangement also places the carboxylate groups in opposite sides, thus reducing electrostatic repulsion. Other new off-diagonal peaks that were observed in 30 mM NaCho include H19-H15$_e$, H19-H15$_a$, H21-H2$_a$, H21-H11$_{a,e}$, H22-H5. These new contacts also validate the anti-parallel arrangement. The volume of the off-diagonal peaks were determined by integration and used to qualitatively examine the changes in the relative distance between protons as the concentration of NaCho was increased. The volume of the off-diagonal peak for geminal protons H16$_a$-H16$_e$ was referenced to 100.00 in 2, 20 and 30 mM and the integrations for other correlations are shown in Table 2-2. The integrations observed in 2 mM for protons

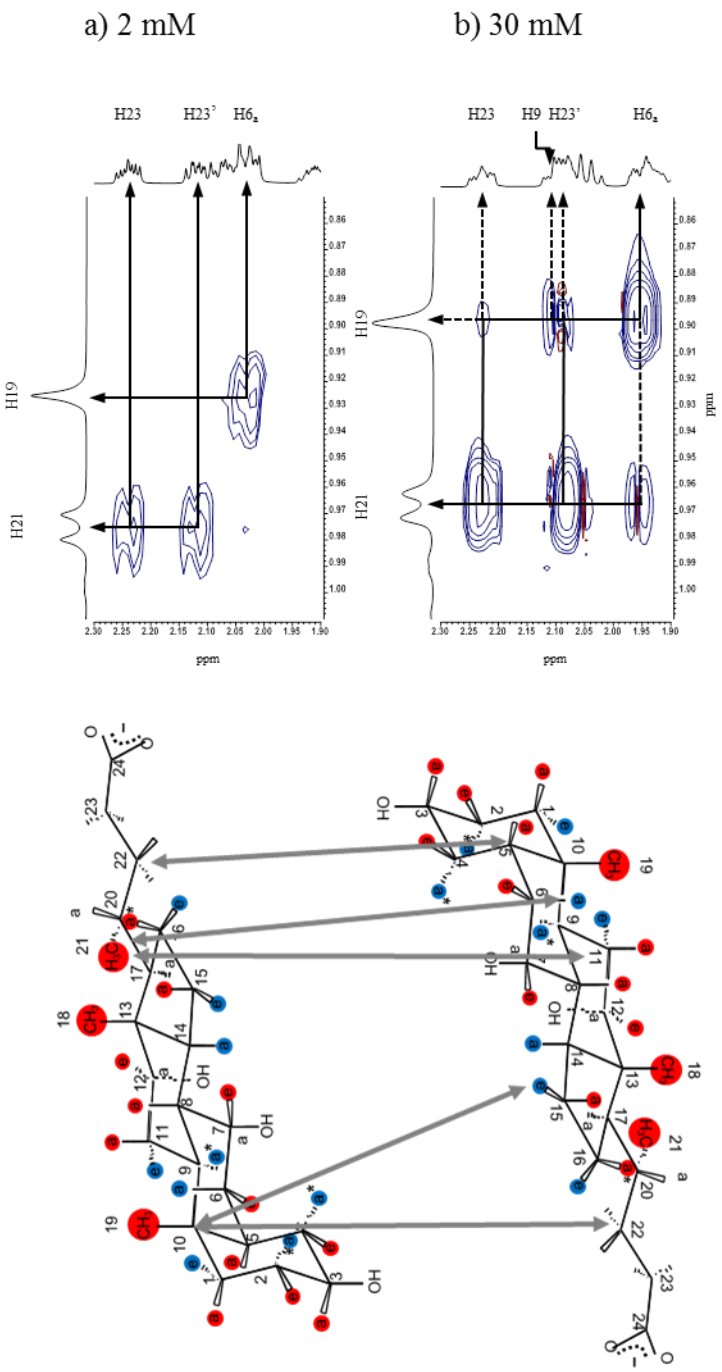


**Figure 2-5:** ROESY spectra obtained for a) 2 mM and b) 30 mM. New contacts observed for primary micelles are shown with dashed arrows. Below ROESY spectra is a schematic diagram of new contacts observed in 30 mM ROESY spectrum. NaCho monomers arranged in an anti-parallel fashion. New contacts are shown in grey.

| Cross Peak Volumes | 2 mM | 20 mM | 30 mM |
|---|---|---|---|
| H1a - H1e | 124.41 | 100.9 | 89.5 |
| H1e - H2a | 17.25 | 9.25 | 6.9 |
| H1a - H3 | 12.17 | 11.43 | 13.34 |
| H2a - H21 | | | 0.8 |
| H3 - H5 | 13.01 | 11.23 | 12.54 |
| H3 - H18 | | 0.36 | 0.23 |
| H4a - H4e | 128.05 | 100 | 107.05 |
| H5 - H19 | 10.6 | 12.7 | 14.5 |
| H5 - H22' | | | 1.23 |
| H6a - H6e | 123.65 | 95.02 | 90.15 |
| H6a - H7 | 25.86 | 13.06 | 12.02 |
| H6a - H19 | 18.21 | 11.48 | 11.73 |
| H9a - H14 | 15.97 | 11.8 | 19.53 |
| H11a,e - H19 | 48.17 | 38.36 | 40.7 |
| H11a,e - H21 | | | 1.72 |
| H12 - H18 | 12.23 | 6.38 | 8.19 |
| H15a - H15e | 76.09 | 88.5 | 102.8 |
| H15a - H16e | 21.15 | 13.6 | 3.4 |
| H15a - H19 | | | 2.5 |
| H15e - H19 | | | 0.95 |
| H15a - H23 | | 0.43 | |
| H15e - H23' | 6.32 | 6.07 | 9.18 |
| **H16a - H16e** | **100 (ref)** | **100 (ref)** | **100 (ref)** |
| H16e - H22' | 16.17 | | |
| H19 - H23 | | 1.61 | 0.26 |
| H19 - H23' | | 0.69 | 0.33 |
| H21 - H23’ | 7.71 | 4.55 | 8.05 |
| H22’ - H23’ | 9.18 | 10.16 | 8.6 |
| H23 - H23' | 41.94 | 39.8 | 59.54 |

**Table 2-2**: Cross peak volumes observed in ROESY spectra for 2, 10, 20 and 30 mM NaCho.

within 5 Å of each other on the monomer decreased as primary micelles were formed. With a few exceptions, the volume of most of the cross peaks diminished or did not change significantly as micelles formed. This trend is expected as some of the protons on the NaCho monomer come in closer proximity to protons in neighboring monomers and their magnetization is transferred to other protons. For example, cross peaks involving H19 that were present in both the monomer and primary micelles ($H6_a$ and $H11_{a,e}$) decreased in volume as new contacts were observed at 20 and 30 mM.

## CONCLUSIONS

This study demonstrates the remarkable enhancement in sensitivity and spectral resolution achieved by the new 700 MHz NMR spectrometer equipped with the cryogenic probe. Because of this significant improvement, we were able to monitor changes in each and every resonance corresponding to protons in NaCho monomers and micelles. In the previous studies by our group on these micelles, only those resonances that were well resolved could be followed with certainty. Our interpretation was greatly facilitated by the theoretical predictions that take into account the presence of paramagnetic fields generated by lone electron pairs. This analysis indicated the plausibility of the proposed barrel-like model that places the monomers (four or six) in an antiparallel arrangement so that the 'head' and 'tail' of neighboring monomers interact to form the top and bottom of the barrel. In addition, a H-bond belt that includes OH-7 and OH-12 was proposed to surround the middle region of the micelle. This model was confirmed by the new through-space interactions revealed by ROESY experiments as the monomers associated to form primary micelles. This validated model supports previous models proposed in our group as well as the disklike model proposed by Kawamura *et al*.

Finally, it is clear that while hydrophobic forces play a significant role in the micellization of NaCho, H-bonding interactions do have just as significant of a contribution to this process.

# CHAPTER 3

# NMR CHARACTERIZATION OF SECONDARY MICELLES OF SODIUM CHOLATE

## INTRODUCTION

Bile salts are amphipathic compounds derived from cholesterol.[63] Bile salts are a major component in bile and aid in the adsorption and digestion of lipids.[64] Bile salts have a different structure from classical surfactants; they are facial amphiphiles due to their rigid steroid backbone and the presence of methyl groups on the hydrophobic face and hydroxyl groups on the opposite face.[65, 66] Above the critical micelle concentration (*cmc*) for bile salts, monomer associate to form primary micelles. Sodium cholate (NaCho) has a *cmc* value around 16 mM and between 4-6 monomers associate to form micelles (aggregation number).[25] Above 50 mM, a second micellization takes place where primary micelles aggregate to form secondary ones.[10]

As discussed in the previous chapter of this dissertation, several models have been proposed on the molecular structure of bile salt primary micelles.[10, 33] Our own work validates the anti-parallel arrangement of four (or six) monomers in a barrel-like micelle. Although bile salt primary micelle formation, size and shape have been extensively studied, there is less information of the formation and structure of secondary micelles. Previous studies in our laboratory using a 500 MHz NMR spectrometer led to the postulation of a model for secondary micelles in which the barrel-like primary micelles stack on top of each other. Because of the broadening of the NMR resonances upon association of the primary micelles, it was not possible to follow all the changes in the 25

resonances in the complex region of the spectrum (see Chapter 1, NMR Studies of Bile Salts). This chapter revisits the characterization of secondary micelles with a 700 MHz NMR instrument that provides high spectral resolution. The previously proposed model is refined and its accuracy is tested.

## MATERIALS AND METHODS

**Chemicals.** $D_2O$, NaOD, NaCho and DSS (4,4-dimethyl-4-silapentane-1-sulfonate, Na salt) were purchased from Sigma-Aldrich Chemical Co, St. Louis, MO.

**Preparation of NaC micelles.** The concentrations used were 20, 30, 50, 100 and 200 mM in $D_2O$. The solutions were sonicated in a bath sonicator (Cole- Parmer 8890) for about 15 minutes and the pH was adjusted with NaOD at physiological pH (7.4).

**Spectral Acquisition.** $^{1}H$ and $^{13}C$ and 2D-NMR spectra were acquired with a Varian INOVA 500 and 700 MHz NMR spectrometers, Palo Alto, CA. The following acquisition parameters were used for 1H: a minimum of 16 scans, relaxation delay of 1.000 second, 45º pulse width, and 25 ºC. For gHSQC spectra, 4 scans per increment and 128 increments were used. For ROESY experiments, the relaxation delay was 1.000 sec, the mixing time was 300 ms, 8 scans were acquired per FID and 256 increments, the spectral width extended from -1 to 9.5 ppm.

**Data Analysis.** All spectra were analyzed using MestReC software, version 4.7.0 or the newer MestReNova, version 7.1.2 (Santiago de Compostela, Spain). A coaxial insert containing 1.0 mM 4,4-dimethyl-4-silapentane-1-sulfonate, sodium salt (DSS) dissolved in $D_2O$ was inserted in the NMR tube and used for signal locking and referencing of NMR spectra.

## RESULTS AND DISCUSSION

### 1D NMR analysis and results

Previous studies on NaCho primary micelles (see Chapter 2) resulted in the proper assignments of all $^{1}H$ resonances in NaCho at lower concentrations (20 and 30 mM). For the current study HSQC experiments were performed to track the chemical shifts for all NaCho resonances as the concentration increased (50 mM, 100 mM and 200 mM) (data not shown). Figure 3-1 shows the labeled NaCho monomer protons, the hydrophilic protons are highlighted in blue and hydrophobic protons in red. Because the tail of the monomer is flexible and can adopt many orientations, the tail protons were not differentiated as being hydrophilic or hydrophobic. Figure 3-1 also shows $^{1}H$ NMR spectra collected for 30, 50 and 100 mM NaCho for the complex spectral region (1.00 – 2.30 ppm). As the concentration increased and primary micelles began to aggregate into secondary micelles (at ~ 50 mM), changes in chemical shift and significant line broadening were observed. As seen by the changes in chemical shifts shown with arrows, some protons became deshielded while other became shielded during the secondary micellization step. To aid in the interpretation of the changes in chemical shift, these trends were compared to theoretical calculations performed using the polarizable continuum medium (PCM) in which the NaCho monomer was placed in media of different dielectric constants, chloroform ($\varepsilon = 4.9$), methanol ($\varepsilon = 32.63$) and water ($\varepsilon = 78.39$). The results of these predictions are included in Chapter 2. As discussed in Chapter 2, most protons become more deshielded (higher $\delta$) as the polarity of the solvent increases. However, a few protons follow the opposite trend due to the presence of

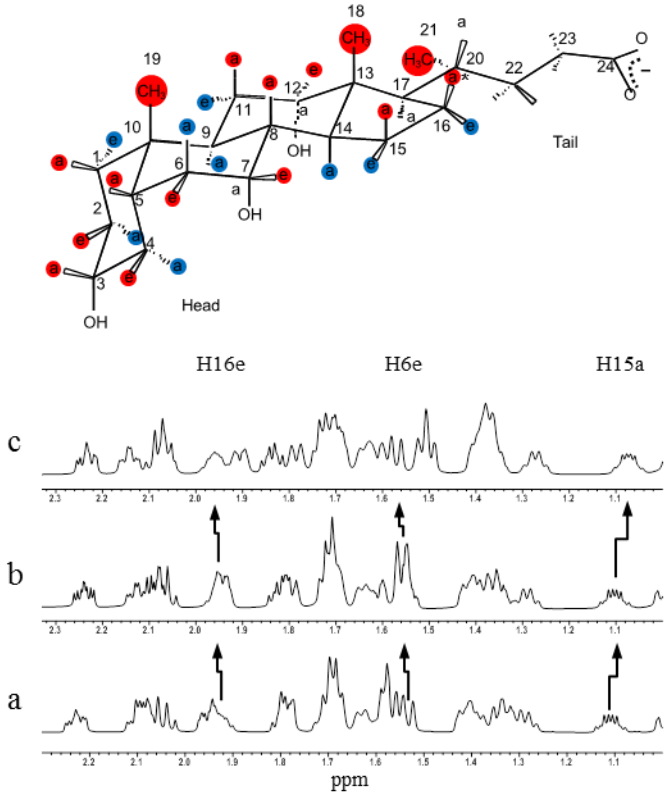


**Figure 3-1:** Labeled NaCho monomer and $^{1}$H NMR spectral collected for 30, 50 and 100 mM NaCho. Protons on the hydrophilic and hydrophobic face are shown in blue and red respectively. $^{1}$H NMR spectra collected for a) 30 mM, b) 50 mM and c) 100 mM NaCho showing the complex spectral region between 1.00 and 2.30 ppm. Concentration-dependent changes in chemical shift are highlighted for H16e, H6e and H15a with black arrows.

oxygen lone pairs in their vicinity. In the non-polar solvent (chloroform) these lone pairs deshield the neighbor protons whereas in water, they interact with the solvent and their deshielding effect is reduced. These trends were used in the studies presented in Chapter 2 and in this chapter for the analysis of experimental results.

**Interpretation of Experimental Trends**

We have calculated the difference between chemical shifts for each proton at different concentrations with respect to those at 20 mM to extract trends that could aid us to understand the organization of NaCho secondary micelles at the molecular level (Figures 3-2 and 3-3).

**Hydrophobic Face**

As primary micelles aggregate to form secondary ones, one would not expect any changes to occur in the hydrophobic core. Therefore, the protons in the hydrophobic core are not expected to change in chemical shift /molecular environment. However, changes in chemical shift were observed for the methyl groups (H18 and H19), H7, H8, $H11_a$, H12 and $H15_a$. The protons in the methyl groups (H18 and H19) as well as H8 are located in the central core of the micelles. H7 and H12 are protons attached to carbons with adjacent hydroxyl groups; these protons are orientated toward the core of the micelle. Similarly, $H11_a$ and $H15_a$ are located at the interface between the hydrophobic/hydrophilic faces. Compared to the theoretical trends all of these protons sense a more hydrophobic environment as secondary micelles are formed. The changes in chemical shift for these protons are shown in Figure 3-2A. In addition, protons on the first ring that are also on the hydrophobic face of the NaCho monomer include: $H1_a$, $H2_e$, H3, $H4_e$ and $5_a$. Protons H3 and $H5_a$ are located in the core of the micelle and H1a, $H2_e$ and $H4_e$ are oriented toward the core of the micelle. As secondary micelles are formed,

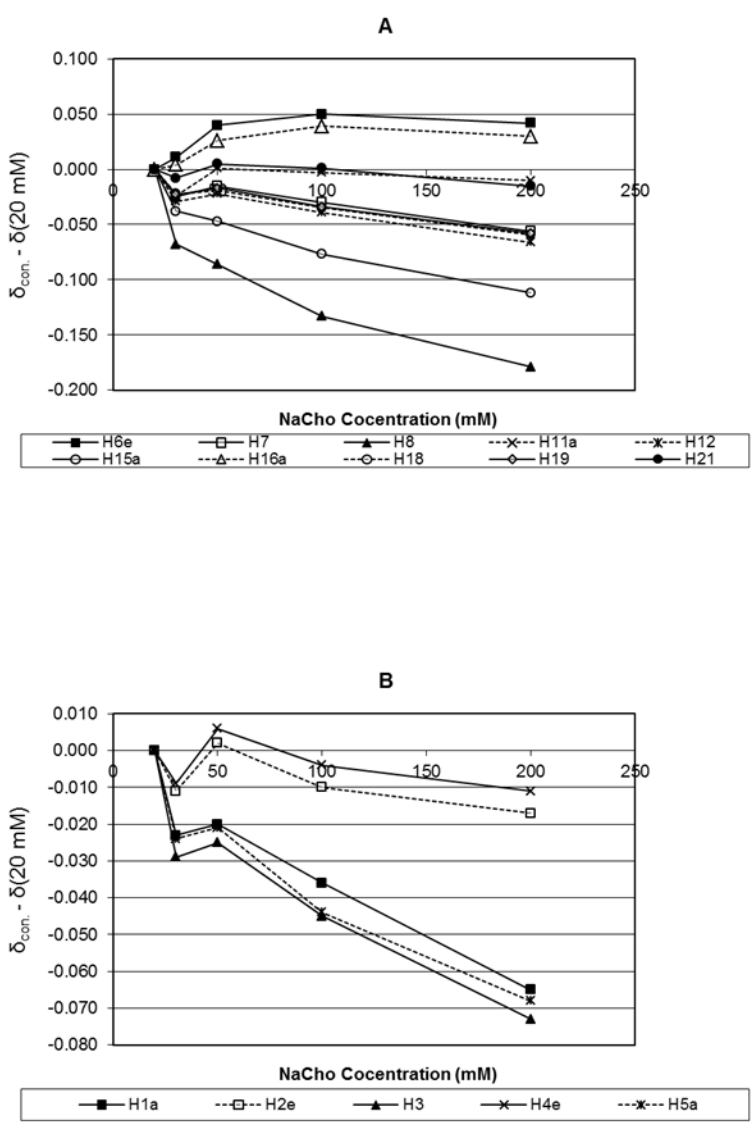


**Figure 3-2: C**hanges in chemical shift for protons on the hydrophobic face. Changes in chemical shifts observed for NaCho as primary micelles (20 mM) aggregate to form second micelles. Graphs A and B show the changes for protons located on the hydrophobic face of NaCho.

these protons also sense a more hydrophobic environment. The changes in chemical shift for these protons are shown in Figure 3-2B. These trends suggest that the primary micelles become more tightened and as a result, their cores are more hydrophobic as the second micellization occurs. It is also proposed that the aggregation of primary micelles enables the extension of the hydrogen-bond belts surrounding each primary micelle so that they become longer and tighter belts that hold together the secondary micelles. In addition, the tightening of the micelles would cause $H2_e$, $H4_e$, H7, $H11_a$, H12, and $H15_a$ to be positioned more toward the core of the micelle and away from the aqueous solvent.

The only exception on the hydrophobic face that sensed a more polar environment was H16a. This proton is located at the interface between the hydrophobic and hydrophilic face. As the secondary micellization takes place and the hydrophobic core becomes more compact, this proton may be pushed away slightly from the core and experience a less hydrophobic environment.

**Hydrophilic Face**

Depending on the 3D molecular arrangement of secondary micelles, the tops/bottoms ($COO^-$ and OH-3 groups) of the primary micelles within the secondary micelle structure should be in closer proximity to protons on neighboring primary micelles. This could cause a more polar environment in the vicinity of some of the protons on the hydrophilic face. Notable changes in chemical shift were observed for protons H14, $H15_e$, $H16_e$ and H17 (Figure 3-3A) that are located around the central hydrogen-bond belt. As the concentration of NaCho increased above 50 mM, these protons sensed a more polar environment. To explain this trend, these protons have to be in the vicinity of a polar moiety, more polar than water. They are likely to be near the

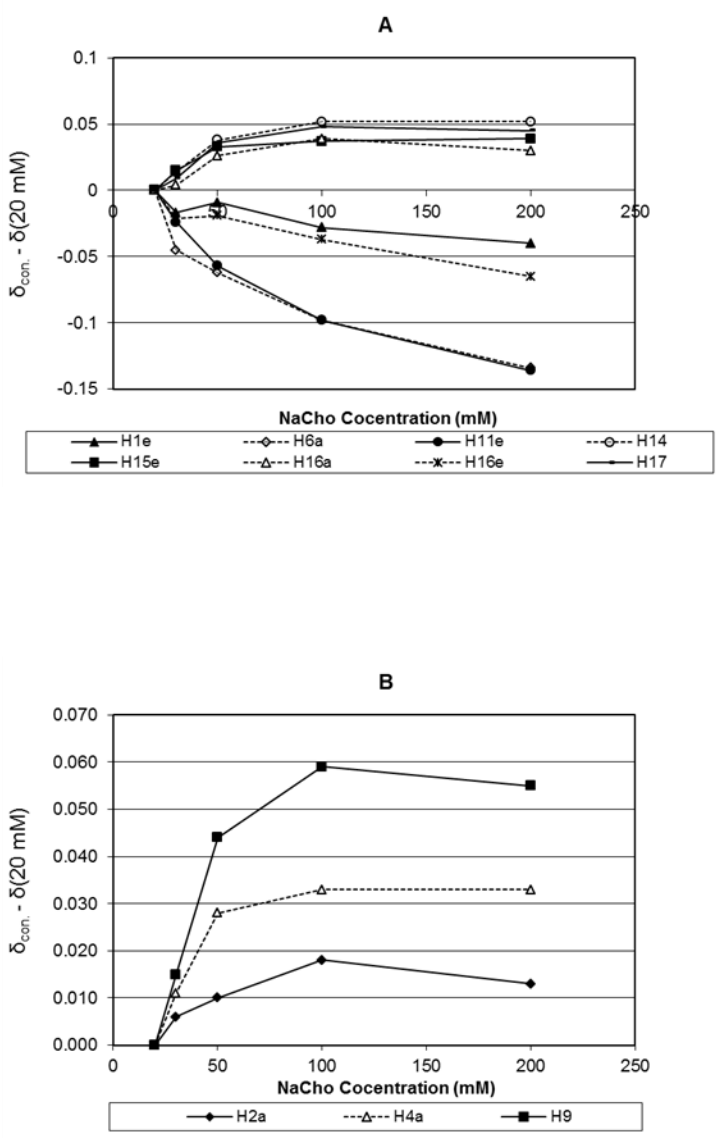


**Figure 3-3:** Changes in chemical shift for protons on the hydrophilic face. Graphs A and B show changes in chemical shifts for protons located on the hydrophilic face of NaCho.

$COO^-$ or OH groups of the neighboring primary micelles. Therefore, as aggregation occurs, the tops/bottoms of primary micelles are proposed to be in the vicinity of the central hydrogen-bond belt of its neighboring primary micelle. However, another possible arrangement of primary micelles within the secondary ones could place the central hydrogen-bond belt of one micelle next to its neighbor's central region. Because these protons are already in the proximity to hydroxyl groups within their own primary micelle, being near additional hydroxyl groups may not lead to the increasing changes in chemical shifts observed; therefore, this arrangement is less likely.

The only proton around the hydrogen bond belt that showed a trend opposite (sensed a more hydrophobic environment) to the others mentioned above was H9a (see Figure 3-3A). It is possible that the hydrogen bond belt in primary micelles interacts with the belts of neighboring micelles creating an extended hydrogen bond network. The formation of this extended hydrogen bond network could change the orientation of the hydroxyl lone pairs thus decreasing their deshielding effect on H9a. This would create a less polar environment around H9a.

Protons on the first ring (hydrophilic face) of the NaCho monomer include $H1_e$, $H2_a$, and $H4_a$. $H1_e$ sensed a more hydrophilic environment as secondary micelles formed. $H1_e$ would be closest in proximity to the top/bottom of the neighboring micelles. On the other hand, $H2_a$ and $H4_a$ sensed a more hydrophobic environment as secondary micelles formed. This may be due to the hydroxyl groups at position 7 and 12 interacting and creating an extended hydrogen bond belt network with the top/bottoms of neighboring primary micelles. This interaction may diminish the deshielding effect of the electron lone pairs of the hydroxyl groups and cause these protons to sense a more hydrophobic environment.

**Proposed Secondary Micelle Model**

As the concentration of NaCho increases beyond 50 mM, primary micelles begin to aggregate and form secondary ones. It is proposed that primary micelles stack together in two ways. First, the tops and bottoms of primary micelles stack together to form columns, these are held together by ion dipole and water mediated interactions. Secondly, it is also proposed primary micelles stack together in a staggered-stacked arrangement where the top/bottom of one primary micelle is in the vicinity of the central hydrogen-bond 'belt' of the neighboring micelle (see Figure 3-4).

**Confirmation of the Proposed Micellar Arrangement by Two-dimensional NMR studies**

2D-NMR experiments such as $^{1}H$-$^{1}H$ ROESY or NOESY can be used to determine which protons are within 5 Å of each other. Under these conditions, magnetization is transferred through space and cross peaks are observed connecting the resonances corresponding to these protons. ROESY spectra were collected for 30 mM (primary micelles), 50 mM (primary and secondary micelles are present), 100 and 200 mM (secondary micelles only). These spectra were compared to reveal possible new cross peaks as secondary micelles formed. These new peaks include contacts between $H9_a$-H21 (see Fig. 3-5), $H9_a$-H23', $H11_e$-H21, H9-$H2_a$, H21-$H15_e$, $H11_e$-$H6_a$, H12-$H15_a$ and $H16_a$-$H4_e$. However, there is significant spectral overlap at 100 mM NaCho and assignments were more difficult. For example, a new cross peak was observed with $H16_a$ and was correlated to a resonance where $H4_e$ and H22 overlapped. To determine if $H16_a$ was correlated to $H4_e$ or H22, other known off-diagonal peaks correlating to H4e or H22 were examined. The cross peak between $H4_e$ and $H4_a$ (which is observed at all NaCho concentrations) aligned with the cross peak connecting $H4_e$ and $H16_a$. Therefore, the new

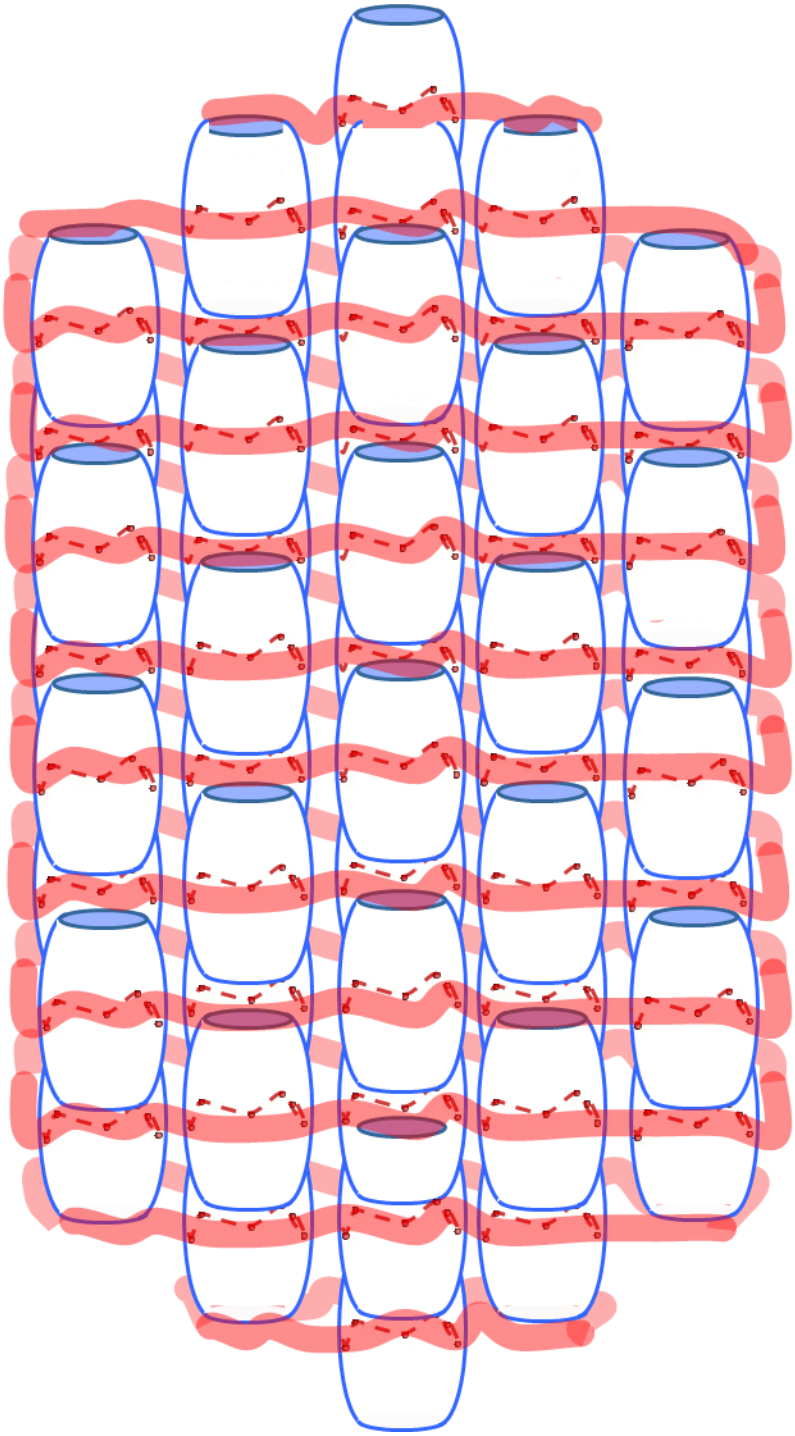

**Figure 3-4:** Proposed model for NaCho secondary micelles. Primary micelles stack together in a staggered-stacked arrangement and held together by ion dipole and water mediated interactions. The extended hydrogen-bond 'belt' is shown in red.

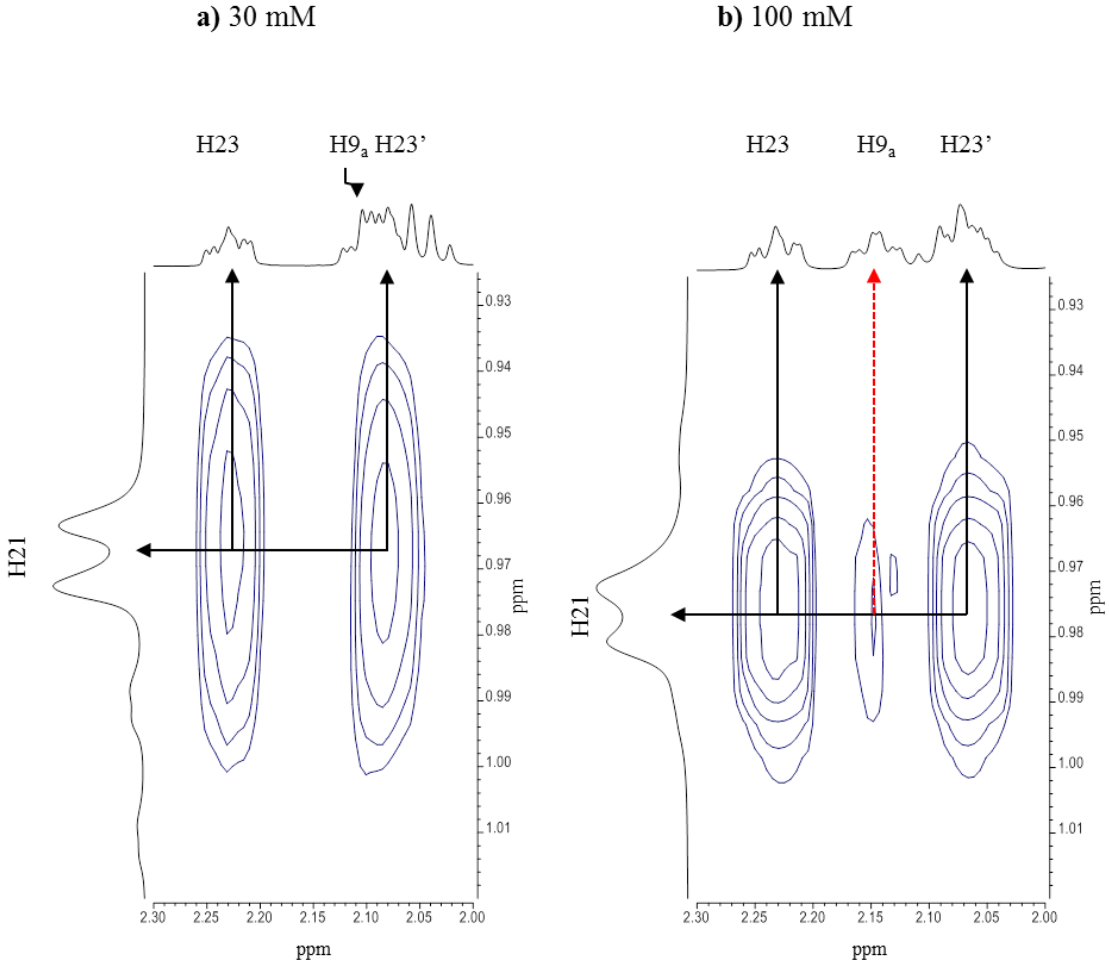


**Figure 3-5**: ROESY spectra collected for a) 30 and b) 100 mM NaCho. New cross peaks present in secondary micelles are shown with red dotted arrows.

contact was assigned to H4e and H16a. Assignments were made using this method in other cases where there was significant spectral overlap. Contacts that support the staggered-stacked arrangement include the new contacts mentioned above with the exception of H12-H15$_{a,}$ H4-H23' and H16$_{a}$-H4$_{e}$. These contacts are possible in the primary micelle model as described in Chapter 2. However, they were not observed in ROESY spectra at 30 mM NaCho. This indicates that these protons must be further than 5 Å away from each other in primary micelles. However, the trends for changes in chemical shift for protons on the hydrophobic face indicated the tightening of primary micelles in the secondary micelle arrangement. This observation is supported by the presence of these new contacts placing them closer together in secondary micelle concentrations (100 mM).

## CONCLUSIONS

A more detailed model has been proposed and partially tested for the arrangement of primary micelles within secondary ones. As discussed in Chapter 2, both hydrophobic interactions and H-bonding play equally important roles in the formation of primary micelles. However, the main force in the formation of secondary micelles is attributed to H-bonding and the increase in the strength of these interactions as the H-bond belts that surround individual primary micelle interact with neighboring ones and become elongated and surround the larger aggregate (see Fig. 3-4). As this elongation takes place, increase in cooperativity leads to tighter belts that make the core of the individual primary micelles even more hydrophobic.

Although the new through-space interactions support the staggered packing of linear stacks of NaCho primary micelles, further studies are needed to validate the proposed model.

# CHAPTER 4

# NMR STUDY OF THE IMPACT OF SALT CONCENTRATION, CATION SIZE AND CHARGE ON SODIUM CHOLATE PRIMARY MICELLES

## INTRODUCTION

In the previous chapters of this dissertation, the molecular arrangements of primary and secondary micelles of sodium cholate (NaCho) were explored at physiological pH and in the absence of additional salts. In this chapter, the impact of mono- and divalent cations is investigated at neutral and basic pH.

The formation of micelles of any surfactant is affected by ionic strength, temperature, and pH.[25] For bile salt micelles and with the use of noninvasive methods such as potentiometry[25], derivative spectrophotometry[46] and light scattering[28, 67], Reiss and co-workers determined *cmc* values for bile salts at various ionic strengths.[25] The results obtained with each method were compared to previously published values and showed that different methodologies may lead to different *cmc* values. Furthermore, the comparison was difficult because parameters such as pH, ionic strength, and temperature had not been specified in some previous reports. Using potentiometry, the results for sodium cholate showed the *cmc* decreased from 7.3 to 6.85 mM as the NaCl concentration increased from 0.10 to 0.20 M. Similarly, for sodium glycocholate the *cmc* decreased from 9.44 to 5.91 mM as the concentration of NaCl increased.[25] This is attributed to the reduction of the screening effect that the anionic carboxylate groups provide.

The impact of temperature on *cmc* for NaCho was investigated by Garidel *et al*. with the use of isothermal titration calorimetry.[29] The *cmc* values reported by the researchers for NaCho in 0.1 M NaCl, showed a slight decrease (from 12.5 to 10 mM) as the temperature increased from ~11 C to 26 ºC. At higher temperatures, the *cmc* increased and reached 15.5 mM at ~ 70 ºC.[29]

Regarding the impact of salt concentration on *cmc*, review of the literature shows that as the concentration of NaCl is increased from 0.001 to 0.5 M, the *cmc* decreased from 7.6 to 2.1 mM at pH 7.0 and from 8.3 to 2.6 mM at pH 9.[25, 68] This effect can be explained by the reduction of electrostatic repulsions at higher ionic strength. As a result, the micellization takes place at lower concentrations.[69]

Salt concentration also affects the aggregation number *n*. For example, light scattering studies of NaCho at pH ~ 6.8, showed *n* to change from 6 to 8 as the concentration of NaCl was increased from 0.5 to 1 M. Using ultracentrifugation, the values for *n* were evaluated for NaCho at pH of ~ 9 and shown to increase from 4 to 6 as the concentration of NaCl was varied from 0.05 to 0.3 M.[10]

Although the previous studies do show the impact of salt concentration and pH, they do not reveal the conformational/structural changes that take place at the molecular level. This chapter focuses on the exploration of the impact of both pH and salts of mono- and divalent of various sizes. Both salt concentration and pH have been increased beyond physiological conditions to gain insight on the possibility of manipulating these parameters for future studies to enhance drug uptake and release by NaCho micelles.

This study follows the model presented in Chapter 2 in which four (or six) NaCho monomers associate in an anti-parallel arrangement and form a barrel-shaped micelle. In this model, a cooperative hydrogen-bond ‘belt’ is formed with the hydroxyl groups on C7

and C12. This water-mediated belt surrounds the outer central region of the micelle. In addition, the top and bottom of the 'barrel' are held by water-mediated hydrogen bonds between the carboxylate ions and the OH groups at C3.

With the use of one- and two-dimensional NMR spectroscopy, the impact of the concentration of NaCl, $NH_4Cl$, $MgCl_2$ and $CaCl_2$ on the compactness and arrangement of NaCho primary micelles is investigated at physiological pH and at pH 9.1. Lower pH values were not tested because the pKa of NaCho is between 4.6 and 5.5 and the protonation of the carboxylate group leads to the precipitation of the micelles at pH values of 6.5 or lower.[54]

## MATERIALS AND METHODS

**Chemicals.** Sodium Cholate (NaCho) and $NH_4Cl$ were obtained from Sigma-Aldrich (St. Louis, MO). Reagent grade NaCl was obtained from EMD Chemicals, Inc. (Gibbstown, NJ). $MgCl_2$ and DSS (4,4-dimethyl-4-silapentane-1-sulfonate, Na salt) were purchased from Aldrich Chemical Co., Inc. (Milwaukee, WI). NANOpure water (Barnstead, resistivity of $18M\Omega cm^{-1}$) was used for all aqueous solutions.

**Sample preparation.** The appropriate amount of NaCho was weighed and placed in a 20-mL vial. Nanopure water was added to attain a final concentration of 200 mM in $H_2O$. This stock solution was used to prepare 20 mM NaCho solutions with various salt concentrations. Aqueous solutions (1.0 M) of NaCl, $NH_4Cl$, $MgCl_2$, and $CaCl_2$ were prepared. The correct amount of these salt solutions was pippetted to create 20 mM NaCho solutions with final salt concentrations of 0.15, 0.30, 0.45, or 0.60 M. The solutions were sonicated in a bath sonicator (Cole-Parmer 8890) for about 15 minutes. The pH was adjusted using 0.1 M and 0.05 M NaOH or HCl to achieve final pH values of

7.4 ± 0.1 and 9.1 ± 0.1. Less than 10 μL were needed to adjust the pH. Therefore, the contribution of $Na^+$ from the pH adjustment did not alter significantly the final salt concentration.

**One-dimensional NMR studies.** NMR experiments were performed on a Varian Inova 500 MHz spectrometer (Palo Alto, CA) equipped with a triple resonance probe. The frequency used for $^1H$ was 500.1 with a total number of 128 scans. All one-dimensional spectra were processed using MestReC Version 2.01 (Santiago de Compostela, Spain) on a personal computer. All acquisitions were carried out at 25ºC. A coaxial insert containing 1.0 mM 4,4-dimethyl-4-silapentane-1-sulfonate, sodium salt (DSS) dissolved in $D_2O$ was inserted in the NMR tube and used for signal locking and referencing of NMR spectra.

## RESULTS AND DISCUSSION

This study explores the impact of salt concentration and pH on the formation of primary micelles of sodium cholate (NaCho). With the use of NMR spectroscopy, we have investigated the effects of cation size and charge on primary micelles. The observed trends at each pH will be presented first. Then, with the aid of the theoretical predictions discussed in Chapter 2, these experimental trends are interpreted and models are proposed to account for the effects of increasing salt concentration as well as cation size and charge on the arrangement of primary micelles.

**Effect of the addition of NaCl, $NH_4Cl$, $MgCl_2$ and $CaCl_2$ to NaCho primary micelles at pH 7.4.** Figure 4-1 shows the NaCho molecule with the labeling scheme and the spectra acquired for a solution of 20 mM NaCho only (trace a) and those containing 0.6 M of $NH_4Cl$ (trace b), NaCl (trace c), and $MgCl_2$ (trace d). No trace is included for

0.6 M $CaCl_2$ because significant precipitation took place at this concentration and at 0.45 M. The spectra are arranged by decreasing ionic diameter and increasing charge; with $NH_4^+$, $Na^+$, $Mg^{2+}$ having ionic diameters of 296 pm, 204 pm, and 144 pm, respectively.[14] The proton labels correspond to the number of the carbon to which they are attached. Axial and equatorial protons are designated with the letters *a* or *e*, respectively. The resonances labeled in the spectra correspond to the three methyl groups H18, H19, and H21, as well as those related to H3, H7, and H12, the protons attached to carbons with a bound hydroxyl group. These resonances can be easily assigned as they are well resolved. In general, Fig. 4-1 shows that the addition of these salts caused the shielding of the chosen protons. Relative to trace a, the most significant changes in both chemical shift and broadening are observed in trace d ($MgCl_2$). Conversely, the presence of $NH_4Cl$ led to relatively minor decreases in chemical shift and did not cause broadening.

*Changes in chemical shifts.* The changes induced by the addition of salts were evaluated. Figure 4-2 shows the net changes in chemical shifts with respect to NaCho only (no additional salts) at pH 7.4. The chemical shift values for all of the resonances examined in this study were obtained by $^1H$ NMR one-dimensional spectral data. Graphs A, B, C, and D correspond to the results obtained upon addition of increasing concentrations of $NH_4Cl$, NaCl, $CaCl_2$ and $MgCl_2$, respectively. In these graphs, the errors in the measurements are represented by the size of the symbol. Overall, the chemical shifts of the chosen resonances decreased (became more shielded) as the salt concentration increased. H21 followed this trend but the degree of change in chemical shift was lower relative to those for the other resonances. This trend was observed with three salts ($NH_4Cl$, NaCl, $MgCl_2$) but not in the presence of $CaCl_2$, graph C. The presence of $NH_4Cl$ led to the smallest changes in chemical shift, followed by NaCl, $CaCl_2$ and

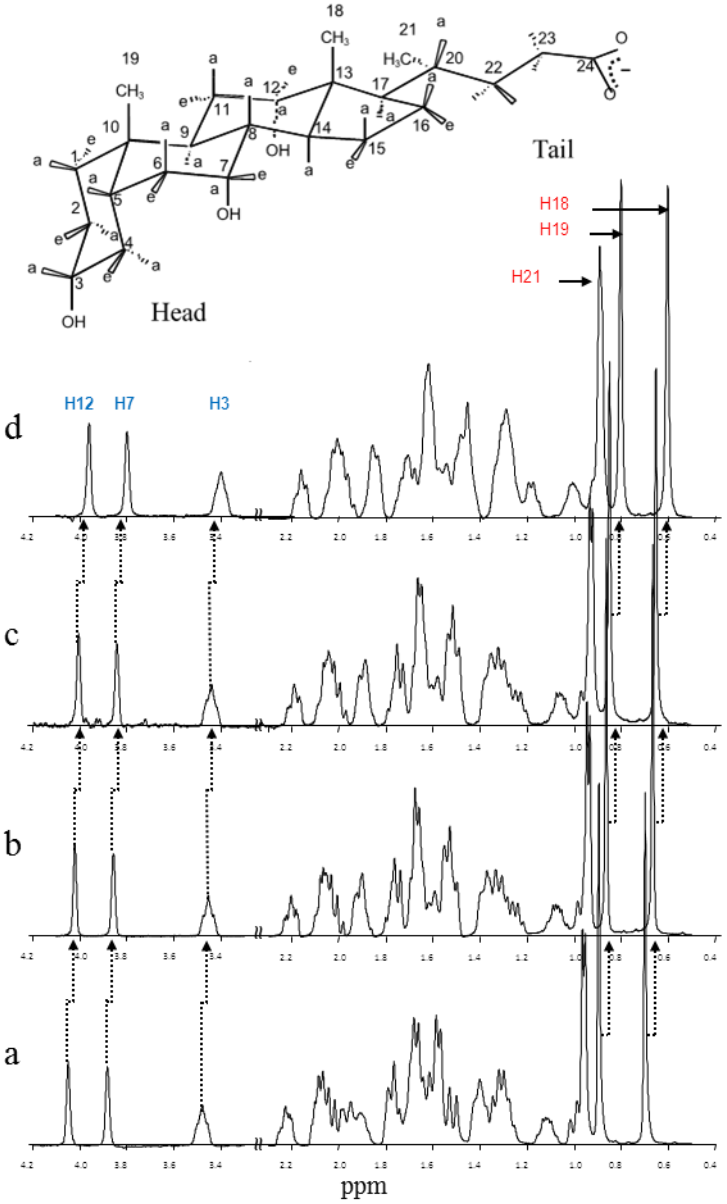


**Figure 4-1:** NaCho molecule with labeling scheme and $^{1}H$ spectra acquired for a solution of a) 20 mM NaCho only and those containing b) 0.6 M $NH_4Cl$ c) 0.6 M NaCl and d) 0.6 M $MgCl_2$.

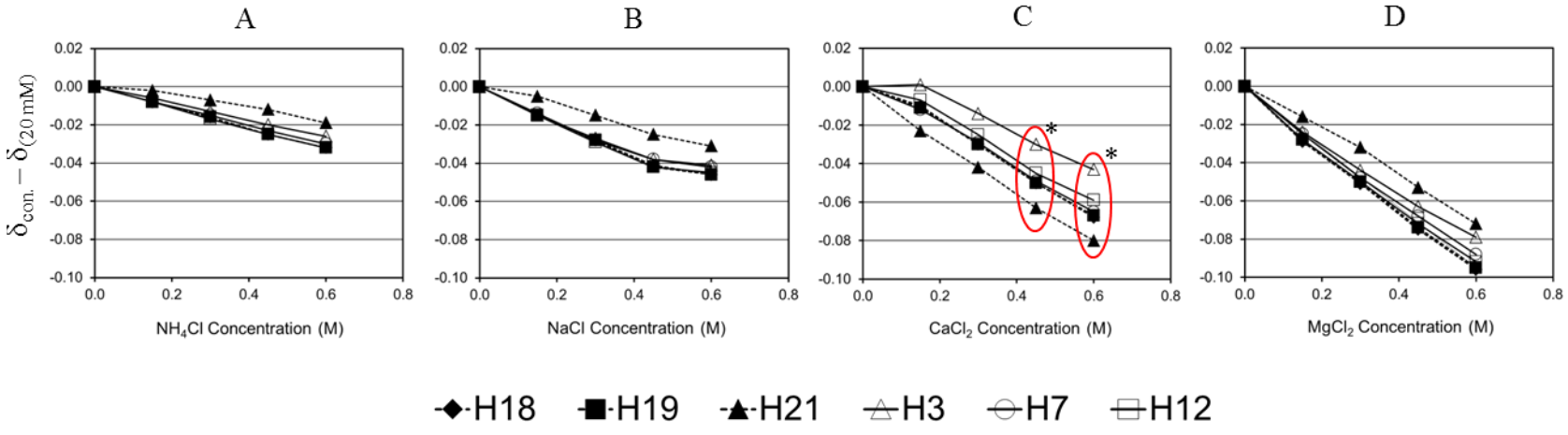


**Figure 4-2**: Changes in chemical sift for primary micelles in the presence of salt at pH 7.4.Changes in chemical shift with respect to NaCho only (no additional salt) at pH 7.4 with A) $NH_4Cl$ B) NaCl C) $CaCl_2$ and D) $MgCl_2$. In graph C 0.45 and 0.6 M $CaCl_2$ are in red circles and denoted with an asterisk. These concentrations are not truly reflected in the graphs due to micelle precipitation

$MgCl_2$. As shown in Graph 2B, at NaCl concentrations of 0.45 M or greater, a plateau was reached. $MgCl_2$ induced the greatest changes in chemical shifts. Indeed, the decreases in chemical shifts were nearly twice greater than those seen with NaCl.

*Changes in linewidths*. Figure 4-3 shows the changes in linewidth for these resonances at pH 7.4. The addition of various salts led to significant changes in linewidth in the resonances corresponding to the methyl protons. In the presence of $NH_4Cl$ and NaCl, the resonances became narrower, with increasing concentrations up to 0.45 M. Further increases resulted in the increase in linewidth. With $CaCl_2$, slight broadening was observed with all resonances. However, linewidths at higher $CaCl_2$ concentrations are not reliable due to micelle precipitation. With $MgCl_2$, the opposite was observed. Indeed, up to 0.3 M the resonances were wider but narrowing was observed at higher concentrations. The resonances corresponding to H3, H7, and H12 exhibited a decrease in linewidth similar to methyl protons in $NH_4Cl$ and NaCl. Linewidth studies for $MgCl_2$ showed the broadening of the H3, H7, and H12 resonances as the concentrations was increased.

**Effect of the addition of NaCl, $NH_4Cl$, and $MgCl_2$ to NaCho primary micelles at pH 9.1.**

*Changes in chemical shifts.* Figure 4-4 shows the changes in chemical shift with increasing salt concentration at pH 9.1. Overall, and just as with the solutions at pH 7.4, shielding was observed in the chosen resonances as the salt concentration increased. For each salt, the decrease in chemical shift was comparable for the various resonances with the exception of H21, whose chemical shift decreased to a lesser extent (except in the presence of $CaCl_2$). When $NH_4Cl$ was used as the electrolyte, a small decrease in chemical shift was observed (Fig. 4-4A). NaCl induced greater changes in chemical shift above 0.45 M compared to pH 7.4. In the presence of $CaCl_2$, the decreases in chemical

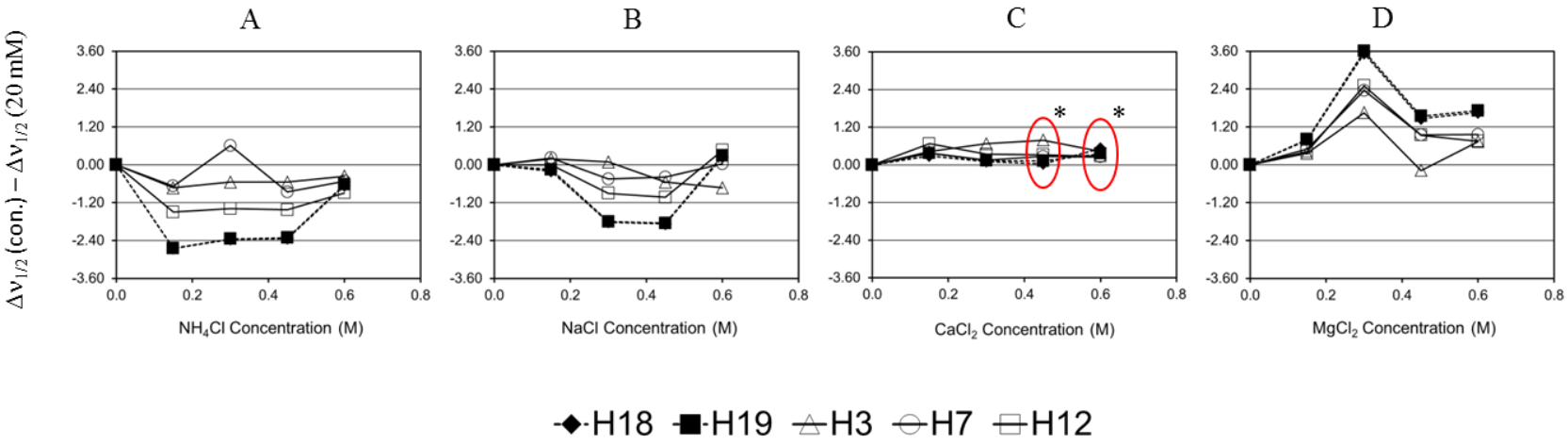


**Figure 4-3:** Changes in linewidth for primary micelles in the presence of salt at pH 7.4. Changes in linewidth with respect to NaCho only (no additional salt) at pH 7.4 with A) $NH_4Cl$ B) NaCl C) $CaCl_2$ and D) $MgCl_2$. In graph C 0.45 and 0.6 M $CaCl_2$ are in red circles and denoted with an asterisk. These concentrations are not truly reflected in the graphs due to micelle precipitation

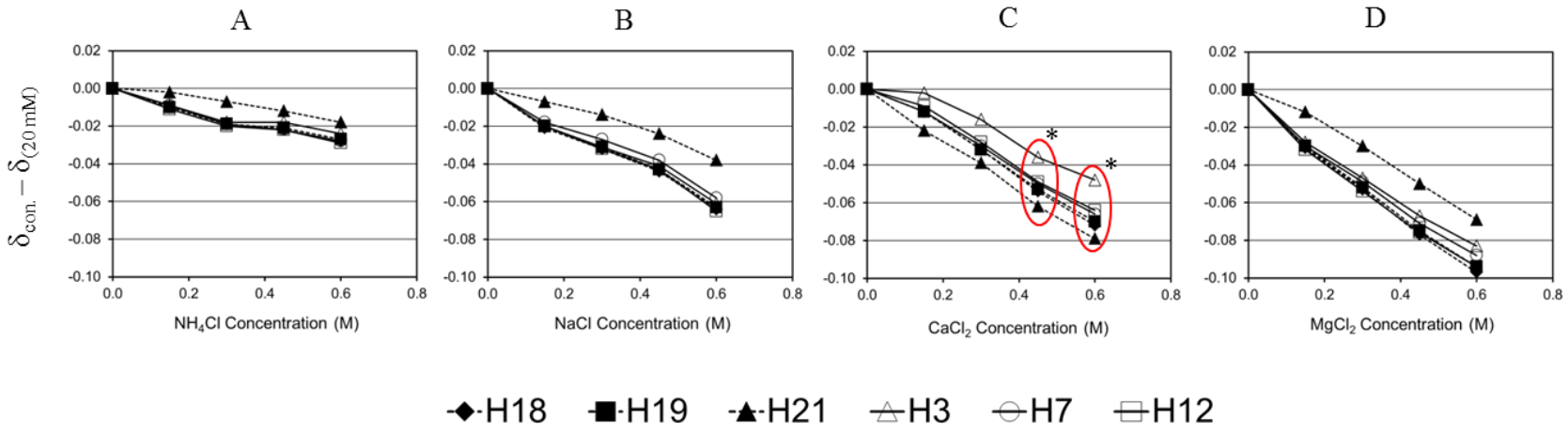


Figure 4-4: Changes in chemical sift for primary micelles in the presence of salt at pH 9.1. Changes in chemical shift with respect to NaCho only (no additional salt) at pH 9.1 with A) $NH_4Cl$ B) NaCl C) CaCl2 and D) $MgCl_2$. In graph C 0.45 and 0.6 M CaCl2 are in red circles and denoted with an asterisk. These concentrations are not truly reflected in the graphs due to micelle precipitation

shifts were similar to those seen at pH 7.4. As also observed at 7.4, the presence of $CaCl_2$ resulted in a smaller decrease in chemical shift for H3 at the higher pH (9.1). On the other hand, and just as observed at pH 7.4, H21 showed the greatest decrease in chemical shift. Relative to the other salts and as observed at pH 7.4, $MgCl_2$ also caused the greatest degree of change in chemical shifts at the higher pH of 9.1.

*Changes in linewidths*. Figure 4-5 shows the changes in linewidth for the selected resonances for 20 mM NaCho at pH 9.1 as the salt concentration was increased. For $NH_4Cl$, there was an increase in linewidth that reached a maximum at 0.45 M. NaCl caused an increase in linewidth at 0.15 M, but above this concentration no significant changes in linewidth were observed. In the presence of $CaCl_2$, resonances became broadened as the salt concentration increased to 0.3 M. $CaCl_2$ concentrations of 0.45 and 0.6 M are shown in red circles denoted with an asterisk because the obtained spectral does not represent the 20 mM concentration of NaCho or the salt concentration due to micelle precipitation. The linewidth study using $MgCl_2$ shows a similar trend with the exception of H18, which became narrower at 0.15 M. The greatest degree of broadening occurred at 0.3 M, subsequent additions of $MgCl_2$ resulted in a decrease in linewidths.

**Interpretation of Trends**

**Cation size and charge at pH-7.4:**

$NH_4^+$, $Na^+$, $Ca^{2+}$ and $Mg^{2+}$ were chosen as electrolytes in this study to explore the impact of ionic diameter and charge on NaCho micelles. The four electrolytes resulted in the decrease of chemical shifts for the chosen resonances. To aid in the interpretation of the experimental trends, the theoretical predictions of chemical shifts reported in Chapter 2 were used. The chemical shifts were theoretically predicted for resonances corresponding to a NaCho monomer in isolation, and then surrounded by chloroform,

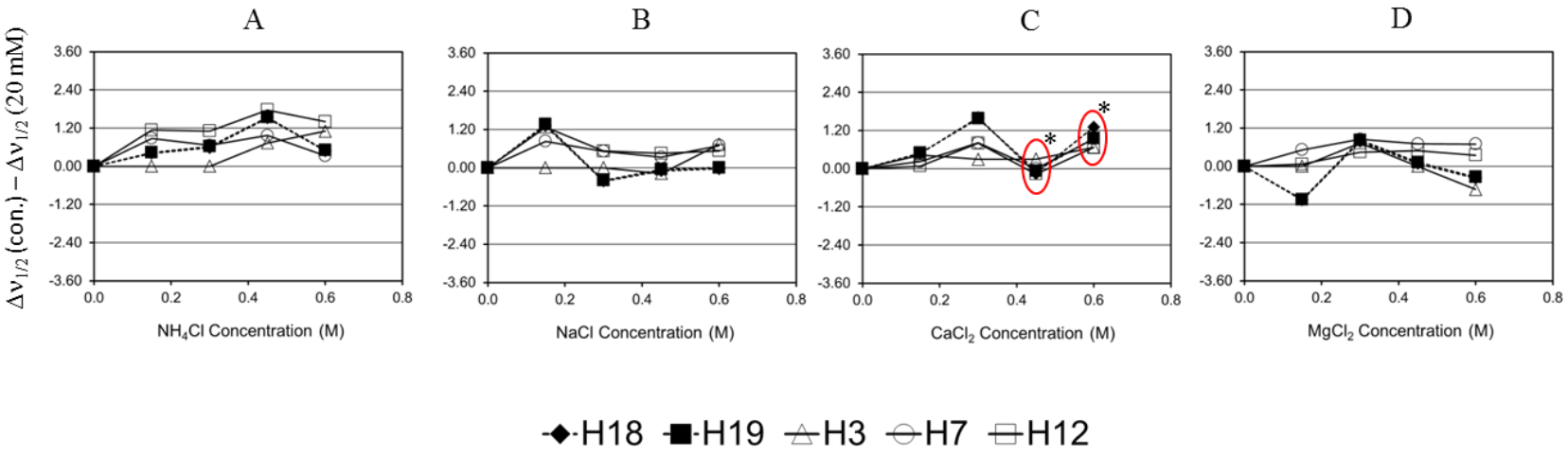


**Figure 4-5:** Changes in linewidth for primary micelles in the presence of salt at pH 9.1. Changes in linewidth with respect to NaCho only (no additional salt) at pH 9.1 with A) $NH_4Cl$ B) NaCl C) $CaCl_2$ and D) $MgCl_2$. In graph C 0.45 and 0.6 M $CaCl_2$ are in red circles and denoted with an asterisk. These concentrations are not truly reflected in the graphs due to micelle precipitation

methanol, or water. Those calculations predict the deshielding for methyl protons H18 and H19 as the polarity of the solvent increases. However, H21 protons which are closer to the $COO^-$ groups are expected to become more shielded as the solvent polarity increases and diminish the deshielding effect of the carboxylate oxygens. Protons H3, H7 and H12 were predicted to increase their chemical shift (more deshielded) with increasing solvent polarity.

Linewidth studies were carried out for methyl protons (H18 and H19) as well as H3, H7 and H12. Linewidths for H21 were not included in this study due to the splitting pattern (doublet) and the spectral overlap with the H1a resonance. This made it difficult to measure accurately the linewidth of the H21 resonance. For the interpretation of changes in linewidth, it is necessary to understand the causes for these variations. Linewidth is often evaluated as the peak width at half height, $\Delta\nu_{1/2}$. High resolution NMR spectra of small molecules is inversely related to the effective spin-spin relaxation time ($T_2$*) which is related to slight variations in the magnetic field sensed by the sample. For small spherical molecules, $T_2$* is long thus resulting in small linewidths, in the order of a few Hertz. Linewidths are also affected by the motional correlation time ($\tau_c$), the time it takes for the molecule or molecular ensemble to rotate one radian. As the molecular weight increases, so does $\tau_c$ and $T_2$ decreases resulting in line broadening. Similarly, when monomers form aggregates in solution, the mobility of the aggregate decreases thus enhancing $\tau_c$ and decreasing $T_2$.[15] Assuming that the tumbling time of primary micelles in each case did not vary significantly, line broadening will be interpreted in terms of decreases in $T_2$ values.

As discussed below, each electrolyte caused unique changes in the spectral traces of NaCho. These variations result from the different ionic diameter and charge of the

chosen cations. Taking into account both the changes in chemical shifts and in linewidths, the paragraphs below postulate the nature of the interactions between each salt and the NaCho micelles.

*Postulates of possible interactions between $NH_4Cl$ and NaCho:* $NH_4^+$, with the largest ionic diameter of 296 pm, resulted in the smallest changes in chemical shift. This is proposed to be due to the lower charge density of $NH_4^+$. This factor limits the strength with which this cation interacts with oxygen lone pairs in the OH groups and with the carboxylate group. As the concentration of $NH_4^+$ increased, the methyl protons became more shielded. The theoretically predicted trends suggest a decrease in polarity around H18 and H19 but the opposite effect around H21. Cations positioned in the proximity of carboxylate groups in the top and bottom of the micelle may reduce the deshielding effect caused by the oxygens in this moiety. As a result, the H21 protons are relatively more shielded.

The same predictions show that as the solvent polarity increases, H3, H7, and H12 protons become deshielded. In this study, as salt concentration increased, the resonances corresponding to H3, H7, and H12 became more shielded. This effect can be attributed to $NH_4^+$ ions interacting with the lone pairs on the hydroxyl groups forming both the H-bond central belt (H7 and H12) and the top/bottom of the micelle as well as with carboxylate ions thus reducing the deshielding effect of these moieties on their neighboring protons.

Linewidth studies for $NH_4Cl$ showed an initial narrowing of the resonances related to the three methyl groups after the first few additions of $NH_4Cl$, suggesting that the core of the micelle is less compact, as modeled in Figure 4-6b. In order for the

micelle to expand, the hydrogen-bond network involving the OH groups at C7 and C12 must be weakened or disrupted. As a result, protons H7 and H12 are expected to be slightly further from neighboring protons and their resonances become narrower. The narrowing of the resonance corresponding to H3 also suggests the weakening of interactions in the top and bottom networks of the micelle; this can be attributed to $NH_4^+$ ions that interact with the OH group at C3 and carboxylate ions. As the $NH_4Cl$ concentration increased from 0.45 to 0.6 M, the linewidth for each of the chosen resonances increased to values similar to those observed in the absence of $NH_4Cl$. This suggests that after the initial expansion of the micelles, $NH_4^+$ ions may be integrated within the hydrogen-bonding central belt as well as with the top and bottom networks and bring the micelle back to a more compact state (see Figure 4-6c).

*Postulates of possible interactions between NaCl and NaCho:* To determine if the changes in NaCho micelles are affected by the size of the cation, NaCl was chosen and compared to $NH_4Cl$. Given that $Na^+$ (diameter: 204 pm) is smaller than $NH_4^+$ (diameter: 296 pm), its charge density is greater and, therefore, it has the ability to interact with electronegative moieties more effectively than $NH_4^+$. These enhanced interactions are reflected by the greater decreases in chemical shifts observed when NaCl, rather than $NH_4Cl$, was added. The significant decrease in chemical shifts seen for H18 and H19 resonances suggests that the core of the micelle senses a less polar environment. The decrease in chemical shift for H21, on the other hand, indicates that this methyl group is not deshielded as much in the presence of NaCl. Given the location of this methyl group near the carboxylate groups, the decrease in chemical shift suggests the presence of $Na^+$ ions in either or both the top and bottom ionic/H-bond networks as well as the central H-

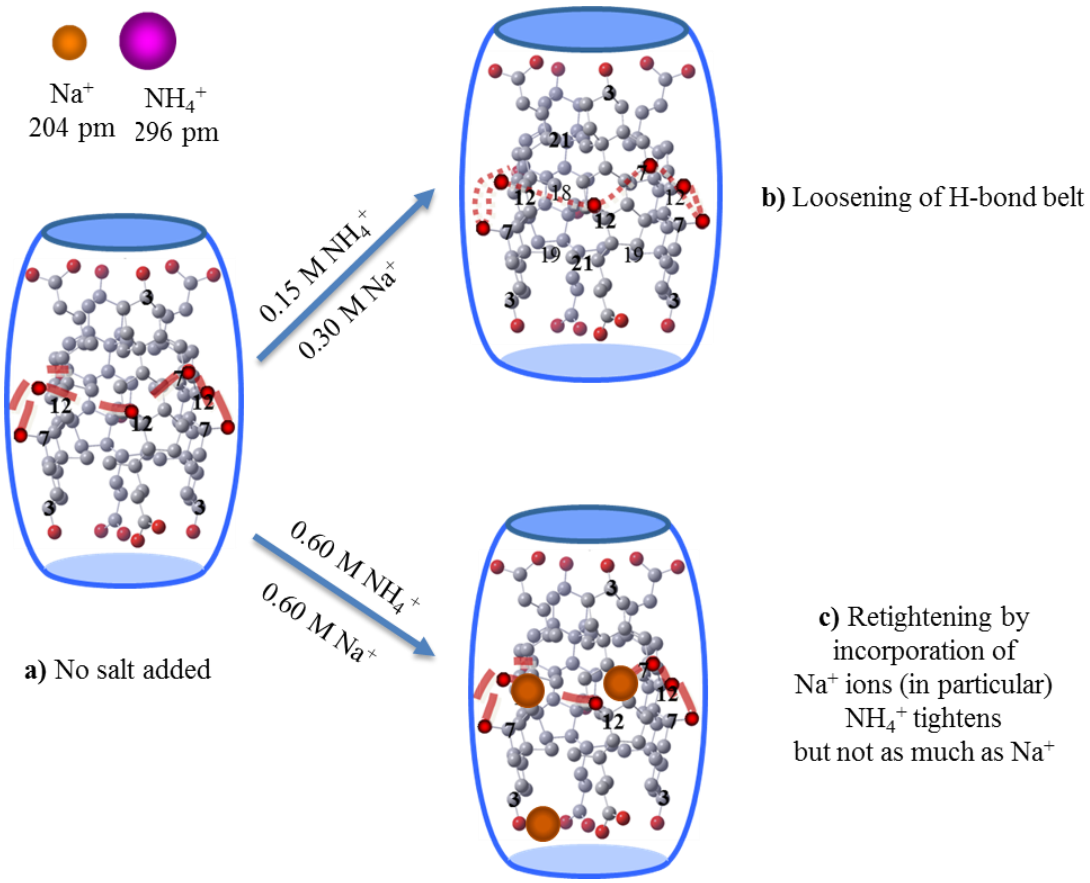


**Figure 4-6:** Primary micelle model in the presence of $NH_4^+$ and $Na^+$ at pH 7.4. a) Primary micelle model with no salt added b) cartoon showing the additions of 0.15 M $NH_4^+$ or 0.30 M $Na^+$ caused loosening of the hydrogen-bond belt and c) cartoon showing at 0.6 M $NH_4^+$ or $Na^+$ there is incorporation of cations ($Na^+$ is represented in this model) into the hydrogen-bonding networks leading to a more compact micelle.

bond belt. This possibility is supported by the shielding of the H3, H7, and H12 protons that suggests that $Na^+$ ions effectively interact with carboxylate ions and hydroxyl lone pairs thus reducing their deshielding effect on neighboring protons. Using NaCl as the electrolyte shows an interesting difference when compared to the other salt species. Indeed, upon reaching 0.45 M, smaller changes in chemical shifts were observed. Possible reasons for this trend are offered below.

Linewidth studies for NaCl showed narrowing of the resonances corresponding to the methyl groups (H18 and H19) as the salt content increased. The magnitude of change was not as large as that observed with $NH_4Cl$, suggesting that the compactness of the micelles is not as affected. It is possible that with the first addition of NaCl there is little impact on the hydrogen-bond central belt as the $Na^+$ ions are expected to be preferentially attracted to the carboxylate ions. As the concentration of NaCl increases the hydrogen-bond belt may become weakened (see Fig.4- 6b) but not as much as with $NH_4Cl$. $NH_4^+$ is a larger ion (296 pm diameter) and thus the charge is delocalized over a greater volume that could possibly affect various adjacent OH groups, causing greater disruption of the central H-bond belt. $Na^+$, on the other hand, being smaller (204 pm diameter) could affect a more localized environment and lead to less loosening of the micelle, as reflected by the smaller decrease in linewidths. In the last addition of NaCl, line broadening was observed suggesting $Na^+$ ions are becoming integrated into the hydrogen-bond network by metal ion-dipole interactions creating a more compact micelle (see Fig. 4-6c).

*Postulates of possible interactions between $CaCl_2$ and NaCho:* To determine if the degree of changes in NaCho micelles is affected by cation charge, $CaCl_2$ was chosen and compared to NaCl because they have similar ionic diameter ($Ca^{2+}$ = 200 pm and $Na^+$ = 204 pm). Changes in chemical shift were greater than those observed in the presence of

NaCl (Fig. 4-3c). These protons became shielded as the salt concentration increased. Changes in chemical shift for these protons above 0.45 M are not truly reflected in the graphs due to micelle precipitation. Unlike the other salts, in the presence of $CaCl_2$, H21 showed the greatest change in chemical shift followed by H18 and H19. The decrease in chemical shift (shielded) for H21 suggests nearby COO- groups are interacting with $Ca^{2+}$ ions thus inhibiting their deshielding effect on neighboring protons. The degree of shielding observed is significantly greater than trends observed with +1 cations. This suggests that the increase in cation charge can more effectively interact with $COO^-$ groups. The trends observed with H18 and H19 suggests the core of the primary micelles is becoming less polar. H3, H7 and H12 also became shielded as salt concentration was increased. $Ca^{2+}$ ions are interacting with the lone pairs on hydroxyl groups and carboxylate ions thus reducing the deshielding effect of these moieties on their neighboring protons. Interestingly, H3 showed the smallest decrease in chemical shift. This suggests $Ca^{2+}$ ions are preferentially interacting with COO- groups. This is to be expected given the very high value of $K_{sp}$ for $CaCO_3$ ($K_{sp} \sim 10^{-9}$).[70] Both the greater charge density and the size of $Ca^{2+}$ (200 pm in diameter) contribute to its strong interaction with $COO^-$ where the oxygens are about ~ 220 pm apart.

Linewidth studies for $CaCl_2$ showed trends different from the other salts examined in that the changes in linewidths observed were much smaller. In the presence of $CaCl_2$, H18 and H19 became slightly broadened suggesting that either the core of the primary micelles is becoming tighter and/or that the screening effect provided by the negatively charged COO- is diminished and aggregation may take place. The linewidths corresponding to H3, H7 and H12 also became broadened. If these changes were due to tightening of the micelles, one could propose that $Ca^{2+}$ ions do not disrupt the hydrogen-

bond networks as seen with $NH_4Cl$ and NaCl but can integrate themselves into these networks forming metal ion-dipole interactions at the top/bottom (OH-3 and $COO^-$) and central region (OH-7 and OH-12) thus creating a more compact primary micelles (see Fig. 4-7b). However, the possibility of aggregation (see Fig. 4-7c) cannot be ruled out, particularly since at concentrations of 0.45 M and above, precipitation occurs. ). Details on how aggregation is taken place are hard to discern, $Ca^{2+}$ can reduce the screening effect that keep primary micelle in solution causing micelle aggregation. However, it is also possible that $CaCl_2$ can bridge primary micelles together through the $COO^-$ groups of primary micelles causing aggregation to occur. Linewidth changes cannot distinguish between these possibilities and further studies are needed.

*Postulates of possible interactions of $MgCl_2$ and NaCho:* To determine the impact of the size and charge of the cation on NaCho micelles, the results obtained with $MgCl_2$ were compared to those obtained with NaCl and $CaCl_2$. $Mg^{2+}$ is doubly charged and has the smallest ionic diameter (144 pm) of the cations tested in this work. Compared to $Na^+$, $NH_4^+$ and $Ca^{2+}$, $Mg^{2+}$ caused the greatest degree of shielding. H18 and H19 are thus proposed to be in less polar environments and H21 in a more polar surrounding when $MgCl_2$ is added. Both the smaller size and greater charge $Mg^{2+}$ lead to a greater attraction toward the hydroxyl lone pairs and negative charges on carboxylate ions. As a result, the deshielding effect of these moieties on neighboring protons is diminished and leads to greater shielding.

Linewidth studies for the chosen resonances showed the initial broadening, unlike the trends seen in the presence of NaCl or $NH_4Cl$. This trend suggests that as the concentration of $MgCl_2$ is increased, the micelles may become more compact until they peak at 0.3 M (see Fig. 4-8b). It is possible that $Mg^{2+}$ ions are small enough to integrate

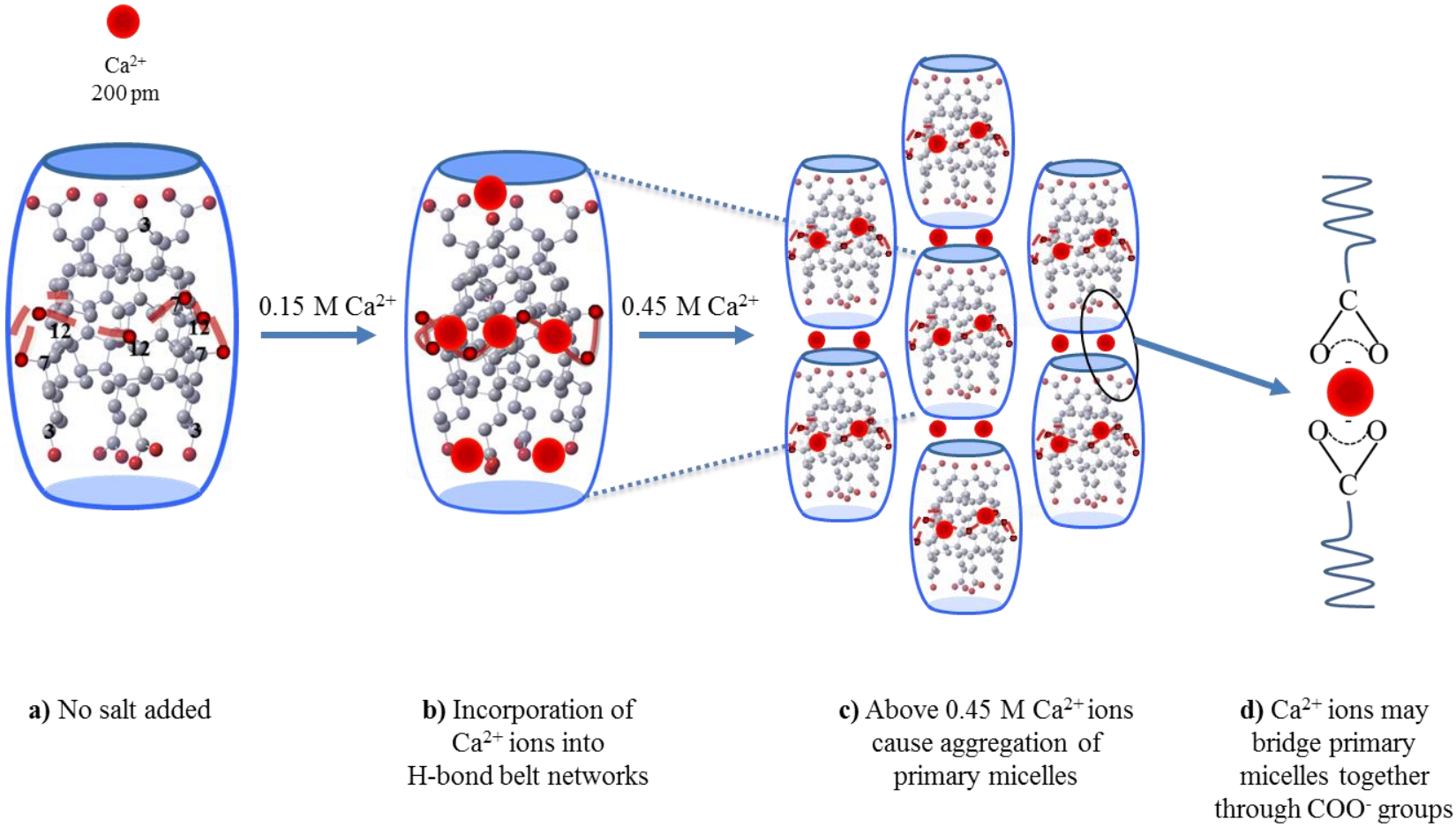


**Figure 4-7:** Primary micelle model in the presence of $Ca^{2+}$ at pH 7.4. a) Primary micelle model with no salt added b) cartoon shows that in the presence of $Ca^{2+}$ ions, incorporation into the hydrogen-bonding networks leads to a more compact micelle c) cartoon showing the possibility of micelle aggregation above 0.45 M $CaCl_2$ and d) schematic diagram showing that $Ca^{2+}$ ions can bridge primary micelles together through $COO^-$ groups.

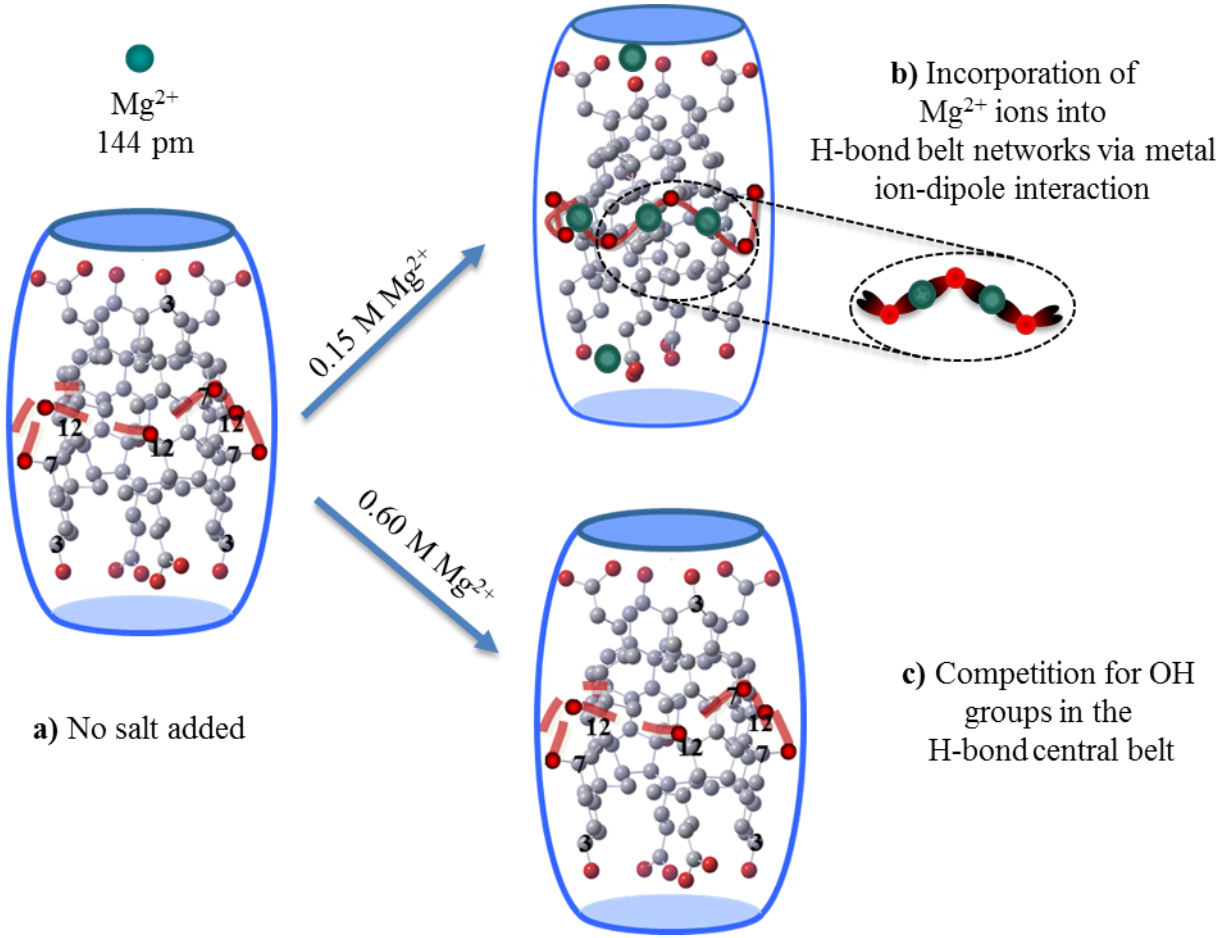


**Figure 4-8**: Primary micelle model in the presence of $Mg^{2+}$ at pH 7.4. a) Primary micelle model with no salt added b) cartoon of primary micelle in the presence of 0.15 M $MgCl_2$. $Mg^{2+}$ ions are incorporated into the hydrogen bond networks via metal ion-dipole interactions and c) cartoon of a loosened primary micelle due to competition of excess $Mg^{2+}$ ions that may compete for OH groups in the hydrogen-bond -$Mg^{2+}$ central belt.

within the central hydrogen-bonding as well as the top and bottom networks through metal ion-dipole interactions after the first addition of $MgCl_2$. At concentrations above 0.3 M $MgCl_2$ there is a decrease in linewidths, suggesting the partial loosening of the micelles (see Fig. 4-8c). This trend may be attributed to the excess $Mg^{2+}$ ions that may compete for the OH groups in the H-bond-$Mg^{2+}$ central belt. As the OH group interacts with both $Mg^{2+}$ ions integrated into the H-bond belt and excess external $Mg^{2+}$ ions, the strength of the belt is reduced.

**Cation size and charge at pH-9.1:**

To understand the effects of pH on NaCho micelles, studies similar to those discussed above were carried out at pH 9.1. Lower pHs were not tested because as the pH begins to approach the pKa value (pKa 4.6-5.5)[54] of cholic acid, the carboxylate group becomes partially protonated and the micelles begin to precipitate at pH values of 6.5 and below. For a solution of 20 mM NaCho only, the chemical shift of the chosen resonances increased at the higher pH, with the exception of that for H21, which decreased at pH 9.1 (see supplemental information). The changes in chemical shifts for all NaCho resonances followed the trends observed in the theoretical predictions obtained using solvents of increasing polarity. This indicates that the presence of a greater concentration of negatively charged OH- groups in the solvent leads to a more polar environment at pH 9.1.

Linewidth studies for a solution of 20 mM NaCho only from 7.4 to 9.1 showed a narrowing of the chosen resonances as the pH increased, suggesting that NaCho micelles are less compact (see Fig. 4-9). The loosening effect observed can be attributed to the disruption or weakening of the hydrogen-bond network involving OH groups at C7 and

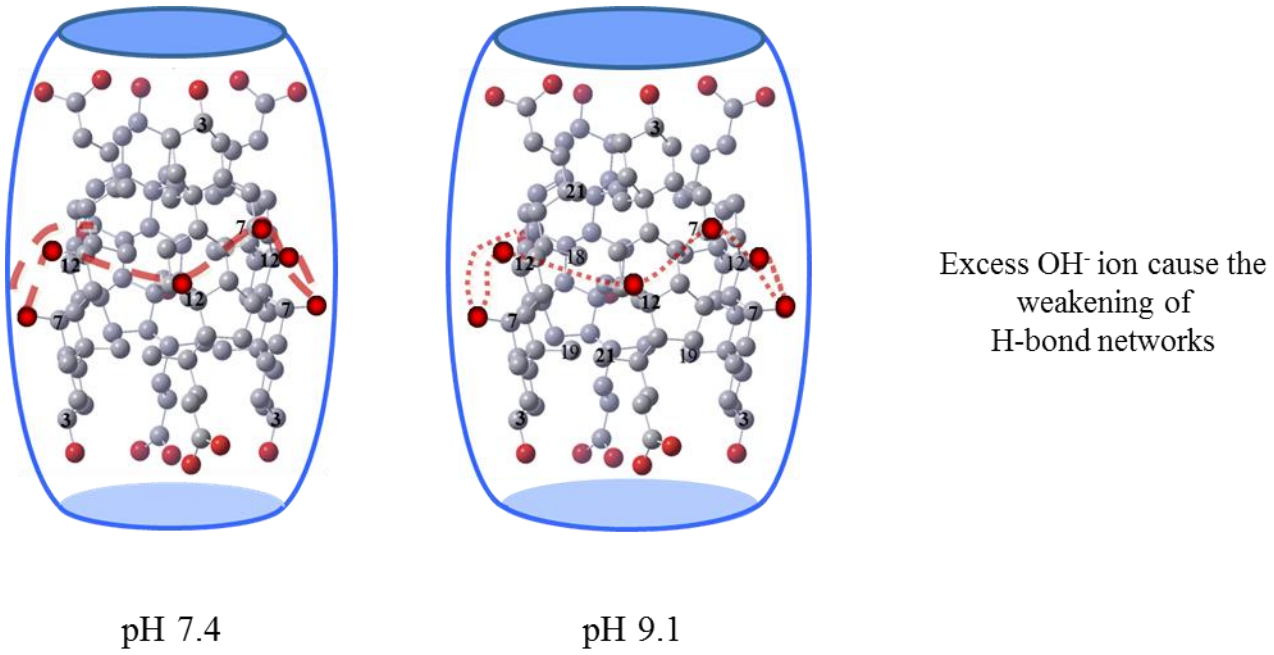


**Figure 4-9:** Cartoon of primary micelle at pH 7.4 and 9.1. As pH increases the excess OH- ions cause the weakening of the hydrogen-bond networks

C12 due to the attraction between the abundant hydroxide ions toward the hydroxyl groups in NaCho micelles.

*Postulates of possible interactions of $NH_4Cl$ and NaCho:* Each electrolyte caused shielding of the chosen protons, similar to the trends seen at pH 7.4. As the salt concentration increased, the chosen protons became more shielded. The reasons for the observed shielding are similar to those discussed for pH 7.4.

As observed at pH 7.4, the first addition of $NH_4Cl$ led to a decrease in chemical shift of the chosen proton resonances at pH 9.1. At $NH_4Cl$ concentrations greater than 0.3 M, smaller changes in chemical shift were observed. The reduced shielding effect observed at pH 9.1 can be attributed to the attraction of $NH_4^+$ ions toward the excess hydroxide ions present in the solution.

Changes in the linewidths of the chosen resonances showed a trend opposite to that seen at pH 7.4. Indeed, at higher concentrations, the linewidths increased, suggesting that tighter micelles may be formed. At pH 9.1, the loosened micelle may enable $NH_4^+$ ions to integrate into the hydrogen-boding network and/or reduce the disrupting effect of $OH^-$ on the network. Both possibilities could lead to tighter micelles after the second addition of $NH_4Cl$, as represented in Figure 4-10b. Linewidths continued to increase as $NH_4^+$ concentration increased until a plateau was observed around 0.45 M. This plateau may indicate that at this high $NH_4^+$ concentration, the maximum number of $NH_4^+$ ions may have been integrated in the hydrogen-bond central belt as well as the top and bottom networks. As a result, the greatest level of compactness could have been reached and further addition of $NH_4Cl$ could not cause greater line broadening.

*Postulates of possible interactions of NaCl and NaCho:* NaCl also reduced the chemical shifts of NaCho resonances to a greater degree than $NH_4Cl$. This trend suggests

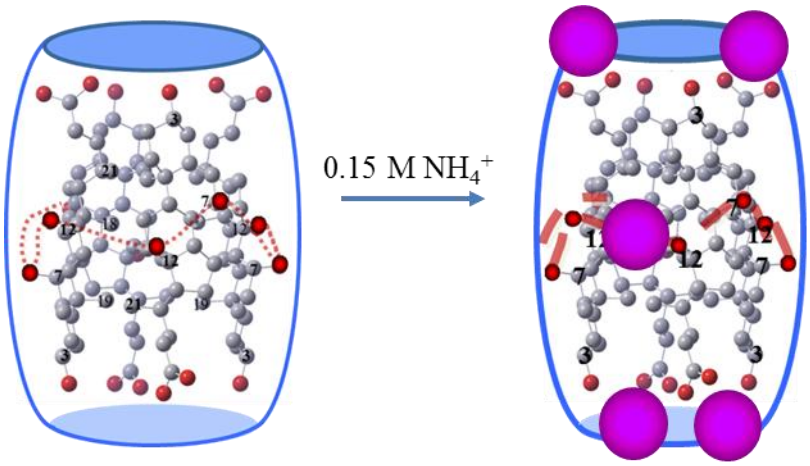


**a)** No salt added at pH 9.1

**b)** Incorporation of $NH_4^+$ ions tightens the primary micelle

**Figure 4-10:** Primary micelle model in the presence of $NH_4^+$ at pH 9.1. a) Cartoon of primary micelle at pH 9.1 with no salt added and b) above 0.15 M $NH_4Cl$ $NH_4^+$ ions incorporate into the hydrogen-bond network that leads to a more compact micelle.

that, compared to $NH_4^+$ ions, $Na^+$ ions are more effective in reducing the deshielding effect that excess hydroxide ions in the solvent have on NaCho protons. Compared to the results at pH 7.4, each addition of NaCl resulted in slightly greater degree of shielding at pH 9.1.

Linewidth studies showed line broadening after the first salt addition. It is possible that $Na^+$ ions are small enough to be disrupt the hydrogen-bond belt and interact with the oxygen lone electron pairs through metal ion-dipole interactions and/or they may reduce the effect of $OH^-$ in the weakening of the H-bond networks (see Figure 4-11). Either effect would result in more compact micelles. Similar to the trend observed at pH 7.4, the linewidths became narrower after 0.15 M NaCl; with a smaller magnitude of change. The smaller degree of change could result from the attraction between excess hydroxide ions and $Na^+$ ions thus limiting the impact of $Na^+$ around the central hydrogen-belt network as seen in pH 7.4. Above 0.45 M NaCl line broadening was observed suggesting the compaction of micelles. This trend suggests that $Na^+$ ions may be integrating into the hydrogen-belt as well as the top and bottom networks through metal ion-dipole interactions.

*Postulates of possible interactions between $CaCl_2$ and NaCho:* Similar to trends observed at pH 7.4, in the presence of $CaCl_2$ chemical shifts for NaCho protons became more shielded than when NaCl was present. $Ca^{2+}$ ions having a greater charge are more effective in reducing the deshielding effect of OH- ions thus leading to more shielding. However, the degree of change in chemical shift was slightly less than at pH 7.4. This may be due to $Ca^{2+}$ ions interacting with $OH^-$ ions in solution as well as OH and COO- groups on the NaCho micelles. H21 showed the greatest decrease in chemical shift followed by H18 and H19. The changes in chemical shift indicate that H3 was the least

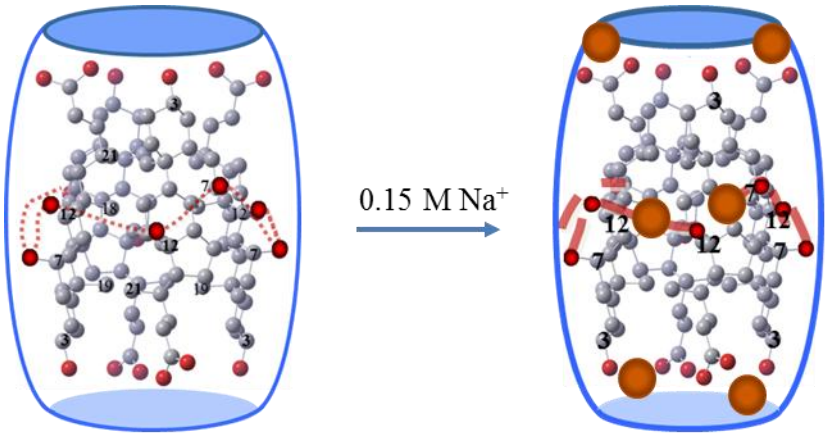


**Figure 4-11:** Primary micelle model in the presence of $Na^+$ at pH 9.1. a) Cartoon of primary micelle at pH 9.1 with no salt added and b) above 0.15 M NaCl, $Na^+$ ions incorporate into the hydrogen-bond network that leads to a more compact micelle.

affected proton. The interactions between $Ca^{2+}$ ions and the $COO^-$ groups cause H21 to sense a more hydrophilic environment. In addition, the interactions between $Ca^{2+}$ ions and hydroxyl groups would cause H3, H7 and H12 to become shielded as $CaCl_2$ concentration increases.

Linewidth studies showed slight broadening for all resonances as $CaCl_2$ concentrations increased. Similar to NaCl, it is possible that $Ca^{2+}$ ions are small enough to be integrated into the hydrogen-bond belt (by metal ion-dipole interactions) and/or reduce the effect of $OH^-$ ions in the weakening of the H-bond networks. At 0.3 M $CaCl_2$, H18 and H19 showed the greatest degree of broadening. This indicates that either the core of the primary micelles becoming more compact or aggregation of primary micelles takes place (see Figure 4-12).

Interactions between $Ca^{2+}$ ions and hydroxyl groups result in the broadening of the resonances for H3, H7 and H12. Above this concentration, primary micelles are most compact and begin to precipitate out of solution. Linewidth studies above 0.45 M are not reliable due to micelle precipitation.

*Postulates of possible interactions of $MgCl_2$ and NaCho:* Similar to the results obtained at pH 7.4, the greatest decrease in chemical shift was observed when using $MgCl_2$ as the electrolyte. $Mg^{2+}$ ions have the greatest impact on the degree of change in chemical shift due to the greater attraction toward hydroxide ions. The degree of change in linewidth is smaller than pH 7.4 due to the attraction between $Mg^{2+}$ ions and excess hydroxide ions. This attraction may reduce the impact of $Mg^{2+}$ ions on the hydrogen-bond networks seen in pH 7.4. Linewidth studies showed that after the first addition of $MgCl_2$ the linewidth decreased. The narrowing of linewidths was more pronounced in H18 and H19, suggesting that at 0.15 M $MgCl_2$, there may not be enough $Mg^{2+}$ ions to

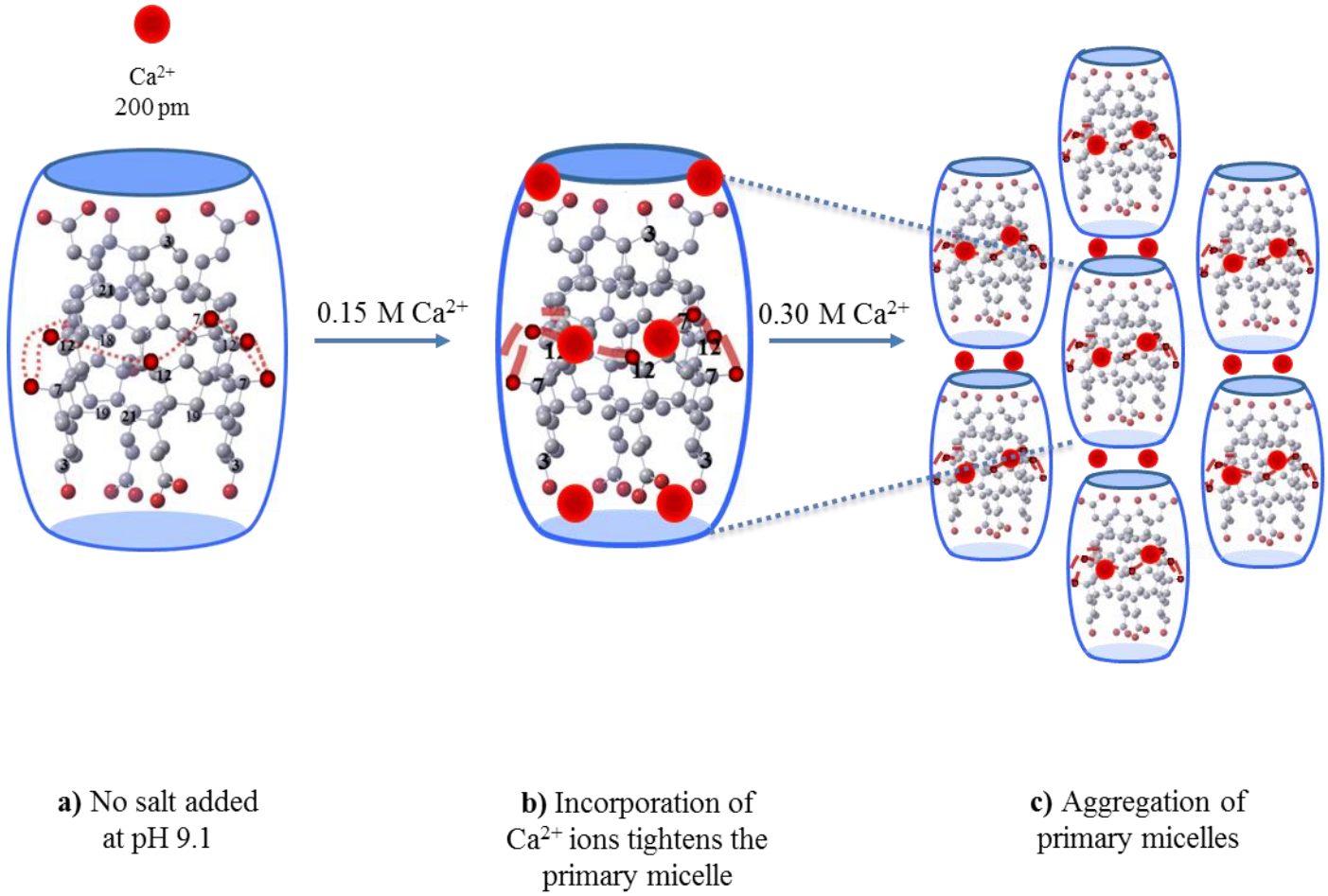


**Figure 4-12:** Primary micelle model in the presence of $Ca^{2+}$ at pH 9.1. a) Cartoon of primary micelle at pH 9.1 with no salt added and b) Incorporation of $Ca^{2+}$ ions causing the tightening of primary micelles and c) Above 0.30 M $CaCl_2$ there is aggregation of primary micelles that leads to micelle precipitation above 0.45 M $CaCl_2$

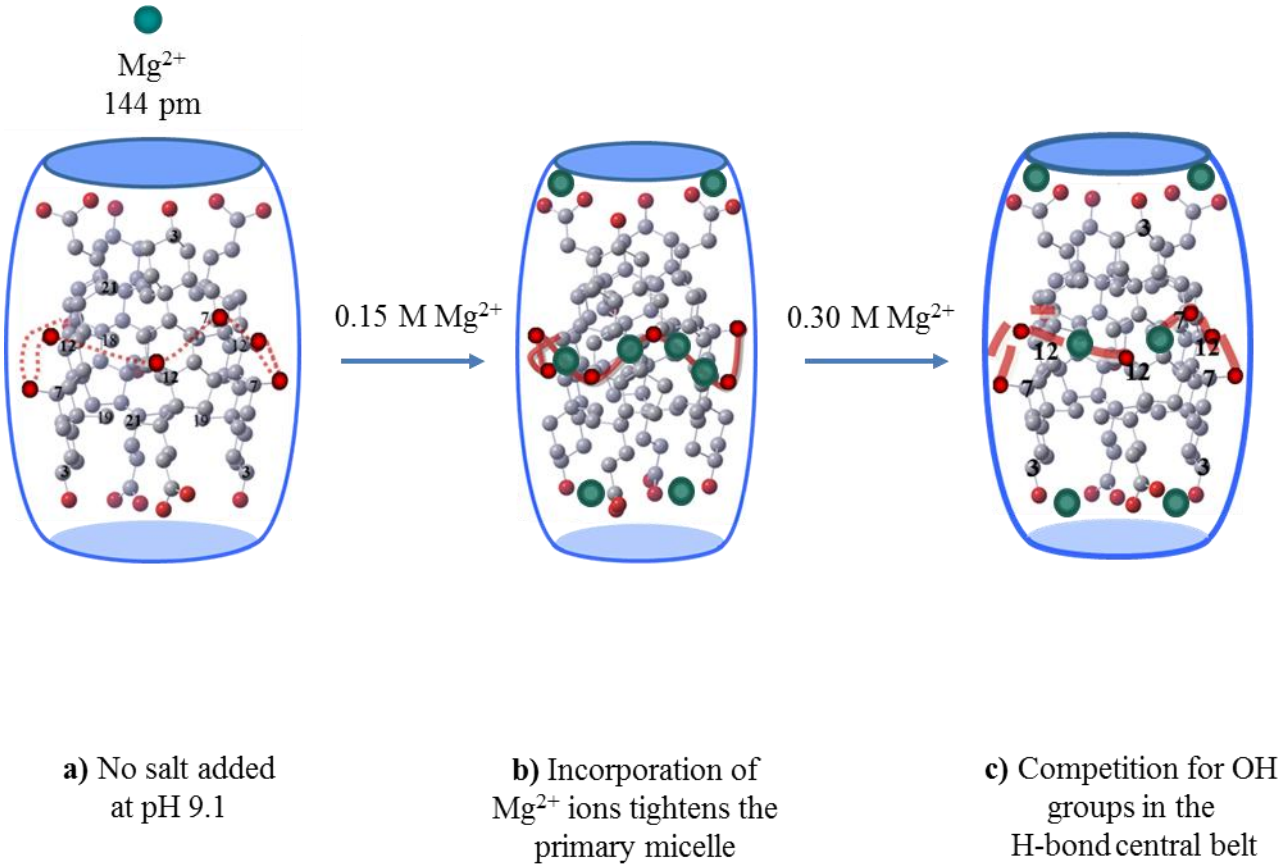


**Figure 4-13:** Primary micelle model in the presence of $Mg2^{+}$ at pH 9.1.a) Cartoon of primary micelle at pH 9.1 with no salt added and b) $Mg^{2+}$ ions integrate themselves into the hydrogen-bond network and create a more compact micelle and c) Above 0.30 M, $Mg^{2+}$ ions lead to the partial weakening of the networks as $Mg^{2+}$ ions interact with the OH groups of NaCho

tighten the looser hydrogen-bond belt expected at pH 9.1. With increasing concentration, enough $Mg^{2+}$ ions may be available to integrate themselves into the hydrogen-bond network through metal ion-dipole interactions and create a more compact micelle (see Figure 4-13b). Above 0.3 M $MgCl_2$, a decrease in linewidth was observed. This observation suggests that 0.3 M $MgCl_2$, the number of $Mg^{2+}$ ions incorporated in the H-bond networks may have reached its maximum and further addition of $Mg^{2+}$ ions lead to the partial weakening of the networks as $Mg^{2+}$ ions interact with the OH groups of NaCho (see Figure 4-13c).

**CONCLUSIONS**

As expected, both ionic and H-bonding interactions are affected by the presence of mono-and divalent cations. Between $NH_4^+$ and $Na^+$, and at pH 7.4, the larger size of $NH_4^+$ leads to a more effective disruption of the H-bond belt, as reflected by the narrowing of the resonances. At pH 9.1, the micelles are not as tight as at pH 7.4 and the addition of $NH_4^+$ leads to tightening of the micelles, suggesting that $NH_4^+$ ions can intercalate within the H-bond loose belt.

For the divalent cations, $Ca^{2+}$ with its larger size relative to $Mg^{2+}$, causes the greatest degree of aggregation at both pH values. This can be attributed to $Ca^{2+}$'s high affinity toward the $COO^-$ group. The screening effect provided by the negative charge of the $COO^-$ groups diminishes significantly and aggregation of primary micelles ensues. $Mg^{2+}$, on the other hand, and because of its smaller size, causes the tightening of primary micelles at both pH values because it can become incorporated into the H-bond belt. At higher concentrations of $Mg^{2+}$ this effect diminishes because the excess $Mg^{2+}$ ions compete for the OH groups forming the belt.

These studies do demonstrate that the tightness of these micelles can be modified by changes in pH and salt composition and concentration. It would be beneficial to investigate simultaneously the aggregation number. NMR data have provided very helpful information but further studies with independent methods need to be pursued.

# CHAPTER 5

# NMR STUDY OF THE IMPACT OF SALT CONCENTRATION, CATION SIZE AND CHARGE ON SODIUM CHOLATE SECONDARY MICELLES

## INTRODUCTION

Beyond the *cmc*, primary micelles begin to associate to form larger (70 nm)[14] secondary micelles. Relatively less detailed information is available regarding the formation of secondary micelles. Previous studies have explored the impact of pH and salt concentration on bile salt micelles. However, those studies were limited to primary micelles.

The current study explores the effect of pH and salt addition on secondary micelles. The concentrations of 50 and 100 mM NaCho were selected because at 50 mM NaCho primary and secondary micelles coexist and at 100 mM only secondary micelles exist.

This study follows the model for secondary micelles presented in Chapter 3. Barrel-shaped primary micelles aggregate into secondary micelles via ion-dipole and hydrogen-bonding interactions that connect the top and bottom of the primary micelles. The central hydrogen-belt network proposed for primary micelles is extended and strengthened as neighboring micelles become linked to each other.

## MATERIALS AND METHODS

**Chemicals.** Sodium Cholate (NaCho) and $NH_4Cl$ were obtained from Sigma-Aldrich (St. Louis, MO). Reagent grade NaCl was obtained from EMD Chemicals, Inc. (Gibbstown, NJ). $MgCl_2$ and DSS (4,4-dimethyl-4-silapentane-1-sulfonate, Na salt) were purchased from Aldrich Chemical Co., Inc. (Milwaukee, WI). NANOpure water (Barnstead, resistivity of $18M\Omega cm^{-1}$) was used for all aqueous solutions.

**Sample preparation.** The appropriate amount of NaCho was weighed and placed in a 20-mL vial. Nanopure water was added to attain a final concentration of 200 mM. This stock solution was used to prepare 50 and 100 mM NaCho solutions varying in ionic strength. Aqueous solutions (1.0 M) of NaCl, $NH_4Cl$, and $MgCl_2$ were prepared. The correct amount of these salt solutions was pippetted to create 50 and 100 mM NaCho solutions to reach final salt concentrations of 0.15, 0.30, 0.45, or 0.60 M. The solutions were sonicated in a bath sonicator (Cole-Parmer 8890) for about 15 minutes. The pH was adjusted using 0.1 M and 0.05 M NaOH or HCl to achieve final pH values of $7.4 \pm 0.1$ and $9.1 \pm 0.1$. Less than 10 μL were used to adjust the pH and the contribution of $Na^+$ from the pH adjustment did not significantly alter the total salt concentration.

**One-dimensional NMR studies.** NMR experiments were performed on a Varian Inova 500 MHz spectrometer (Palo Alto, CA) equipped with a triple resonance probe. The frequency used for $^1H$ was 500.1 with a total number of 128 scans. All one-dimensional spectra were processed using MestReC Version 2.01 (Santiago de Compostela, Spain) on a personal computer. All acquisitions were carried out at 25ºC. A coaxial insert containing 1.0 mM 4,4-dimethyl-4-silapentane-1-sulfonate, sodium salt (DSS) dissolved

in $D_2O$ was inserted in the NMR tube and used for signal locking and referencing of NMR spectra.

## RESULTS AND DISCUSSION

As an extension to the study on NaCho primary micelles, we have investigated the effects of cation size and charge on secondary micelles with the use of NMR spectroscopy. The trends observed for each NaCho concentration (50 and 100 mM) at the two pH values will be presented first.

### Effect of the addition of NaCl, $NH_4Cl$, and $MgCl_2$ to NaCho secondary micelles at pH 7.4.

#### 1) Effect on 50 mM solutions of NaCho.

*a) Changes in chemical shift.* The impact of salt addition on the $^1H$ NMR spectrum of NaCho micelles is seen in Figure 5-1. The changes in chemical shift ($\Delta\delta$) were evaluated with respect to the chemical shifts of a solution of 50 mM NaCho (no salt added) at pH 7.4. The chemical shift values for all of the resonances examined in this study were obtained by $^1H$ NMR one-dimensional spectral data. Results obtained upon the addition of increasing concentrations of $NH_4Cl$, NaCl, and $MgCl_2$ are shown in graphs a, b, and c respectively. In these graphs, the standard deviations (n = 3) in the measurements are represented by the size of the symbol. In these studies, $CaCl_2$ was not included due to micelle precipitation even at the lowest concentration (0.15 M) tested. Overall, as salt concentration increased, the changes in chemical shifts became more negative for the chosen resonances, indicating that the corresponding protons became more shielded (decreased in $\delta$). The smallest changes in chemical shift occurred in the presence of $NH_4Cl$, followed by NaCl. The decreases were greater for NaCl than for $NH_4Cl$. The

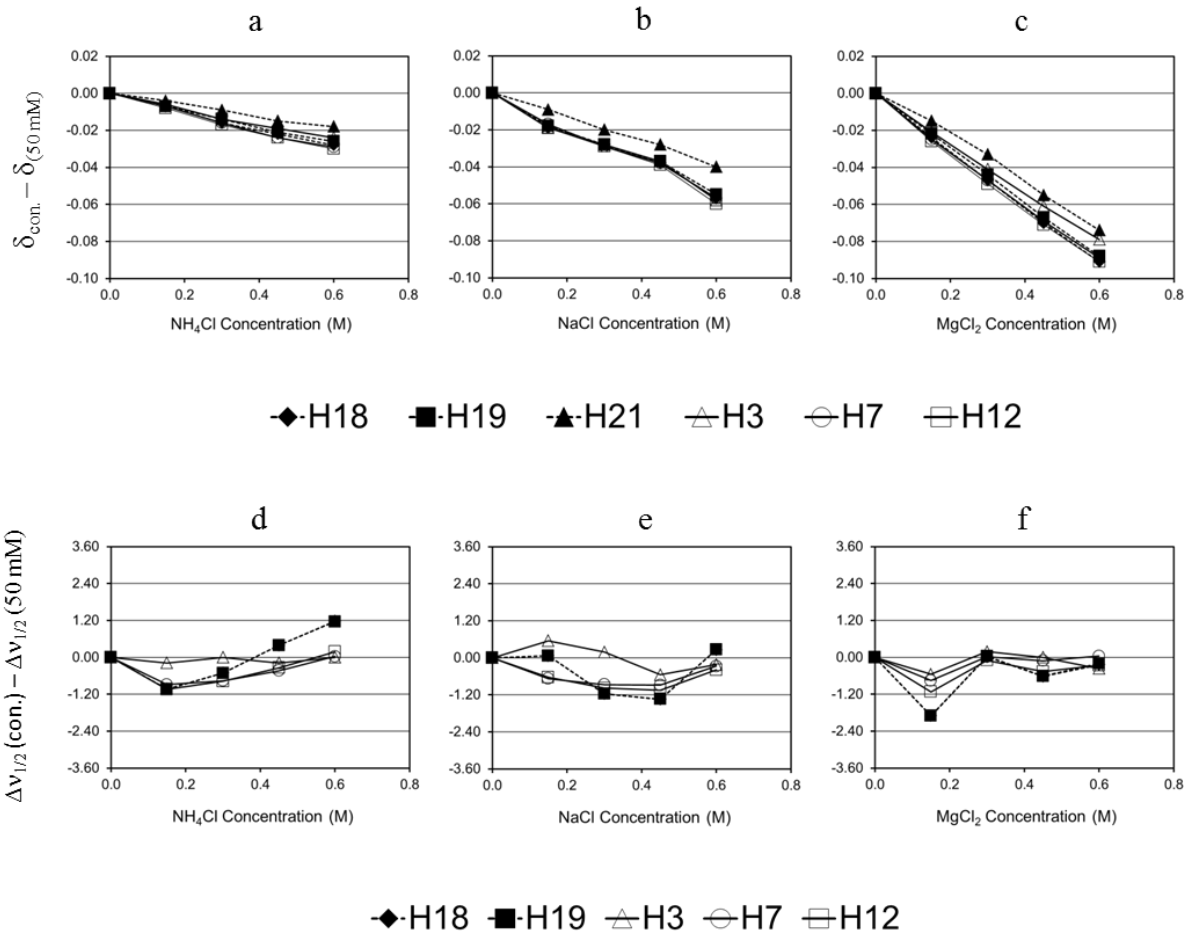


**Figure 5-1.** Changes in chemical shifts (a, b and c) and linewidths (d, e and f) with the addition of $NH_4^+$ (a and d), $Na^+$ (b and e) and $Mg^{2+}$ (c and f) to 50 mM NaCho at pH 7.4

addition of $MgCl_2$ produced the greatest changes in chemical shifts, as shown in Fig. 5-1c.

*b) Changes in linewidth.* Figure 5-1 shows the changes in linewidth for the chosen resonances with respect to a 50 mM NaCho solution at pH 7.4. With each addition of salt, significant changes in linewidth were observed.

$NH_4Cl$: As the $NH_4Cl$ concentration increased, an initial decrease in linewidth was observed for the chosen resonances (see Figure 5-1d). However, at 0.3 M and above, resonances became broader, with H18, H19, and H12 showing the greatest increase in linewidth.

NaCl: When the concentration of NaCl was increased from 0.15 M to 0.45 M, an overall decrease in linewidth was observed (see Figure 5-1e). The methyl resonances (H18, H19), H7 and H12 were impacted the most at 0.3 M. Above 0.45 M, the chosen resonances increase in linewidth.

$MgCl_2$: With the first addition of $MgCl_2$, a decrease in linewidth was seen, particularly in the resonances corresponding to H18 and H19. However, further additions resulted in increasing linewidths (see Figure 5-1f).

**2) Effect on 100 mM solutions of NaCho.**

*a) Changes in chemical shift.* Figure 5-2 shows the changes in chemical shift ($\Delta\delta$) caused by each salt relative to the $\delta$'s seen for a 100 mM NaCho solution at pH 7.4 without any additional salt.

$NH_4Cl$: The first addition of $NH_4Cl$ did not significantly impact the chemical shifts of the chosen resonances. At 0.45 M, and above, a plateau was reached (see Figure 5-2a).

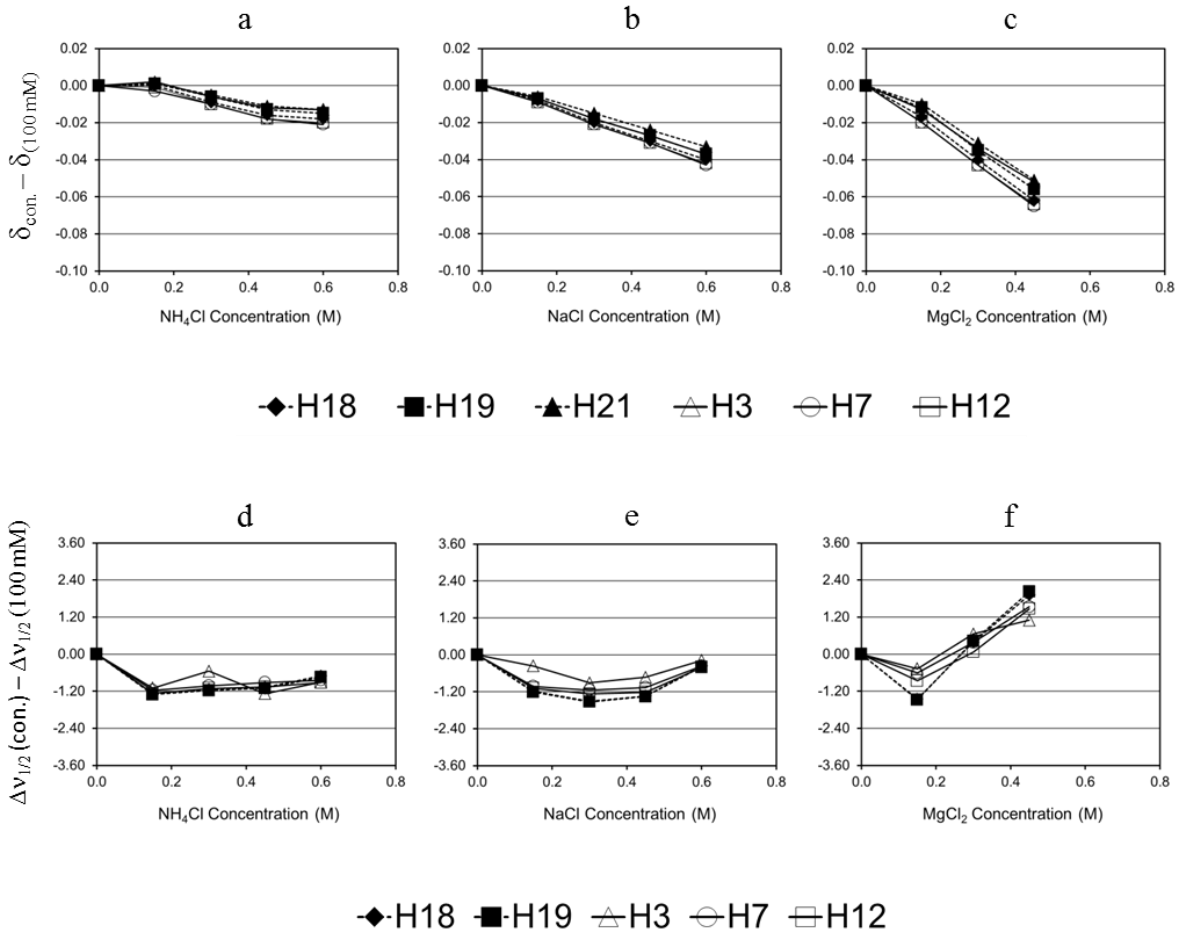


**Figure 5-2.** Changes in chemical shifts (a, b and c) and linewidths (d, e and f) with the addition of $NH_4^+$ (a and d), $Na^+$ (b and e) and $Mg^{2+}$ (c and f) to 100 mM NaCho at pH 7.4

NaCl: Overall, just as with 50 mM NaCho solutions, as the salt concentration increased, δ's decrease (negative Δδ). This is an indication of shielding of chosen protons. The changes in chemical shifts were smaller relative to those seen for 50 mM NaCho (see Figure 5-2b).

$MgCl_2$: As observed for the 50 mM NaCho solution, $MgCl_2$ resulted in the greatest decrease in chemical shift. An increase to 0.6 M $MgCl_2$ led to precipitation of NaCho micelles (see Figure 5-2c).

*b) Changes in linewidth.* Figure 5-2 shows the changes in linewidth for chosen resonances for 100 mM NaCho solutions at pH 7.4.

$NH_4Cl$: In the first addition of $NH_4Cl$, there is an initial narrowing of resonances, as ionic strength increases, slight broadening is observed (see Figure 5-2d).

NaCl: In the presence of NaCl, linewidths decreased as the salt concentration increased; line narrowing was not as significant as observed in the presence of $NH_4Cl$. At 0.3 M NaCl and above, line broadening was observed (see Figure 5-2e).

$MgCl_2$: As $MgCl_2$ is introduced, a decrease in linewidth is observed (see Figure 5-2f). Unlike the other salts, $MgCl_2$ has the greatest impact on linewidths causing significant broadening above 0.15 M concentrations.

**Effect of the addition of NaCl, $NH_4Cl$, and $MgCl_2$ to NaCho secondary micelles at pH 9.1.**

**1) Effect with 50 mM NaCho Solutions.**

*Changes in chemical shift.* Figure 5-3 presents changes in chemical shift for 50 mM NaCho solutions at pH 9.1. Similar to pH 7.4, changes in chemical shift show a decrease in the chemical shifts as the concentration of each salt increased. The degree of shielding is comparable to that seen at pH 7.4. As the concentration of $NH_4Cl$ increased, the

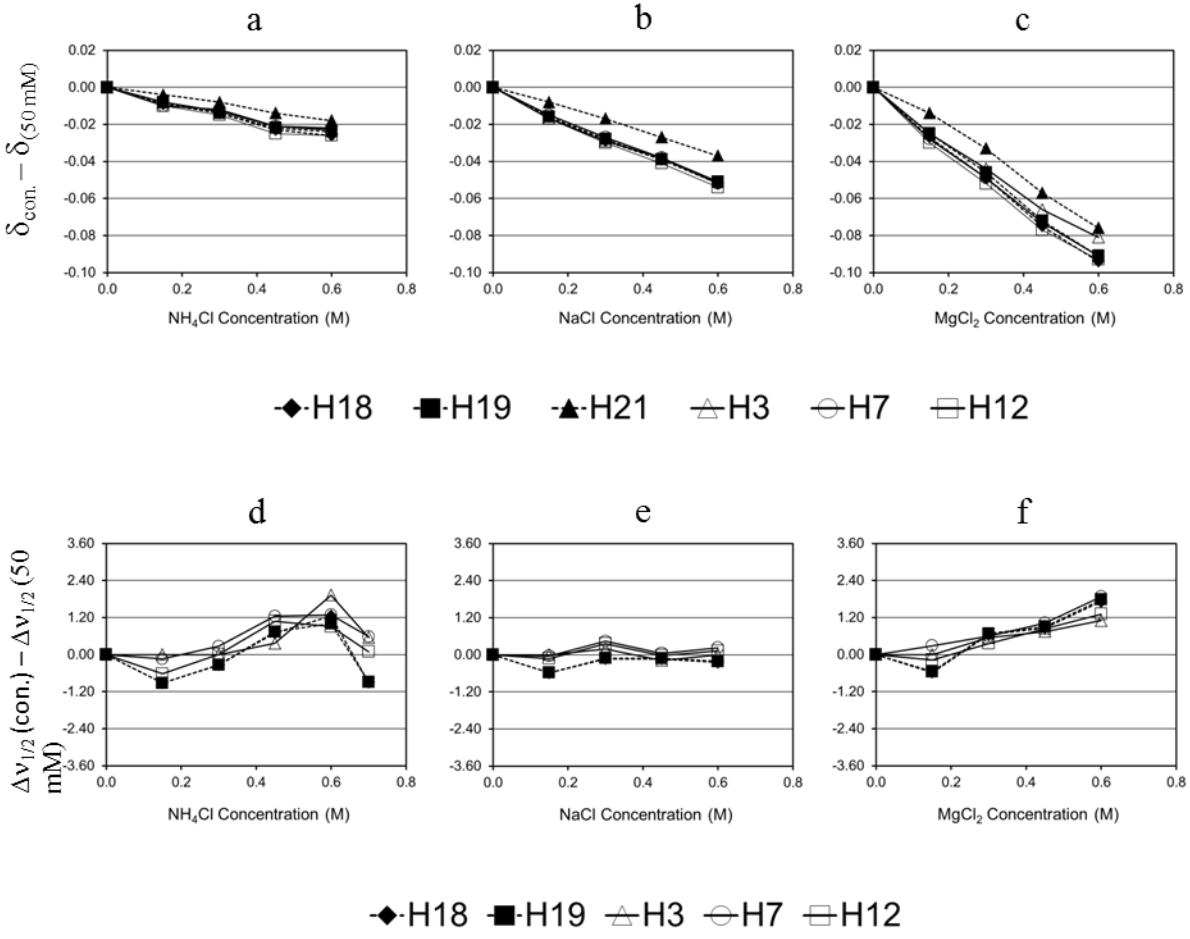


**Figure 5-3.** Changes in chemical shifts (a, b and c) and linewidths (d, e and f) with the addition of $NH_4^+$ (a and d), $Na^+$ (b and e) and $Mg^{2+}$ (c and f) to 50 mM NaCho at pH 9.1.

changes in chemical shift reached a plateau around 0.45 M (see Fig. 5-3a). As expected, $MgCl_2$ caused the greatest decrease in δ for the chosen resonances shown in Figure 5-3c.

*Changes in linewidth.* Figure 5-3 shows the changes in linewidth for the three salts in 50 mM NaCho solution at pH 9.1.

$NH_4Cl$: There were significant changes in linewidth for $NH_4Cl$; in the first addition, the chosen resonances became slightly narrower (see Figure 5-3d). Further additions caused broadening of resonances. Above 0.45 M, the resonances decrease their linewidths. H3 was the exception; only small changes in linewidth were observed as the salt concentration was increased.

NaCl: Smaller changes in linewidth were shown with NaCl addition; resonances corresponding to methyl protons became narrower with the first addition of NaCl (see Figure 5-3e). Above 0.3 M NaCl only slight changes in linewidth were observed.

$MgCl_2$: Similar to the trends seen for NaCl, the first addition of $MgCl_2$ resulted in decreases in linewidth for methyl protons. As the concentration of $MgCl_2$ increased to 0.6 M, significant broadening was observed (see Figure 5-3f).

**2) Effect of 100 mM NaCho Solutions.**

*Changes in chemical shift.* Figure 5-4 shows changes in chemical shifts for solutions of 100 mM NaCho with each of the three salts at pH 9.1. As expected, the chosen resonances decreased their chemical shift as the salt concentration increased. The overall changes in chemical shifts for the three salts are slightly less than those observed for the 50 mM solution of NaCho at pH 9.1. The greatest changes in chemical shift occurred with $MgCl_2$. Above 0.45 M $MgCl_2$, the changes in chemical shifts are not shown due to micelle precipitation.

*Changes in linewidth.* Figure 5-4 shows the changes in linewidth for 100 mM NaCho in the presence of the three salts at pH 9.1.

$NH_4Cl$: Minor changes for chosen resonances were observed for $NH_4Cl$; the first and second additions of $NH_4Cl$ resulted in a decrease in linewidth (see Figure 5-4d).

Above 0.3 M $NH_4Cl$ concentrations, an increase in linewidth is observed and begins to plateau around 0.6 M.

NaCl: Overall, as the concentration of NaCl increases, resonances were slightly broadened (see Figure 5-4e).

$MgCl_2$: Significant changes in linewidth for the chosen resonances were observed in the presence in $MgCl_2$. The greatest change in linewidth occurred between 0.3 and 0.45 M $MgCl_2$ (see Figure 5-4f). The changes in linewidths for 0.45 M are not included in the graph because they were beyond the scale of the graph. The scale was not changed in order to easily compare the changes in linewiths with the other salts studied. These actual values can be found in the supplemental information. Above 0.45 M micelles precipitation was observed.

**Cation size and charge at pH 7.4:**

To explore the impact of ionic diameter and charge on NaCho secondary micelles; the electrolytes chosen in this study include $NH_4^+$, $Na^+$, and $Mg^{2+}$ with ionic diameters of 296, 204, and 144 pm, respectively. In this study, changes in chemical shift ($\Delta\delta$) and linewidths ($\Delta\nu_{1/2}$) were evaluated and were interpreted with the aid of the theoretical predictions presented in Chapter 2.

*Postulates of possible interactions between $NH_4Cl$, NaCl, and $MgCl_2$ with 50 mM NaCho:*

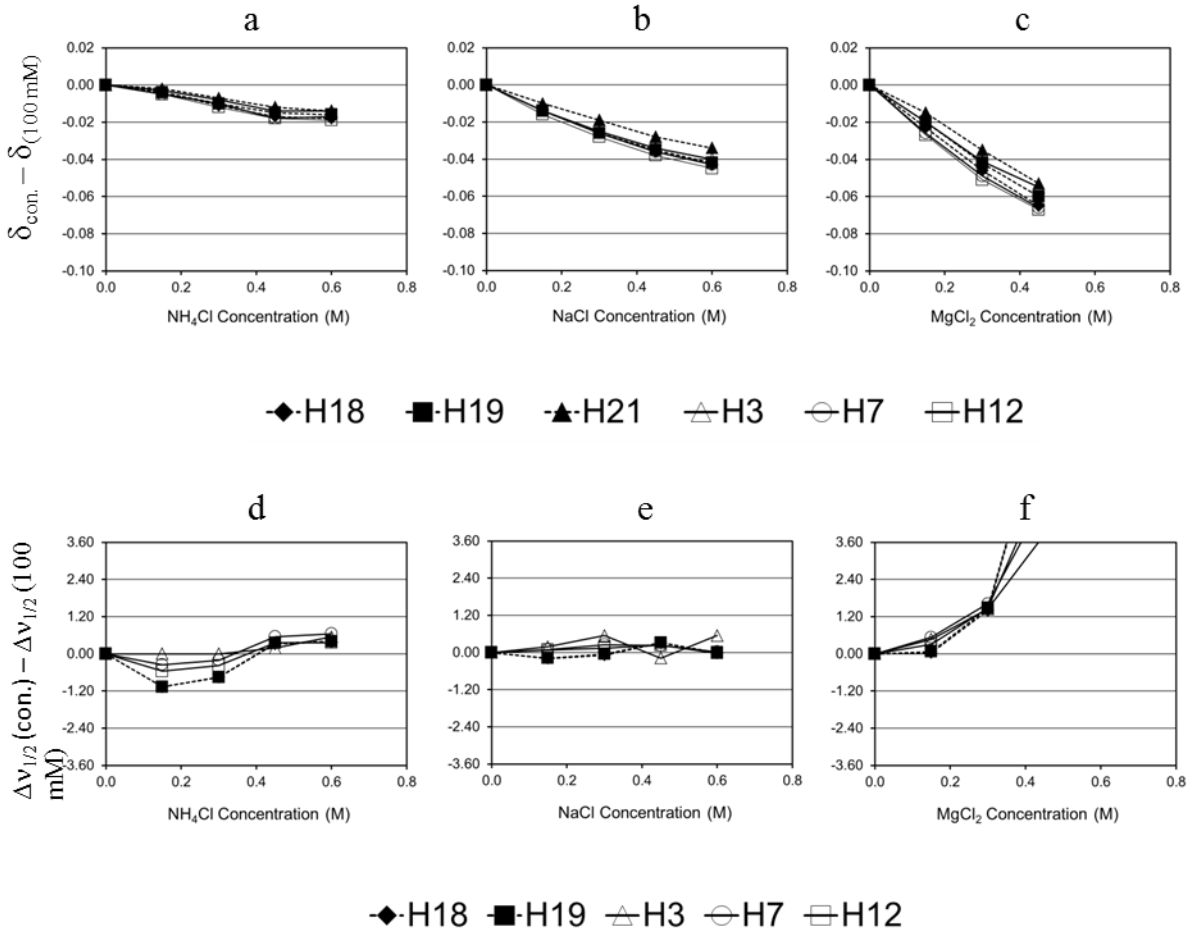


**Figure 5-4.** Changes in chemical shifts (a, b and c) and linewidths (d, e and f) with the addition of $NH_4^+$ (a and d), $Na^+$ (b and e) and $Mg^{2+}$ (c and f) to 100 mM NaCho at pH 9.1.

At 50 mM, both primary and secondary micelles of NaCho co-exist. Although the relative amounts of primary and secondary micelles are not known at this concentration, we have reported that no further changes in chemical shifts and linewidths were observed after a concentration of 100 mM is reached[71], suggesting that only secondary micelles are present at 100 mM and above. In this study we compared chemical shifts and linewidths observed at 50 mM with those reported at 20 mM NaCho (primary micelles) and 100 mM NaCho (secondary micelles). As the electrolyte concentration was increased, changes in chemical shifts and linewidths were calculated with respect to the values recorded without the addition of salt. We selected those resonances because they are well resolved and are associated with key protons in NaCho. H3 is in the head of the molecule, H7 and H12 are connected to C7 and C12, where the OH proposed to form a central H-bonding belt are attached. H18 and H19 are related to the methyl protons located in the hydrophobic core of the micelles. H21 corresponds to the methyl group that is more exposed to the hydrophylic face of NaCho. H21 was not included in linewidth studies due the splitting pattern and spectral overlap with the H1a resonance.

Regarding changes in chemical shifts, the trends observed—overall decrease in $\delta$, or shielding of the corresponding protons—were comparable to those observed with primary micelles undergoing similar variations in salt concentration. However, each electrolyte caused different changes in linewidths suggesting that cation size and charge cause significant variations in the degree of micellar compactness, as discussed next.

$NH_4Cl$: With the first addition of $NH_4Cl$, decreases in linewidths were observed for all resonances except H3, whose linewidth did not change significantly upon addition of $NH_4Cl$. Since H3 is believed to be located at the top and bottom of primary and secondary micelles, this suggests $NH_4^+$ ions are not interacting with these specific areas

in NaCho micelles. On the other hand, the linewidths for H7 and H12 became narrower suggesting that $NH_4^+$ ions are interacting with the lone pairs of the oxygens in the hydroxyl groups at C7 and C12. As a result, the hydrogen-belt network is weakened and the primary and secondary micelles are more loosely packed causing the narrowing of these resonances. As the micelle central-belt is disrupted the linewidths of the three methyl resonances also decreased suggesting the loosening of the hydrophobic core of the NaCho micelles.

At concentrations above 0.30 M $NH_4Cl$, broadening was observed for each of the chosen resonances. This effect may be due to the tightening of primary/secondary micelles or due to association of primary micelles into secondary micelles. NMR spectral changes alone cannot discern which possibility prevails but we favor greater association due to the reduction of the screening effect.

NaCl: With the first addition of NaCl interesting changes in linewidth were observed. H3 became broader; such a trend was not observed for primary and secondary micelles upon addition of $NH_4Cl$. This observation suggests the interaction between $Na^+$ ions and either the $COO^-$ and/or OH-3 groups located at the tops and bottoms of primary micelles. H7 and H12 showed decreases in linewidth similar to those seen for secondary micelles (100 mM) but to a lesser magnitude. These decreases suggest that $Na^+$ ions are weakening the central hydrogen-bond belt network. The disruption of the central belt has a significant impact on the loosening of the micelles core (H18 and H19). Overall, $Na^+$ ions disrupt all areas (top/bottom and central H-bond belt) in NaCho micelles unlike trends seen with the addition of $NH_4Cl$ that only had a significant impact around the central H-bond belt. $Na^+$ ions effectively interact with $COO^-$ due to a smaller ionic

diameter whereas; $NH_4^+$'s size and dispersed charge reduces or eliminates such interactions.

At 0.30 M NaCl, the resonances for H3 as well as H7 and H12 became slightly narrower. This indicates that $Na^+$ ions are beginning to disrupt the central belt to a greater extent than the top and bottom of the micelles. This effect is also reflected through the significant decrease in methyl resonances. The degree of impact with the first addition of salt is less than $NH_4^+$ ions due to $NH_4^+$'s larger size. However, $Na^+$ ions continue to cause disruptions on hydrogen-bond networks until 0.45 M NaCl is reached; unlike tends observed with $NH_4Cl$. This disruption causes the loosening of primary and secondary micelles; it is also possible secondary micelles are breaking apart into primary micelles. Above 0.45 M, all resonances began to broaden, particularly those associated with H18 and H19. H3, H7, and H12 resonances did not broaden to values of 50 mM NaCho in the absence of salt, suggesting the H-bond networks are not as tight. Similar to trends observed with $NH_4^+$ ions, association of primary to secondary micelles is most plausible due to the weakening of the screening effect. The degree of broadening achieved at 0.6 M NaCl is not as significant as seen with $NH_4Cl$. This may be due to the greater disruption caused by NaCl that could lead to an increase in the number of primary micelles. Therefore, the number of exposed negative charges is expected to be greater with NaCl compared to that in the presence of $NH_4Cl$. Even at this high concentration of NaCl, it is possible that the amount of $Na^+$ ions in solution is not enough to screen the increased number of negative charges. As a result, the association of primary micelles into secondary micelles may be less than $NH_4Cl$ based on the degree of broadening for chosen resonances. However, overall association of primary micelles is expected to be greater

with $Na^+$ ions since they are more effective at reducing electrostatic charges around the top and bottom of micelles due to its smaller ionic diameter.

$MgCl_2$: The addition of $Mg^{2+}$ ions caused the largest decrease in linewidths compared to the other salts. Linewidths decreased for all resonances with the first addition of $MgCl_2$ particularly for the three methyl resonances. $Mg^{2+}$ ions disrupt all areas of NaCho micelles similar to NaCl. This trend is unlike trends seen in 20 mM NaCho primary micelles suggesting the loosening of secondary micelles outweighs the tightening of primary micelles seen at 20 mM NaCho. Secondary micelles become loosened through disruption of hydrogen-bonding networks that hold the secondary micelle assembly together. Compared to the other two salts, $Mg^{2+}$ ions are more effective at disrupting micelles as seen in the significant decreases in linewidths for all resonances.

At 0.3 M $MgCl_2$ concentrations, linewidths increased for all resonances. It is possible that this broadening is caused by a less effective screening effect causing the association of primary micelles. Due to the disruption observed at lower concentrations of $MgCl_2$, the amount of primary micelles present may also increase, similar to the effect seen with NaCl. Greater additions of $Mg^{2+}$ did not affect the linewidths significantly. It is possible that the small $Mg^{2+}$ ions can enter into secondary micelles; as a result, primary micelles may be pushed further apart from one another. This effect may be due to the buildup of positive charges. This could result in repulsive forces that keep NaCho primary micelles farther apart from each other thus resulting in a looser secondary micelle. However, this effect is not creating further decreases in linewidths but it is inhibiting the association of primary micelles into secondary micelles.

*Postulates of possible interactions between $NH_4Cl$, NaCl, and $MgCl_2$ with 100 mM NaCho:*

At concentrations of 100 mM NaCho only secondary micelles are present. Similar to 50 mM NaCho, changes in chemical shifts followed the expected trends (decrease in δ); therefore, the focus of this discussion will focus on changes in linewidths as each salt is introduced as well as interpretations for interactions between the various cations and secondary micelles.

$NH_4Cl$: As $NH_4Cl$ was introduced, narrowing of chosen resonances was observed. This effect may be a result of $NH_4^+$ ions being attracted to hydroxyl lone pairs, resulting disruption or weakening hydrogen-bond networks. If $NH_4^+$ ions are in the vicinity of the central H-belt; this could result in loosening of the hydrophobic core indicated by the narrowing of methyl resonances. Indeed methyl resonances were impacted the greatest by the first addition of $NH_4Cl$, as a result, secondary micelles are loosened (see Figure 5-5b). Slight increases in linewidth were observed as the concentration of $NH_4Cl$ increased from 0.3 to 0.60 M (see Figure 5-5c). However, the broadening observed never reached the linewidth values of 100 mM NaCho in the absence of salt. Also, the degree of broadening was significantly less than that seen at 50 mM NaCho concentrations; this may be due to the increased ratio of NaCho to salt concentration.

NaCl: Similar to trends observed with $NH_4Cl$, resonances became narrower with the first addition of NaCl (decrease $\nu_{1/2}$). $Na^+$ ions continued to cause narrowing for all resonances as NaCl was increased to 0.3 M (see Figure 5-5b). Above 0.45 M NaCl, resonances showed slight broadening but never reached the linewidth measured for 100 mM NaCho with no additional salt (see Figure 5-5c). At higher concentrations of NaCl, the degree of broadening observed for all resonances was greater than that observed for

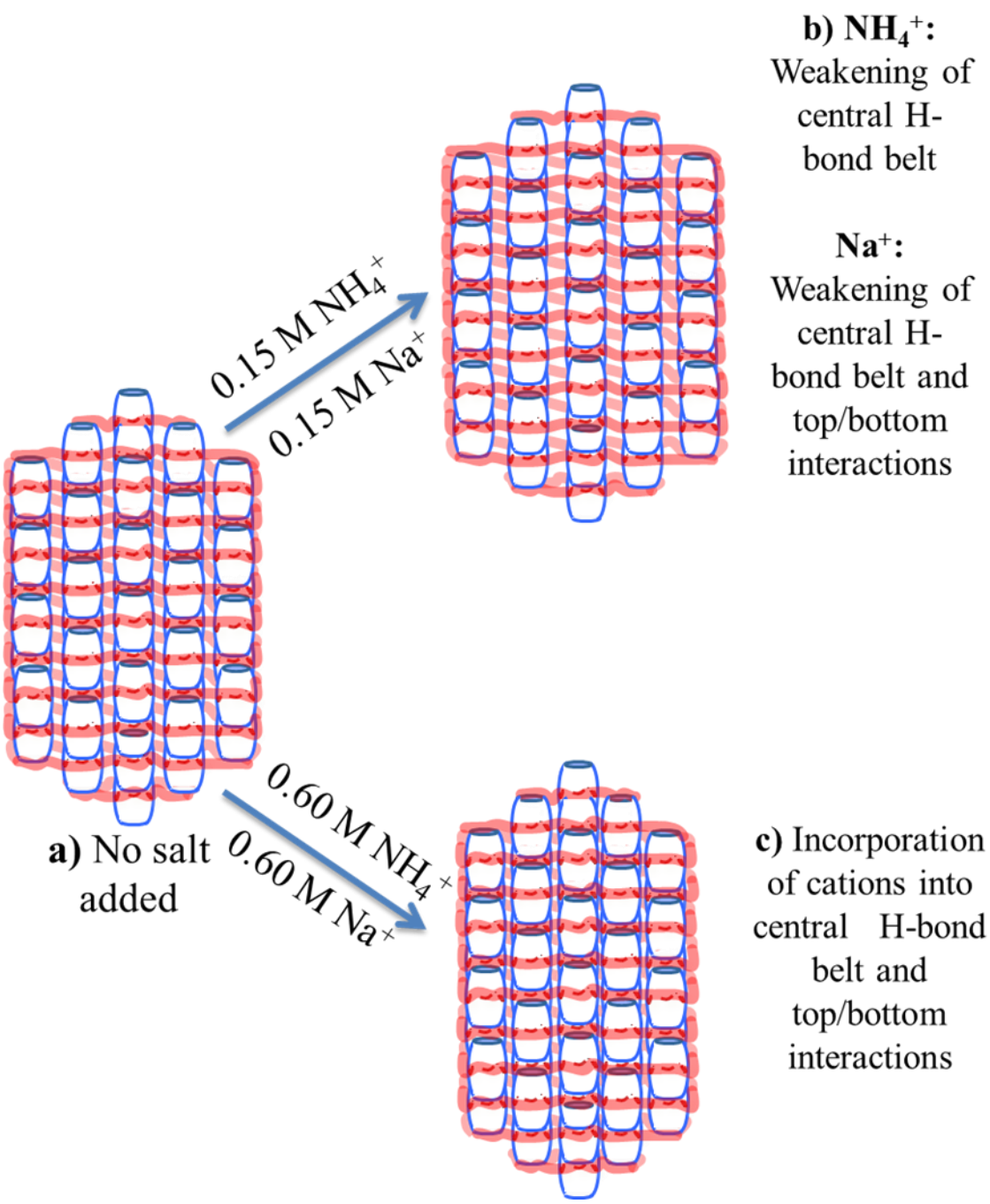


**Figure 5-5**. a) Secondary micelle in the absence of salt b) Cartoon showing $NH_4^+$ and Na+ ions weakening the hydrogen- bonding networks and c) cations are incorporated into these networks resulting in a more compact secondary micelle.

similar concentrations of $NH_4Cl$. This difference in broadening may be due to $Na^+$ ions having a centrally located charge thus, minimizing the screening effect more efficiently. As a result, tighter secondary micelles are formed.

$MgCl_2$: The first addition of $MgCl_2$ produced results similar to those seen with $NH_4^+$ and $Na^+$ ions. However, $Mg^{2+}$ ions resulted in greater decreases in linewidth. The three methyl resonances become significantly narrower than other resonances; this may suggest loosening of secondary micelles (see Figure 5-6b). Above 0.15 M $MgCl_2$ significant broadening for the chosen resonances was observed. Broadening may be caused by either or both aggregation as the $Mg^{2+}$ ions shield the negative charges of COO- and allow for micelles to associate together, and/or the tightening of secondary micelles due to $Mg^{2+}$ becoming incorporated into the hydrogen-bonding networks forming a metal ion-dipole network (see Figure 5-6c). Although both effects may occur simultaneously, aggregation is proposed to be the main cause of line broadening. Indeed, as the concentration of $MgCl_2$ increased from 0.45 to 0.6 M, precipitation of secondary micelles was observed.

**Cation size and charge at pH 9.1:**

*Postulates of possible interactions between $NH_4Cl$, NaCl, and $MgCl_2$ with 50 mM NaCho:*

Similar to the studies at pH 7.4, changes in $\delta$ and $\nu_{1/2}$ were calculated at 50 and 100 mM NaCho with respect to the values recorded in the absence of salt. The trends observed in the $\delta$'s were comparable to pH 7.4 for each NaCho concentration. Increasing salt concentration resulted in the shielding of chosen protons (decrease $\delta$) and as expected, $Mg^{2+}$ ions caused the greatest degree of shielding. However, changes in linewidth varied for each electrolyte, as also seen at pH 7.4, suggesting cation size and

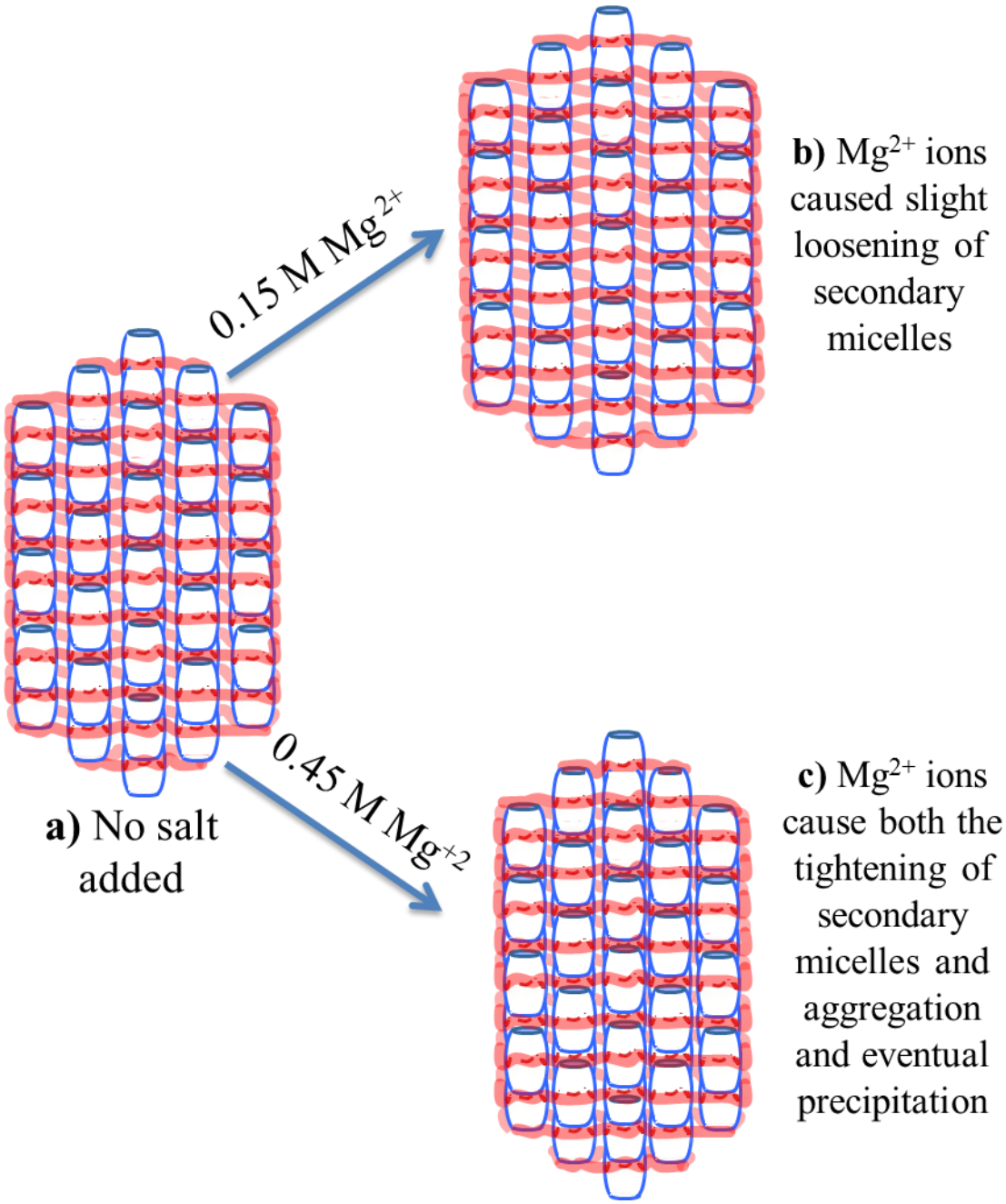


**Figure 5-6.** a) Secondary micelle in the absence of salt b) Cartoon showing at 0.15 M $MgCl_2$, $Mg^{2+}$ ions loosen secondary micelles and c) Above 0.45 M $MgCl_2$, tighter secondary micelles are formed due to the incorporation of $Mg^{2+}$ ions. Aggregation of secondary micelles is also present.

charge play a key role in altering NaCho micelles. Before presenting the interpretations of $\nu_{1/2}$ for each cation, it is relevant to point out that at pH 9.1, the narrower resonances observed suggest that primary and secondary micelles are looser when compared to pH 7.4 (see Figure 5-7). The loosening effect observed at pH 9.1 may be due to the attractions between excess hydroxide ions in solution with hydroxyl groups in NaCho micelles positioned at C3, C7, and C12. This may lead to the weakening of the hydrogen-belt network causing the overall loosening of micelles, including the hydrophobic core, as indicated by narrowing of the resonances for the methyl protons H18 and H19.

$NH_4Cl$: After the first addition of $NH_4Cl$, the linewidths decreased, except for H3. The narrowing of H7, H12, and the three methyl groups suggests secondary micelles are becoming loosened. At this higher pH, excess hydroxide ions are present in solution and are expected to be in the vicinity of the hydrogen-belt network. In the presence of $NH_4Cl$, it is anticipated $NH_4^+$ ions to be attracted to hydroxide ions therefore, causing further disruption around the central hydrogen-belt. Above 0.15 M $NH_4Cl$ linewidths increased, indicating the transition of primary micelles associating into secondary micelles as well as the tightening of secondary micelles. The linewidth for H3 does not significantly increase until 0.45 M $NH_4Cl$, where it began to increase following the other resonances. The linewidths measured for 50 mM NaCho with 0.45 and 0.6 M $NH_4Cl$ were compared to the linewidths for primary and secondary micelles without the addition of salt. The resonances were broader for 50 mM NaCho with 0.45 and 0.6 M $NH_4Cl$ than for secondary micelles. This indicates that at higher salt concentrations secondary micelles are becoming more compact. The tightening of secondary micelles may be due to the incorporation of $NH_4^+$ ions into the hydrogen-bonding networks that hold the primary micelles within the secondary micelles assembly.

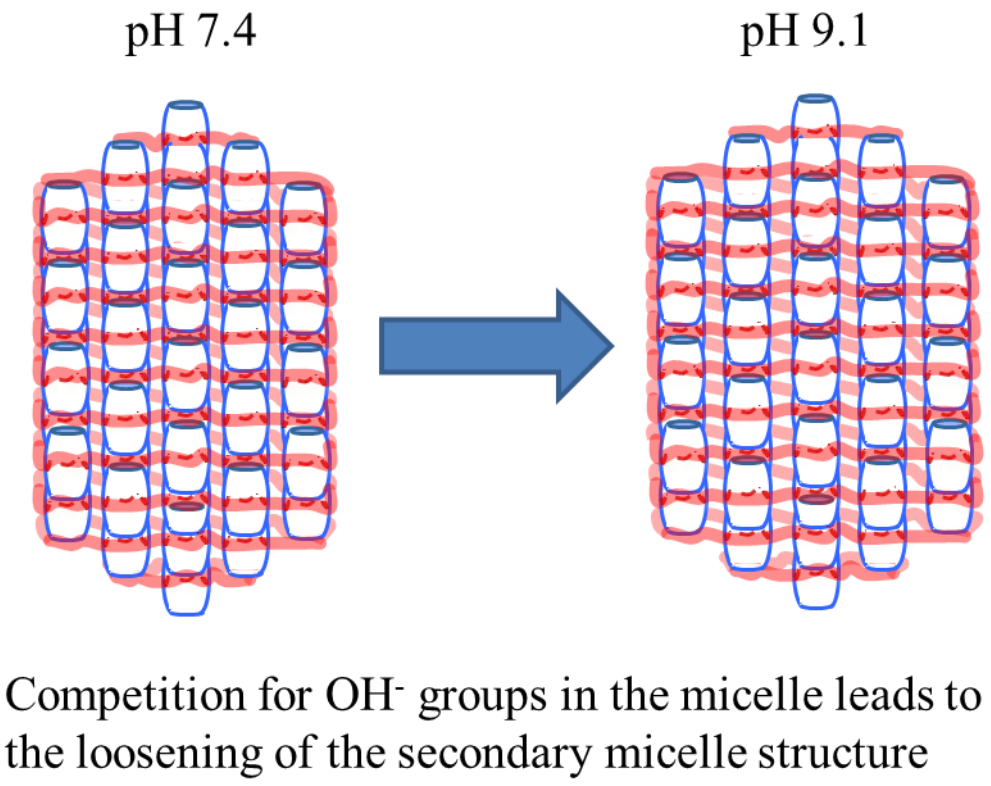


**Figure 5-7.** Secondary micelle in the absence of salt for pH 7.4 and 9.1. At pH 9.1 the presence of OH- ions leads to the overall loosening of the secondary micelle structure.

NaCl: In the presence of 0.15 M NaCl, slight decreases in linewidth occurred for the resonances related to H3, H7, and H12. Decreases in the three methyl resonances were also observed. This indicates loosening of the secondary micelle core. As the concentration of NaCl increased, the resonances slightly broadened suggesting incorporation of $Na^+$ ions in the hydrogen-bond networks and the tightening of the central hydrogen-bond belt (by metal ion-dipole interactions) and/or association of primary micelles into secondary micelles. With the last addition of NaCl, all resonances did not show significant changes in linewidth.

$MgCl_2$: Decreases in linewidth were observed for the three methyl resonances and H12. The linewidth of H3 remained the same but H7 increased its linewidth. The $\nu_{1/2}$ seen after the first addition of $MgCl_2$ was similar to recorded values of primary and secondary micelles; overall $Mg^{2+}$ ions are creating looser secondary micelles by interacting with H-bonding networks holding the secondary micelles together. Above 0.3 M $MgCl_2$, resonances broadened significantly; the impact with $Mg^{2+}$ ions was greater than the other two cations. This effect may be due to the doubly charged nature of the $Mg^{2+}$ ion that can effectively minimize the screening effect. At higher $Mg^{2+}$ concentrations, association of primary micelles and the tightening of secondary micelles may both occur as reflected by the significant increases in linewidth for all resonances.

*Postulates of possible interactions between $NH_4Cl$, NaCl, and $MgCl_2$ with 100 mM NaCho:*

$NH_4Cl$: Unlike the other two salts, the first addition of $NH_4Cl$ caused the narrowing of chosen resonances; and similar to 50 mM NaCho at pH 9.1, the methyl resonances (H18 and H19) were impacted the greatest. This effect may be due to the size of $NH_4^+$ ions; with its larger ionic diameter it can cause greater disruption around the

central hydrogen belt thus, resulting in the loosening of the hydrophobic core in secondary micelles (see Figure 5-8b). Above 0.15 M $NH_4Cl$, the linewidths began to increase and at higher concentrations resonances broaden slightly more than 100 mM NaCho without additional salt; suggesting the tightening of secondary micelles (see Figure 5-8c). This trend begins to plateau around 0.6 M $NH_4Cl$; this may be due to the amount $NH_4Cl$ compared to the increased amount of NaCho relative to 50 mM NaCho.

NaCl: As NaCl is introduced to secondary micelles, slight changes in linewidths were observed; all resonances increased in linewidth except for H18 and H19. This suggests the beginning of the formation of tighter secondary micelles. Above 0.15 M NaCl, resonances broadened with increasing salt concentration; this may be due to the incorporation of $Na^+$ ions into the central hydrogen-belt network through metal ion-dipole interactions as well as around the top and bottom of the micelles leading to the tightening of secondary micelles. Changes in linewidth were not as significant as seen in 50 mM NaCho at similar pH; this may be due to high NaCho concentrations consisting of secondary micelles carrying an overall negative charge. Therefore, it would take higher concentrations of NaCl (above 0.6 M) to see increased broadening or further aggregation that would lead to precipitation.

$MgCl_2$: In the presence of $MgCl_2$, linewidths increased after the first addition of $MgCl_2$ for all resonances, unlike the trends seen for $NH_4^+$ and $Na^+$ ions. Significant broadening was observed between 0.30 and 0.45 M (see Figure 5-10b). As mentioned with NaCl, the presence of the greater negative charge at these NaCho concentrations requires higher salt concentrations. $Mg^{2+}$ is an exception due to its double charge; in fact, with higher $MgCl_2$ concentrations $Mg^{2+}$ ions can overcome the screening effect that holds secondary micelles apart. This effect was observed at and above 0.45 M $MgCl_2$ where

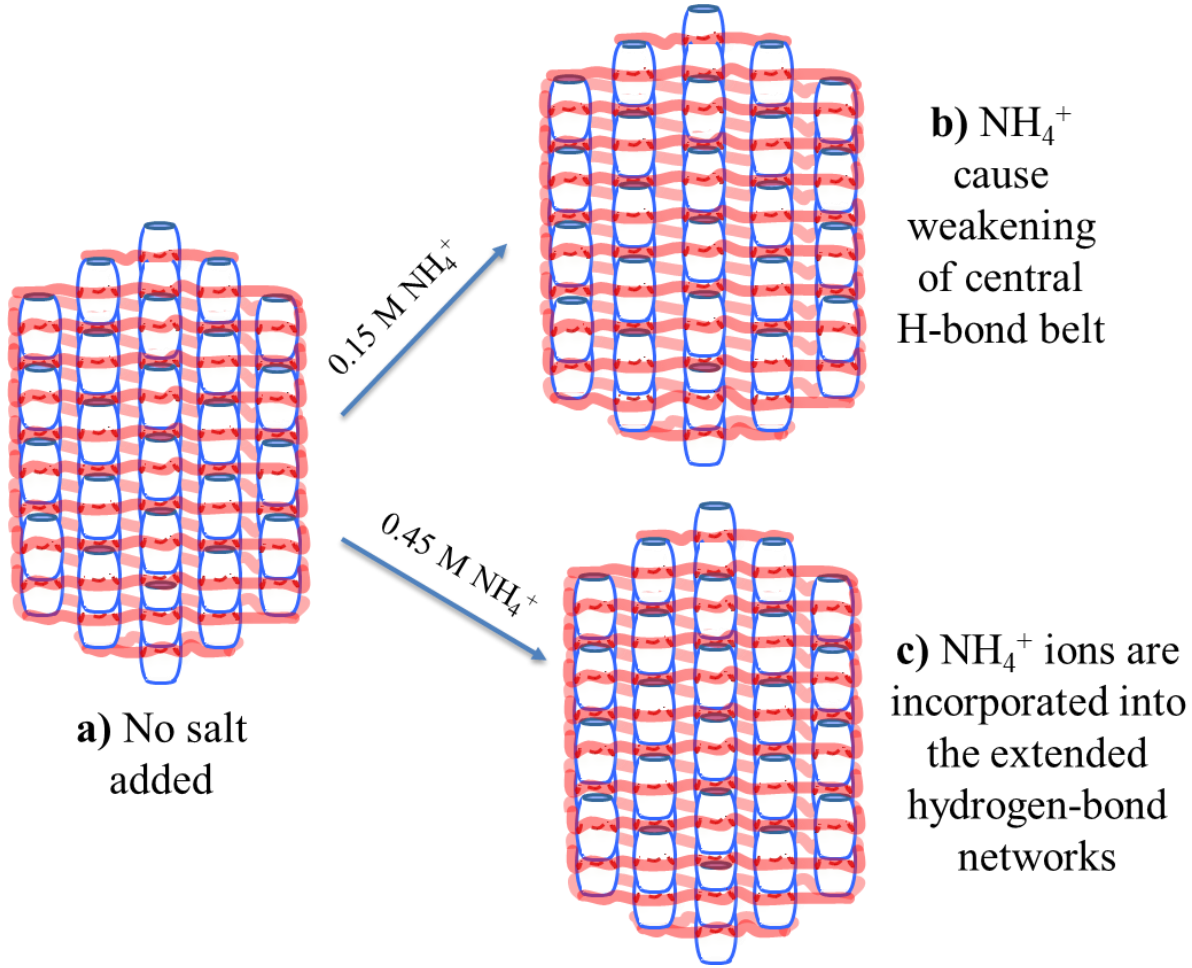


**Figure 5-8.** a) Secondary micelle in the absence of salt at pH 9.1 b) Cartoon showing at 0.15 M $NH_4Cl$ , $NH_4^+$ ions loosen secondary micelles and c) Above 0.45 M $NH_4Cl$, tighter secondary micelles are formed due to the incorporation of $NH_4^+$ ions into the extended hydrogen-bond networks.

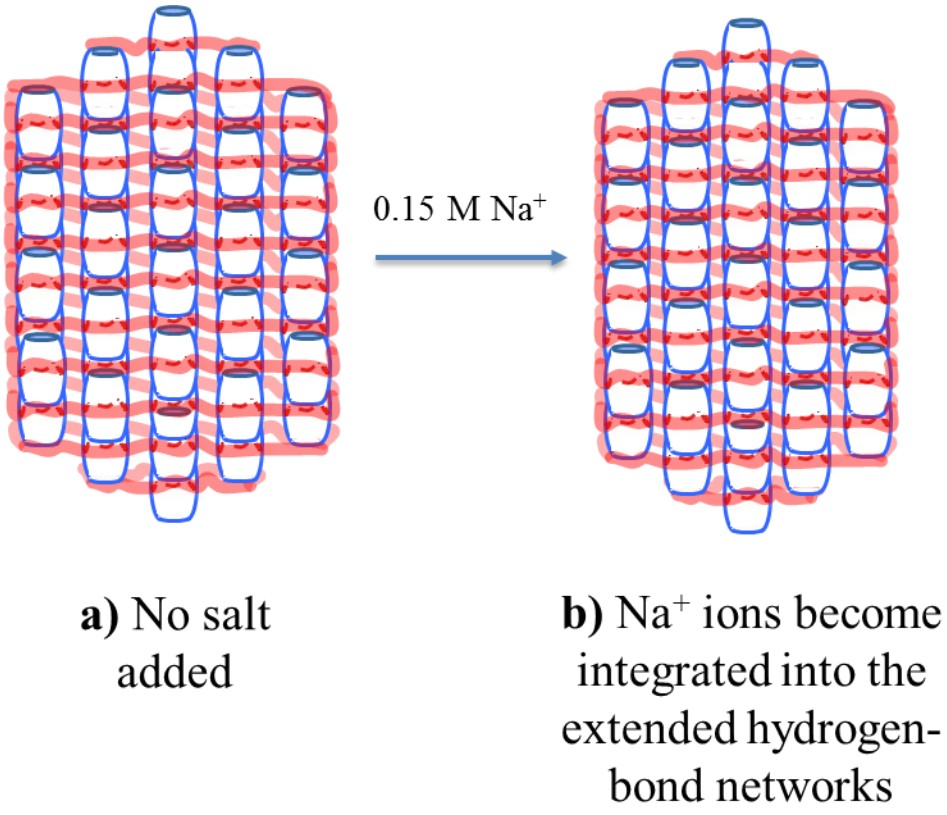


**Figure 5-9**. a) Secondary micelle in the absence of salt at pH 9.1 b) Cartoon showing at 0.15 M NaCl, tighter secondary micelles are formed due to the incorporation of $Na^+$ ions into the extended hydrogen-bond networks.

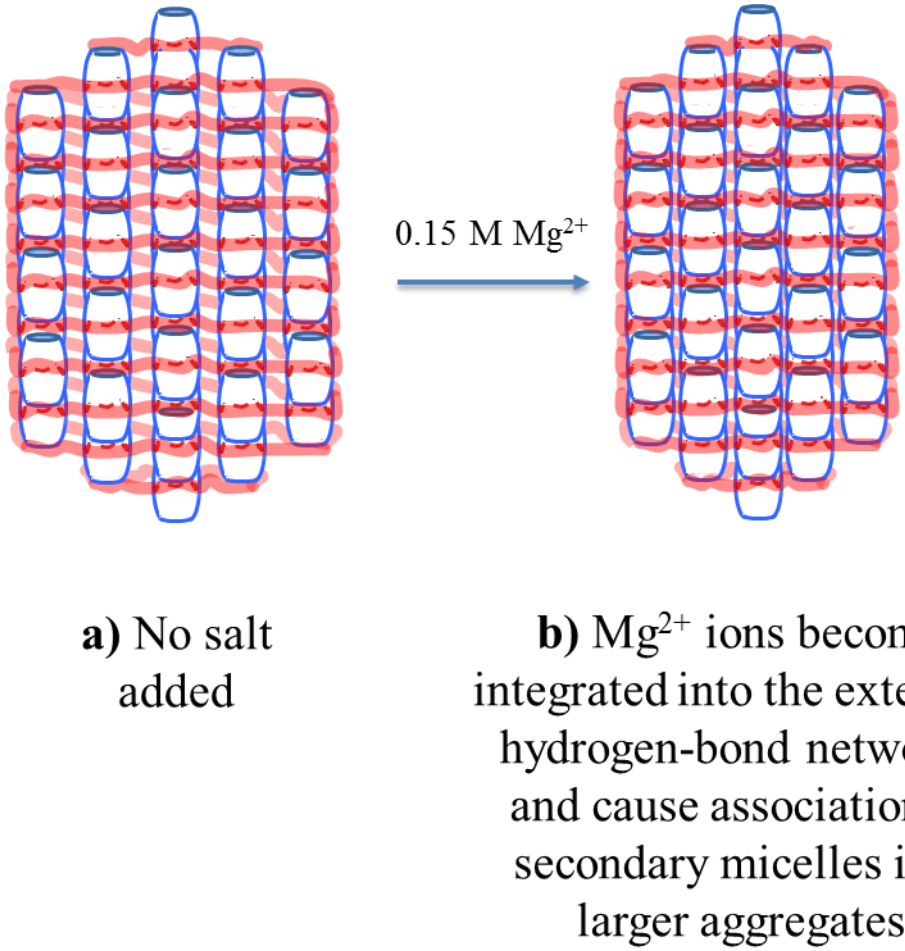


**Figure 5-10.** a) Secondary micelle in the absence of salt at pH 9.1 b) Above 0.15 M $MgCl_2$, $Mg^{2+}$ ions cause association of secondary micelles into larger aggregates. Above 0.45 M $MgCl_2$ precipitation of secondary micelles is observed.

solutions became cloudy due to association of secondary micelles into larger aggregates. This effect is represented by the larger increases in linewidth seen at 0.45 M $MgCl_2$. As these aggregates become larger, micelles begin to precipitate out of solution; this is also supported by visual observations.

## CONCLUSIONS

At 50 mM NaCho primary and secondary micelles co-exist and at 100 mM NaCho, only secondary micelles are present. The following conclusions are limited to the results obtained for 100 mM NaCho because at this concentration only secondary micelles are present.

Comparing the three salts, $NH_4^+$ and $Na^+$ ions caused the greatest disruption of the extended hydrogen-bond belt; this suggests that the size of the ion affects the degree of disruption. As the concentration of monovalent cations increased it is possible these cations cause the tightening of secondary micelles. It is possible that the cations enter the secondary micelles and become integrated into the extended hydrogen bonding networks (by metal ion-dipole interactions) and reinforces them. As expected, $Mg^{2+}$ showed the greatest decrease in chemical shifts compared to the other salts studied. The smaller ionic diameter and larger charge density of $Mg^{2+}$ accounts for the more effective reduction in the screening effect that keep secondary micelles from aggregating. Indeed, $Mg^{2+}$ caused the tightening of secondary micelles and at high $MgCl_2$ concentrations micelle aggregation and eventual precipitation were observed.

The major findings of these studies demonstrate that the tightening or loosening of secondary micelles can be modified by changes in pH and salt concentration. It would

be beneficial to investigate simultaneously the aggregation number and monitor micellar growth as the salt concentration increases for both mono- and divalent cations.

# CHPATER 6

# CONCLUSIONS AND FUTURE DIRECTIONS

The studies included in this dissertation explored the molecular organization of primary and secondary micelles of sodium cholate (NaCho), one of the most abundant primary bile salts produced in our bodies. These micelles were studied at physiological pH and in the absence of additional salts first. In addition, primary and secondary micelles have been studied in the absence of and in the presence of mono- and divalent cations at neutral and basic pH. The impact of salt concentration was explored to understand how primary and secondary micelles interact with cations that vary in size and charge. From nuclear magnetic resonance (NMR) spectral changes in chemical shift and linewidth, the interactions between the different cations ($NH_4^+$, $Na^+$, $Mg^{2+}$ and $Ca^{2+}$) were inferred and models to describe these interactions have been proposed and tested. The paragraphs below summarize the main conclusions of this project and provide possible directions for future research.

## New and Powerful of NMR spectrometer (700 vs 500 MHz)

NMR spectroscopy is an essential tool in chemistry for the characterization and determination of molecular structures. NMR spectroscopy was used throughout all the studies of NaCho primary and secondary micelles presented in this dissertation. Both a 500 and a 700 MHz NMR spectrometer were used to acquire one- and two-dimensional

spectral traces. All salt concentration and pH studies were acquired on the 500 MHz instrument to explore the impact of these parameters on primary and secondary micelles. Then, the presence of the 700 MHz NMR instrument studies on the molecular arrangements of NaCho primary and secondary micelles were obtained. The stronger magnet in this instrument provided greater spectral resolution and sensitivity in the measurements and allowed for faster acquisition times. In addition to the higher magnetic field, this instrument is equipped with a cryogenically cooled probe. This technological advancement enables a three- or four-fold enhancement in sensitivity compared to conventional probes.[72] The increased spectral resolution was crucial for the studies on the molecular arrangements of primary and secondary micelles because twenty-five resonances appear within a narrow spectral region between 1.0 and 2.3 ppm. 2D HSQC experiments examined through-bond interactions between two different types of nuclei ($^{1}H$ and $^{13}C$). This technique and the enhancement of sensitivity and spectral resolution achieved by the 700 MHz spectrometer allowed the confirmation and correction of NaCho assignments and importantly, each resonance could be followed at the various conditions tested. In addition, 2D NMR ROESY was applied to examine through-space interactions (< 5 Å) among NaCho protons in the monomer as well as in primary and secondary micelles. This information was used to test and validate the models proposed for the micellar arrangements.

**Theoretical Predictions**

NMR spectroscopy was applied to explore the changes that take place as NaCho monomers associate to form primary micelles (first micellization) and as primary micelle aggregate to form secondary ones (second micellization). The results from these studies were interpreted based on trends observed for chemical shifts calculated theoretically

using the polarizable continuum medium (PCM) approach for solvents with different dielectric constants. The analysis of these trends played a significant role in the interpretation of experimental data that, in turn, allowed for the postulation of molecular arrangements for primary and secondary micelles. These predictions showed the deshielding of most proton resonances (increase in δ) as the polarity of the solvent increased. However, these predictions showed opposite changes in chemical shift for protons on the hydrophilic face of the NaCho monomer. This is due to the presence of paramagnetic fields generated by lone pair electrons. In a non-polar environment, the oxygen lone pairs present in the OH groups at C3, C7, and C12 cause deshielding of neighboring protons. When the environment becomes more polar, these lone pairs interact with the solvent, thus reducing the deshielding of neighboring protons.

**Primary Micelle Model**

From the interpretations of changes in chemical shifts observed for NaCho protons as the first micellization process occurs, the barrel-like model was postulated for primary micelles. In this model, four (or six) NaCho monomers associate in an anti-parallel arrangement to form primary micelles. These micelles are held together by a central hydrogen-bond 'belt' that includes the hydroxyl groups (OH-7 and OH-12). At the top and bottom of the barrel, the monomers interact with their neighbors via ion-dipole and water-mediated H-bonds. For the first time, the barrel-like model postulated for primary micelles has been validated using through-space magnetization transfer 2D-NMR ROESY techniques. The results from these experiments place protons located on the head of the monomer in the proximity of protons on the tail of the neighboring monomer.

**Secondary Micelle Model**

Previous studies on bile salt micelles had been limited to primary micelles only. There has been little information offered on secondary micelles. A previous study on secondary micelles provided the concentration at which secondary micelles form and postulated (based only on the chemical features of bile salts) that primary micelles aggregate to form secondary ones through hydrogen bonding interactions.[10] In this dissertation, detailed studies on the molecular arrangements of secondary micelles have been presented. For the first time, a model has been proposed on the arrangement of primary micelles within secondary ones. In this model, primary micelles form stacks where the tops and bottoms of neighboring primary micelles are held together through H-bonding and ion-dipole interactions. These stacks interact with neighboring stacks in a staggered fashion and extended H-bonding belts surround the secondary micelle. Hydrogen-bonding plays an important role in the stabilization of these nanostructures.

This model has been partially tested using 2D-NMR ROESY techniques and further studies are needed to validate conclusively the postulated model for secondary micelles. It is proposed however that water pockets are present between the hydrophilic surfaces of primary micelles within the secondary micelles structure (see Figure 6-1). The size and geometry of these pockets are unknown but their study could be potentially useful for the incorporation of hydrophilic compounds that due to their polarity cannot traverse biomembranes. Possible approaches for such studies are mentioned later in this chapter.

**Intercalation of $NH_4^+$ and $Na^+$ into H-bond Belt**

Linewidth studies for NaCl and $NH_4Cl$ showed an overall narrowing of proton resonances suggestive of the loosening of primary micelles. In order for the micelle to

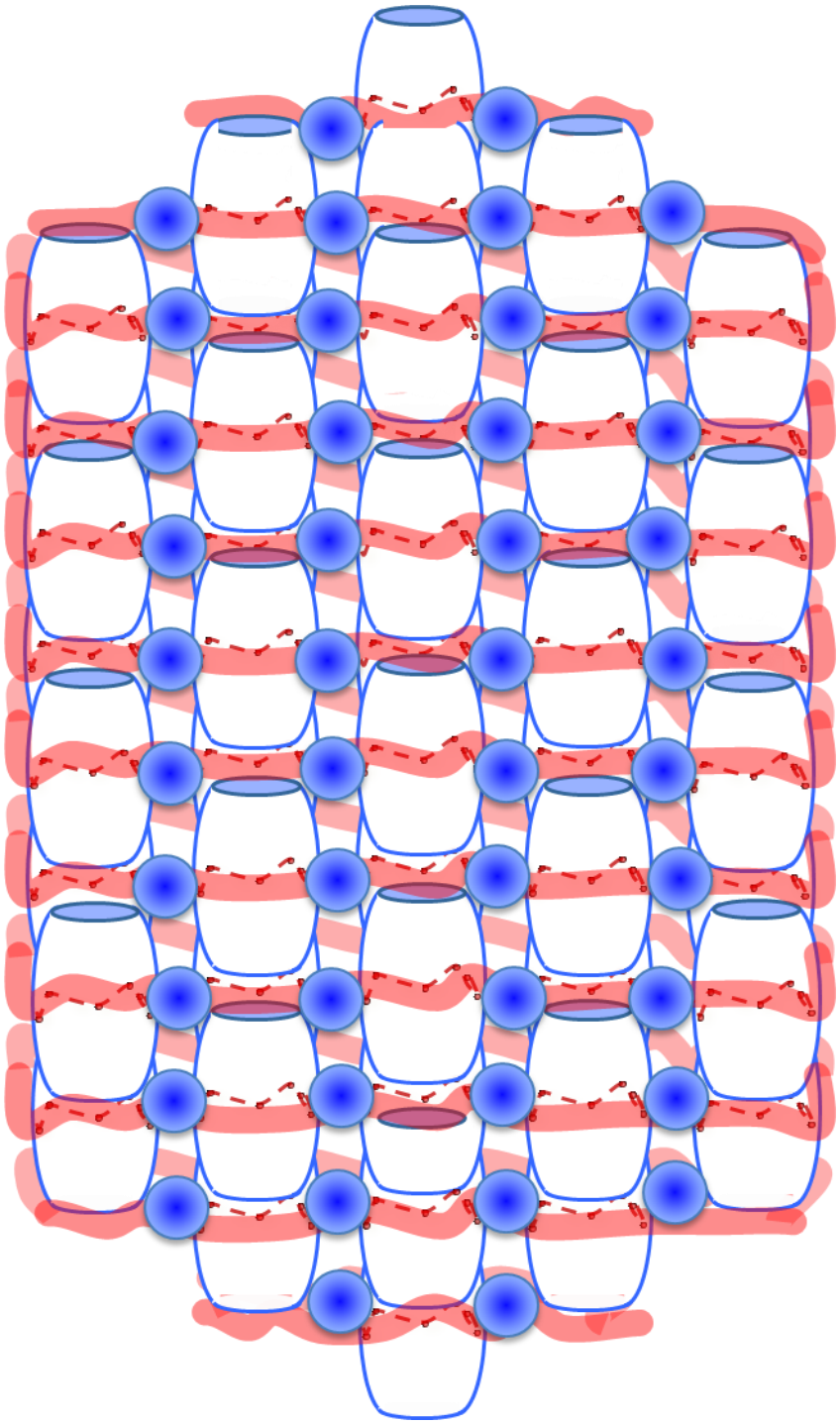

**Figure 6-1**: Proposed model for NaCho secondary micelles showing the presence of water pockets between the hydrophilic surfaces of primary micelles with in the secondary micelle structure.

expand, the hydrogen-bonding network involving the OH groups at C7 and C12 must be weakened or disrupted by $NH_4^+$ or $Na^+$ ions. However, as the salt concentration increased above 0.3 M, the $\Delta\upsilon_{1/2}$ increased indicating the formation of tighter primary micelles. This suggests that after the initial expansion of the micelles, $NH_4^+$ or $Na^+$ ions may be integrated within the hydrogen-bonding central belt as well as within the top and bottom networks and bring the micelle back to a more compact state.

**Aggregation and Precipitation with $Ca^{2+}$ ions**

The divalent cation, $Ca^{2+}$ caused a greater decrease in chemical shift compared to the monovalent cations studied. This is attributed to calcium's higher charge density and smaller ionic diameter that allows for a more effective reduction in the deshielding effect of $OH^-$ groups. Linewidth studies suggest that $Ca^{2+}$ ions lead to more compact micelles. However, $Ca^{2+}$ ions have a high affinity toward the $COO^-$ groups on NaCho located at the tops/bottoms of primary micelles. This interaction leads to the aggregation of primary micelles and at high $CaCl_2$ concentration, micelle precipitation was observed. Further studies are needed to determine the aggregation number of NaCho primary micelles as salt concentration is increased.

**Mg intercalation and tightening**

$MgCl_2$ caused initial broadening at low concentrations (< 0.3 M) and, at concentrations above 0.3 M, a decrease in linewidth was observed. This suggests the partial loosening of the micelles and may be attributed to the excess $Mg^{2+}$ ions that may compete for the OH groups in the H-bond-$Mg^{2+}$ central belt. As the OH groups interact with both internal and external $Mg^{2+}$ ions, the strength of the belt is reduced. At pH 9.1, at higher salt concentrations, the linewidths increased, suggesting that tighter micelles may be formed.

As mentioned in Chapter 4, it is unclear to determine if micelles are becoming more compact or aggregation occurs.

**Future Directions for the Use of Bile Salts as Drug Carriers**

Small hydrophobic molecules easily partition across lipid membranes. However, hydrophilic molecules require a selective transport system or they are otherwise unable to traverse biomembranes.[73] The ability to transport hydrophilic molecules for subsequent intracellular delivery is a difficult challenge but worth pursuing as many drug candidates contain polar moieties. Bile acids have been investigated as carriers of polar molecules.

Kahne and co-workers investigated bile acids derivatives as potential drug delivery transporters. They synthesized derivatives of cholic acid by attaching glucose units to hydroxyl groups on C7 and C12 creating additional hydrogen-bonding groups. As a result, the hydrophilicity of the polar surfaces on the amphiphile was altered. Their findings showed that the overall hydrophobicity of the molecule does not predict how efficient the bile acid will be at transporting polar molecules across the lipid bilayer. Indeed, the more hydrophilic, glycosylated compound was more effective in transporting polar molecules across the membrane. This study demonstrates the use of bile acids as capable transport agents for polar compounds.[73,74] However, the nature of the interactions between polar drug compounds and bile acids was not addressed.

Previous studies on the interactions between sodium cholate and adenosine triphosphate (ATP) revealed H-bonding interactions between ATP with the hydrophilic surface of NaCho primary micelles.[49] ATP was proposed to remain in the "self stacked" conformation allowing the adenosyl moiety of ATP to form H-bonds with the H-bonding central belt of NaCho primary micelles.

To further test the possibility of trapping ATP within the water pockets of secondary micelles, additional studies need to be completed. 2D NMR ROESY studies will provide information on where ATP is interacting with NaCho secondary micelles. We should be able to see new cross peaks between protons of ATP and NaCho if they are within 5Å. However, as mentioned before, the size of these water pockets is unknown; if they are large enough and ATP is indeed trapped inside the water pockets, the distance between ATP and NaCho could be larger than 5 Å. In this scenario, it would not be possible to observe any off-diagonal peaks between ATP and NaCho. Nonetheless, using the knowledge gained from the studies on secondary micelles and the impact of salt concentration and pH, it is possible to adjust the relative size of the water pockets i.e. making them smaller by creating more compact micelles, as a result, contacts between ATP and NaCho would be observed.

In addition to the entrapment of ATP within the water pockets of secondary micelles, it is also expected that ATP will interact with the surface of secondary micelles in a fashion similar to that described for ATP attachment to NaCho primary micelles. Since we are only interested in the trapped ATP, we can explore enzymatic digestion using ATPase as another method to quantify how much ATP is not trapped. Assuming that ATPase cannot enter the secondary micelles, only externally bound and free ATP will be converted to adenosine diphosphate (ADP). The ratio of ATP to ADP can be monitored by $^{31}$P NMR spectroscopy. After determining whether or not ATP can indeed be trapped, exploring ways to enhance ATP uptake and delivery is necessary. We predict that secondary micelles with trapped hydrophilic molecules will cross the lipid membrane. As the concentration of bile salts in the intracellular fluid is lower, this may

cause demicellization where the secondary micelle assembly would break apart into primary micelles thus releasing the trapped hydrophilic molecules.

**Concluding Remarks**

This work produced two detailed models for primary and secondary micelles. This testing would not have been possible without the availability of the new 700 MHz NMR spectrometer equipped with the cryogenically cooled probe. Results from the salt concentration studies can be implemented in future studies for bile salt micelles as drug carriers. The incorporation of molecules can be enhanced by altering the salt concentration to create looser primary and secondary micelles. Once the molecule of interest is incorporated, specific amounts of salt can be added to tighten these micelles. These studies can be implemented to improve the entrapment of both hydrophilic and hydrophobic molecules. In addition, ROESY or NOESY NMR techniques can be used to explore the interactions between bile salt micelles and the molecules of interest.

REFERENCES

1. Shaw, R.; Elliott, W.; Barisas, B. G., Estimation of critical micelle concentrations of bile acids by reversed-phase high performance liquid chromatography. *Mikrochim Acta* **1991,** *105* (4-6), 137-145.

2. le Maire, M.; Champeil, P.; Møller, J. V., Interaction of membrane proteins and lipids with solubilizing detergents. *Biochimica et Biophysica Acta (BBA) - Biomembranes* **2000,** *1508* (1–2), 86-111.

3. Garidel, P.; Hildebrand, A., Thermodynamic properties of association colloids. *Journal of Thermal Analysis and Calorimetry* **2005,** *82* (2), 483-489.

4. Goyal, P.; Aswal, V., Micellar structure and inter-micelle interactions in micellar solutions: Results of small angle neutron scattering studies. *CURRENT SCIENCE-BANGALORE-* **2001,** *80* (8), 972-979.

5. Seddon, A. M.; Curnow, P.; Booth, P. J., Membrane proteins, lipids and detergents: not just a soap opera. *Biochimica et Biophysica Acta (BBA) - Biomembranes* **2004,** *1666* (1–2), 105-117.

6. Nelson, D. L.; Lehninger, A. L.; Cox, M. M., *Lehninger principles of biochemistry*. W.H. Freeman: New York, 2008.

7. London, E.; Brown, D. A., Insolubility of lipids in Triton X-100: physical origin and relationship to sphingolipid/cholesterol membrane domains (rafts). *Biochimica et Biophysica Acta (BBA) - Biomembranes* **2000,** *1508* (1–2), 182-195.

8. Funasaki, N.; Fukuba, M.; Hattori, T.; Ishikawa, S.; Okuno, T.; Hirota, S., Micelle formation of bile salts and zwitterionic derivative as studied by two-dimensional NMR spectroscopy. *Chem Phys Lipids* **2006,** *142* (1-2), 43-57.

9. Stark, R. E.; Leff, P. D.; Milheim, S. G.; Kropf, A., Physical studies of CHAPS, a new detergent for the study of visual pigments. *The Journal of Physical Chemistry* **1984,** *88* (24), 6063-6067.

10. Small, D. M., Size and structure of bile salt micelles: influence and structure, concentration, counterion concentration, pH and temperature. In *E.D Goddard*, Ser., A. C., Ed. Plemum Press: New York, 1968; Vol. 84, pp 31-52.

11. Roda, A.; Hofmann, A. F.; Mysels, K. J., The influence of bile salt structure on self-association in aqueous solutions. *J Biol Chem* **1983,** *258* (10), 6362-70.

12. Hofmann, A. F., Bile Acids: The Good, the Bad, and the Ugly. *News Physiol Sci* **1999,** *14*, 24-29.

13. Navas Díaz, A.; García Sánchez, F.; García Pareja, A., Cholic acid behavior in water and organic solvent: study of normal and inverted aggregates. *Colloids and Surfaces A: Physicochemical and Engineering Aspects* **1998,** *142* (1), 27-34.

14. Small, D. M., The physical chemistry of cholanic acids. *The bile acids* **1971,** *1*, 249-356.

15. O'Connor, C. J.; Ch'ng, B. T.; Wallace, R. G., Studies in bile salt solutions: 1. Surface tension evidence for a stepwise aggregation model. *Journal of Colloid and Interface Science* **1983,** *95* (2), 410-419.

16. Mukhopadhyay, S.; Maitra, U., Chemistry and biology of bile acids. *Current Science* **2004,** *87* (12), 1666-1683.

17. Trauner, M.; Boyer, J. L., Bile Salt Transporters: Molecular Characterization, Function, and Regulation. *Physiological Reviews* **2003,** *83* (2), 633-671.

18. Garidel, P.; Hildebrand, A.; Knauf, K.; Blume, A., Membranolytic activity of bile salts: influence of biological membrane properties and composition. *Molecules* **2007,** *12* (10), 2292-326.

19. Carey, M. C.; Small, D. M., Micelle Formation by Bile-Salts - Physical-Chemical and Thermodynamic Considerations. *Arch Intern Med* **1972,** *130* (4), 506-&.

20. Baskin, R.; Frost, L. D., Bile salt-phospholipid aggregation at submicellar concentrations. *Colloids Surf B Biointerfaces* **2008,** *62* (2), 238-42.

21. Hofmann, A. F.; Small, D. M., Detergent properties of bile salts: correlation with physiological function. *Annu Rev Med* **1967,** *18*, 333-76.

22. Simonović, B.; Momirović, M., Determination of critical micelle concentration of bile acid salts by micro-calorimetric titration. *Mikrochim Acta* **1997,** *127* (1-2), 101-104.

23. Matsuoka, K.; Moroi, Y., Micelle formation of sodium deoxycholate and sodium ursodeoxycholate (part 1). *Biochim Biophys Acta* **2002,** *1580* (2-3), 189-99.

24. Ninomiya, R.; Matsuoka, K.; Moroi, Y., Micelle formation of sodium chenodeoxycholate and solubilization into the micelles: comparison with other unconjugated bile salts. *Biochimica et Biophysica Acta (BBA) - Molecular and Cell Biology of Lipids* **2003,** *1634* (3), 116-125.

25. Reis, S.; Moutinho, C. G.; Matos, C.; de Castro, B.; Gameiro, P.; Lima, J. L., Noninvasive methods to determine the critical micelle concentration of some bile acid salts. *Anal Biochem* **2004,** *334* (1), 117-26.

26. Madenci, D.; Egelhaaf, S. U., Self-assembly in aqueous bile salt solutions. *Current Opinion in Colloid & Interface Science* **2010,** *15* (1-2), 109-115.

27. Matsuoka, K.; Suzuki, M.; Honda, C.; Endo, K.; Moroi, Y., Micellization of conjugated chenodeoxy- and ursodeoxycholates and solubilization of cholesterol into their micelles: comparison with other four conjugated bile salts species. *Chem Phys Lipids* **2006,** *139* (1), 1-10.

28. Mazer, N. A.; Carey, M. C.; Kwasnick, R. F.; Benedek, G. B., Quasielastic light scattering studies of aqueous biliary lipid systems. Size, shape, and thermodynamics of bile salt micelles. *Biochemistry-Us* **1979,** *18* (14), 3064-3075.

29. Garidel, P.; Hildebrand, A.; Neubert, R.; Blume, A., Thermodynamic characterization of bile salt aggregation as a function of temperature and ionic strength using isothermal titration calorimetry. *Langmuir* **2000,** *16* (12), 5267-5275.

30. Zhang, X.; Jackson, J. K.; Burt, H. M., Determination of surfactant critical micelle concentration by a novel fluorescence depolarization technique. *Journal of Biochemical and Biophysical Methods* **1996,** *31* (3–4), 145-150.

31. Lopez, F.; Samseth, J.; Mortensen, K.; Rosenqvist, E.; Rouch, J., Micro- and Macrostructural Studies of Sodium Deoxycholate Micellar Complexes in Aqueous Solutions. *Langmuir* **1996,** *12* (26), 6188-6196.

32. Schurtenberger, P.; Mazer, N.; Kaenzig, W., Static and dynamic light scattering studies of micellar growth and interactions in bile salt solutions. *The Journal of Physical Chemistry* **1983,** *87* (2), 308-315.

33. Kawamura, H.; Murata, Y.; Yamaguchi, T.; Igimi, H.; Tanaka, M.; Sugihara, G.; Kratohvil, J. P., Spin-label studies of bile salt micelles. *The Journal of Physical Chemistry* **1989,** *93* (8), 3321-3326.

34. Campanelli, A.; Candeloro De Sanctis, S.; Giglio, E.; Viorel Pavel, N.; Quagliata, C., From crystal to micelle: A new approach to the micellar structure. *J Incl Phenom Macrocycl Chem* **1989,** *7* (4), 391-400.

35. Campanelli, A. R.; Desanctis, S. C.; Chiessi, E.; Dalagni, M.; Giglio, E.; Scaramuzza, L., Sodium Glycodeoxycholate and Taurodeoxycholate - Possible Helical Models for Conjugated Bile-Salt Micelles. *J Phys Chem-Us* **1989,** *93* (4), 1536-1542.

36. Jacobsen, N. E., *NMR Spectroscopy Explained: Simplified Theory, Applications and Examples for Organic Chemistry and Structural Biology*. Wiley: 2007.

37. Macomber, R. S., *A complete introduction to modern NMR spectroscopy*. Wiley: New York, 1998; p xvii, 382 p.

38. Lambert, J. B., *Organic structural spectroscopy*. Prentice Hall PTR: 1998.

39. Sanders, J. K. M.; Hunter, B. K., *Modern Nmr Spectroscopy: A Guide for Chemists*. Oxford University Press, Incorporated: 1993.

40. Barnes, S.; Geckle, J. M., High resolution nuclear magnetic resonance spectroscopy of bile salts: individual proton assignments for sodium cholate in aqueous solution at 400 MHz. *J Lipid Res* **1982,** *23* (1), 161-70.

41. Ishikawa, H.; Nakashima, T.; Inaba, K.; Mitsuyoshi, H.; Nakajima, Y.; Sakamoto, Y.; Okanoue, T.; Kashima, K.; Seo, Y., Proton magnetic resonance assay of total and taurine-conjugated bile acids in bile. *J Lipid Res* **1999,** *40* (10), 1920-1924.

42. Stevens, R. D.; Ribeiro, A. A.; Lack, L.; Killenberg, P. G., Proton magnetic resonance studies of the aggregation of taurine-conjugated bile salts. *J Lipid Res* **1992,** *33* (1), 21-9.

43. Waterhous, D. V.; Barnes, S.; Muccio, D. D., Nuclear magnetic resonance spectroscopy of bile acids. Development of two-dimensional NMR methods for the elucidation of proton resonance assignments for five common hydroxylated bile acids, and their parent bile acid, 5 beta-cholanoic acid. *J Lipid Res* **1985,** *26* (9), 1068-78.

44. Campredon, M.; Quiroa, V.; Thevand, A.; Allouche, A.; Pouzard, G., NMR studies of bile acid salts: 2D NMR studies of aqueous and methanolic solutions of sodium cholate and deoxycholate. *Magnetic Resonance in Chemistry* **1986,** *24* (7), 624-629.

45. Funasaki, N.; Ueshiba, R.; Hada, S.; Neya, S., Stepwise Self-Association of Sodium Taurocholate and Taurodeoxycholate As Revealed by Chromatography. *The Journal of Physical Chemistry* **1994,** *98* (44), 11541-11548.

46. Funasaki, N.; Hada, S.; Neya, S., Self-Association Patterns of Sodium Taurocholate and Taurodeoxycholate As Studied by Frontal Derivative Chromatography. *The Journal of Physical Chemistry B* **1998,** *103* (1), 169-172.

47. Funasaki, N.; Fukuba, M.; Kitagawa, T.; Nomura, M.; Ishikawa, S.; Hirota, S.; Neya, S., Two-dimensional NMR study on the structures of micelles of sodium taurocholate. *J Phys Chem B* **2004,** *108* (1), 438-443.

48. Puppato, A. J. Analytical and biophysical studies of sodium cholate micelles and phospholipids. Ph.D. Dissertation, University of Louisville, Louisville, 2008.

49. Phillips, S. C. PREPARATION AND CHARACTERIZATION OF METAL OXIDE/ADENOSINE TRIPHOSPHATE/BILE SALT NANOHYBRIDS. Dissertation, University of Louisville, Louisville, 2009.

50. Bauer, E.; Jakob, S.; Mosenthin, R., Principles of physiology of lipid digestion. *Asian-australasian journal of animal sciences* **2005,** *18* (2), 282-295.

51. Santhanalakshmi, J.; Lakshmi, G.; Aswal, V. K.; Goyal, P. S., Small-angle neutron scattering study of sodium cholate and sodium deoxycholate interacting micelles in aqueous medium. *J Chem Sci* **2001,** *113* (1), 55-62.

52. Hildebrand, A.; Beyer, K.; Neubert, R.; Garidel, P.; Blume, A., Temperature dependence of the interaction of cholate and deoxycholate with fluid model membranes and their solubilization into mixed micelles. *Colloids and Surfaces B: Biointerfaces* **2003,** *32* (4), 335-351.

53. Hildebrand, A.; Garidel, P.; Neubert, R.; Blume, A., Thermodynamics of demicellization of mixed micelles composed of sodium oleate and bile salts. *Langmuir* **2004,** *20* (2), 320-8.

54. Cabral, D. J.; Hamilton, J. A.; Small, D. M., The ionization behavior of bile acids in different aqueous environments. *J Lipid Res* **1986,** *27* (3), 334-43.

55. Leibfritz, D.; Roberts, J. D., Nuclear magnetic resonance spectroscopy. Carbon-13 spectra of cholic acids and hydrocarbons included in sodium desoxycholate solutions. *J Am Chem Soc* **1973,** *95* (15), 4996-5003.

56. Kolehmainen, E., Solubilization of aromatics in aqueous bile salts. IV—Two-dimensional 1H NMR study on intra- and inter-molecular interactions in aromatic solubilizate–cholate systems. *Magnetic Resonance in Chemistry* **1988,** *26* (9), 760-764.

57. Sugioka, H.; Moroi, Y., Micelle formation of sodium cholate and solubilization into the micelle. *Biochimica et Biophysica Acta (BBA) - Lipids and Lipid Metabolism* **1998,** *1394* (1), 99-110.

58. Funasaki, N.; Fukuba, M.; Kitagawa, T.; Nomura, M.; Ishikawa, S.; Hirota, S.; Neya, S., Two-Dimensional NMR Study on the Structures of Micelles of Sodium Taurocholate. *J. Phys. Chem. B* **2004,** *108*, 438-443.

59. Miertuš, S.; Scrocco, E.; Tomasi, J., Electrostatic interaction of a solute with a continuum. A direct utilizaion of AB initio molecular potentials for the prevision of solvent effects. *Chemical Physics* **1981,** *55* (1), 117-129.

60. Frisch, M.; Trucks, G.; Schlegel, H.; Scuseria, G.; Robb, M.; Cheeseman, J.; Montgomery Jr, J.; Vreven, T.; Kudin, K.; Burant, J., Gaussian 03, revision C. 02; Gaussian, Inc: Wallingford, CT, 2004. *There is no corresponding record for this reference* **2010**.

61. Wu, C.-K.; Dailey, H. A.; Rose, J. P.; Burden, A.; Sellers, V. M.; Wang, B.-C., The 2.0 Å structure of human ferrochelatase, the terminal enzyme of heme biosynthesis. *Nature Structural & Molecular Biology* **2001,** *8* (2), 156-160.

62. Barnes, S.; Geckle, J. M., High resolution nuclear magnetic resonance spectroscopy of bile salts: individual proton assignments for sodium cholate in aqueous solution at 400 MHz. *J. Lipid Res.* **1982,** *23*, 161-170.

63. Chiang, J. Y., Bile acids: regulation of synthesis. *J Lipid Res* **2009,** *50* (10), 1955-66.

64. Fung, B. M.; Peden, M. C., The nature of bile salt micelles as studied by deuterium NMR. *Biochim Biophys Acta* **1976,** *437* (1), 273-9.

65. Sugioka, H.; Matsuoka, K.; Moroi, Y., Temperature effect on formation of sodium cholate micelles. *J Colloid Interface Sci* **2003,** *259* (1), 156-62.

66. Kratohvil, J. P.; Hsu, W. P.; Jacobs, M. A.; Aminabhavi, T. M.; Mukunoki, Y., Concentration-dependent aggregation patterns of conjugated bile salts in aqueous sodium chloride solutions. *Colloid & Polymer Sci* **1983,** *261* (9), 781-785.

67. Mazer, N. A.; Benedek, G. B.; Carey, M. C., An investigation of the micellar phase of sodium dodecyl sulfate in aqueous sodium chloride solutions using quasielastic light scattering spectroscopy. *The Journal of Physical Chemistry* **1976,** *80* (10), 1075-1085.

68. Campanelli, A. R.; Desanctis, S. C.; Giglio, E.; Pavel, N. V.; Quagliata, C., From Crystal to Micelle - a New Approach to the Micellar Structure. *J Inclusion Phenom* **1989,** *7* (4), 391-400.

69. Oshitani, J.; Takashina, S.; Yoshida, M.; Gotoh, K., Difference in Screening Effect of Alkali Metal Counterions on H-AOT-Based W/O Microemulsion Formation. *Langmuir* **2009,** *26* (4), 2274-2278.

70. Hastings, A. B.; Murray, C. D.; Sendroy, J., STUDIES OF THE SOLUBILITY OF CALCIUM SALTS: I. THE SOLUBILITY OF CALCIUM CARBONATE IN SALT SOLUTIONS AND BIOLOGICAL FLUIDS. *Journal of Biological Chemistry* **1927,** *71* (3), 723-781.

71. Puppato, A. J. Analytical and biophysical studies of sodium cholate micelles and phospholipids. 2008.

72. Kovacs, H.; Moskau, D.; Spraul, M., Cryogenically cooled probes—a leap in NMR technology. *Progress in Nuclear Magnetic Resonance Spectroscopy* **2005,** *46* (2-3), 131-156.

73. Chen, Y.; Ho, D. M.; Gottlieb, C. R.; Kahne, D.; Bruck, M. A., Facial Amphiphiles. *J Am Chem Soc* **1992,** *114* (18), 7319-7320.

74. Venkatesan, P.; Cheng, Y.; Kahne, D., Hydrogen-Bonding in Micelle Formation. *J Am Chem Soc* **1994,** *116* (15), 6955-6956.

# APPENDIX A

## LIST OF ACRONYMS

| | |
|---|---|
| NaCho | sodium cholate |
| *cmc* | critical micelle concentration |
| mM | millimolar |
| SDS | sodium dodecyl sulfate |
| CHAPS | 3-[(3-cholamidopropyl)dimethylammino]-1-propanesulfonate |
| *n* | aggregation number |
| TC | trihydroxyl taurocholate |
| TDC | taurodeoxycholate |
| TCDC | taurochenodeoxycholate |
| NaTDC | sodium taurodeoxycholate |
| NaCl | sodium chloride |
| ESR | electron spin resonance |
| $\tau_c$ | rotational correlation (tumbling) time |
| NMR | nuclear magnetic resonance |
| rf | radiofrequency |
| I | spin quantum number |
| m | nuclear spin quantum number |
| $\gamma$ | magnetogyric ratio |
| *h* | Plank's constant |
| $B_0$ | applied magnetic field |
| $T_1$ | spin-lattice (longitudinal) relaxation time |
| $T_2$ | spin-spin (transverse) relaxation time |
| $\nu_{1/2}$ | linewidth at half height |
| FID | free induction decay |
| FT | Fourier transform |
| B | magnetic field |
| $\sigma$ | shielding tensor |
| $\sigma_{diamag}$ | diamagnetic shielding tensor |
| $\sigma_{paramag}$ | paramagnetic shielding tensor |
| $\delta$ | chemical shift |
| ppm | parts-per-million |
| J | coupling contant |
| Hz | Hertz |
| COSY | COrrelation SpectroscopY |
| TOCSY | Total COrrelation SpectroscopY |
| HETCOR | HETeronuclear CORrelation spectroscopy |
| NOESY | Nuclear Overhauser Effect SpectroscopY |

| | |
|---|---|
| HSQC | gradient heteronuclear single quantum correlation spectroscopy |
| HMBC | gradient heteronuclear multiple bond correlation spectroscopy |
| HMQC | heteronuclear multiple quantum correlation spectroscopy |
| NaTC | sodium taurocholate |
| ABB | antiparallel back-to-back |
| PBB | parallel back-to-back |
| AFF | antiparallel face-to-face |
| ABF | antiparallel back-to-face |
| PFF | parallel face-to-face |
| PBF | parallel back-to-face |
| BA | bile acids |
| BS | bile salts |
| PL | phospholipids |
| ITC | isothermal titration calorimetry |
| $D_2O$ | deuterium oxide |
| NaOD | sodium deuteroxide |
| DSS | 4,4-dimethyl-4-silapentane-1-sulfonic acid |
| gHSQC | gradient heteronuclear single quantum correlation spectroscopy |
| PCM | polarizable continuum model |
| ε | dielectric constant |
| OH | hydroxyl |
| $COO^-$ | carboxylate |
| H-bond | hydrogen bond |
| $NH_4Cl$ | ammonium chloride |
| $CaCl_2$ | calcium chloride |
| $MgCl_2$ | magnesium chloride |
| NaOH | Sodium hydroxide |
| HCl | hydrochloric acid |
| pm | picometer |
| $T_2^*$ | effective spin-spin relaxation time |
| Ksp | solubility product constant |
| nm | nanometer |
| con. | concentration |
| Δ | Change |
| ATP | adenosine triphosphate |
| ADP | denosine diphosphate |

# APPENDIX B

## SUPPLEMENTAL INFORMATION

| proton label | 2 Mm | 10 mM | 20 mM | 30 mM |
|---|---|---|---|---|
| **H1A** | **1.018** | 1.017 | 1.012 | 0.989 |
| **H1E** | **1.807** | 1.806 | 1.803 | 1.786 |
| **H2A** | **1.343** | 1.341 | 1.347 | 1.353 |
| **H2E** | **1.640** | 1.635 | 1.639 | 1.628 |
| **H3** | **3.508** | 3.507 | 3.500 | 3.471 |
| **H4A** | **2.035** | 2.034 | 2.042 | 2.053 |
| **H4E** | **1.689** | 1.689 | 1.690 | 1.681 |
| **H5** | **1.446** | **1.447** | **1.439** | **1.415** |
| **H6A** | **2.026** | **2.022** | 2.004 | 1.959 |
| **H6E** | 1.510 | **1.509** | **1.521** | **1.532** |
| **H7** | **3.909** | **3.907** | **3.902** | **3.877** |
| **H8A** | **1.670** | **1.670** | **1.641** | **1.581** |
| **H9A** | **2.072** | **2.072** | **2.083** | **2.098** |
| **H11A** | **1.639** | **1.607** | **1.605** | **1.581** |
| **H11E** | **1.618** | **1.607** | **1.605** | **1.581** |
| **H12** | **4.079** | **4.079** | **4.072** | **4.043** |
| **H14** | **1.776** | **1.776** | **1.780** | **1.794** |
| **H15A** | **1.170** | **1.165** | **1.150** | **1.112** |
| **H15E** | **1.667** | **1.665** | **1.679** | **1.694** |
| **H16A** | **1.918** | **1.910** | **1.920** | **1.924** |
| **H16E** | **1.325** | **1.322** | **1.309** | **1.288** |
| **H17** | **1.670** | **1.668** | **1.680** | **1.689** |
| **H18** | **0.731** | **0.729** | **0.724** | **0.702** |
| **H19** | **0.925** | **0.924** | **0.919** | **0.896** |
| **H20** | **1.429** | **1.428** | **1.416** | **1.398** |
| **H21** | **0.975** | **0.974** | **0.975** | **0.967** |
| **H22A** | **1.737** | **1.735** | **1.729** | **1.706** |
| **H22E** | **1.306** | **1.306** | **1.316** | **1.331** |
| **H23A** | **2.240** | **2.240** | **2.241** | **2.225** |
| **H23E** | **2.117** | **2.115** | **2.105** | **2.079** |

**Table B-1:** Chemical shift values for all protons in NaCho for 2, 10, 20 and 30 mM.

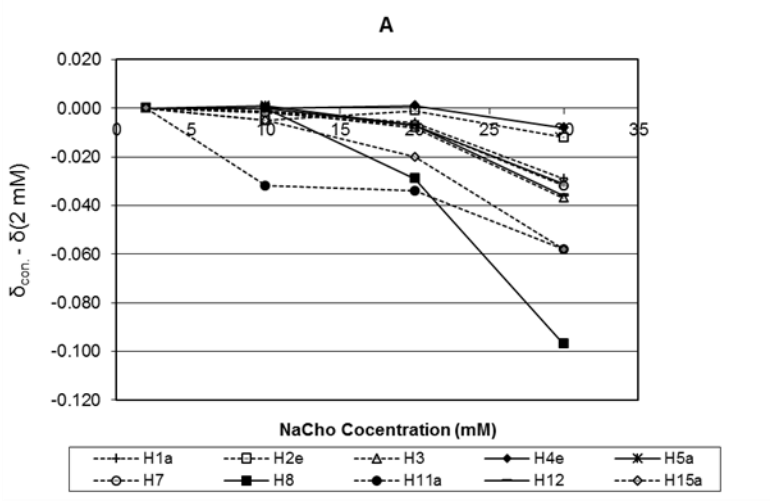


**Figure B-1:** Changes in chemical shifts for primary micelles.

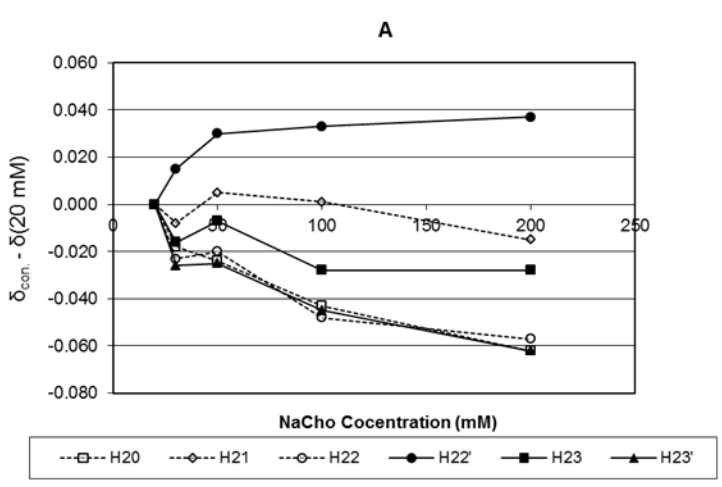


**Figure B-2**: Changes in chemical shifts for protons located on the tail of NaCho (secondary micelles).

| pH | H18 δ (ppm) | H19 δ (ppm) | H21 δ (ppm) | H3 δ (ppm) | H7 δ (ppm) | H12 δ (ppm) |
|---|---|---|---|---|---|---|
| 7.4 | 0.697 | 0.894 | 0.958 | 3.48 | 3.886 | 4.051 |
| 9.1 | 0.701 | 0.897 | 0.957 | 3.485 | 3.888 | 4.055 |

**Table B-2.** Chemical shift values for 20 mM NaCho in the absence of salt at pH 7.4 and 9.1.

| $MgCl_2$ Concentration | H18 Δδ | H19 Δδ | H21 Δδ | H3 Δδ | H7 Δδ | H12 Δδ |
|---|---|---|---|---|---|---|
| 0 | 0 | 0 | 0 | 0 | 0 | 0 |
| 0.15 | 0.033 | 0.068 | 0.183 | 0.465 | 0.531 | 0.305 |
| 0.30 | 1.400 | 1.471 | 1.830 | 1.449 | 1.616 | 1.478 |
| 0.45 | 7.785 | 7.874 | 5.307 | 3.842 | 5.006 | 5.611 |
| 0.60 | n/a | n/a | n/a | n/a | n/a | n/a |

**Figure Table B-3.** Change in chemical shift values for 20 mM NaCho in the presence of $MgCl_2$ with respect to 20 mM NaCho only (no additional salt) at pH 9.1.

APPENDIX C

**Confirmation of the presence of squalene in human eyelid lipid by heteronuclear single quantum correlation spectroscopy**

Douglas Borchman[a*], Marta C. Yappert[b], Sarah E Milliner[b], Ryan J Smith[a], Rahul Bhola[a]

[a] Department of Ophthalmology and Visual Sciences, University of Louisville, Louisville, KY 40202, USA

[b] Department of Chemistry, University of Louisville, Louisville, KY 40202, USA

* Corresponding author: Professor Douglas Borchman

Kentucky Lions Eye Center

301 E. Muhammad Ali Blvd.

Louisville KY, 40202

Tel.: +1 502 852 7435; fax: +15028527450;

Email address: borchman@louisville.edu

**Abstract**

$^{1}$H NMR spectroscopy has been used to quantify squalene in meibum and sebum. Squalene has many beneficial properties and its loss on the surface of skin upon ultraviolet light exposure or in the tear film with dry eye could be detrimental. In this study, we confirm the NMR proton resonance assignments of squalene, squalene in human meibum, and in human eyelid lipid using heteronuclear single quantum correlation spectroscopy. Our results confirm the presence of squalene in eyelid lipid but not in meibum. We speculate that the source of squalene in eyelid lipid could be from sebaceous glands. The beneficial characteristics of squalene including its anti-inflammatory, antioxidant, and antibacterial qualities suggest that the presence of a squalene film could be of significant biological and physical benefit. Its loss in human meibum from patients with dry eye could be detrimental and contribute to the symptoms observed in these patients.

**Key Words**

Lipids; Meibum; NMR; Sebum; Squalene; Tears

**Abbreviations**

EML

human eyelid meibum lipid

HSQC

heteronuclear single quantum correlation spectroscopy

SQ

Squalene

## Introduction

NMR spectroscopy has been a valuable tool for the evaluation of the lipid composition in the ocular lens [1] (reviewed in [2]), human eyelid meibum lipid [3-7] and skin sebum lipid [3,8]. Meibum is produced in the meibomian glands of the eyelids and has many functions: prevent the overflowing of tears, lubricate, improve refraction, inhibit evaporation, physically stabilize the tear film, degrade mucinic clots, provide antibacterial activity, and suppress light [9]. The role of skin sebum is less clear but it has been suggested that sebum may protect the skin from dehydration, ultraviolet radiation, wrinkling, and infection [10,11]. Squalene (SQ), a major component of human sebum [3,12], may serve to protect the skin from UVinduced peroxidation [13,14].

NMR spectroscopy was used to show that SQ reaches concentrations of 4% in human eyelid meibum lipid (EML) [3] and reaches levels of 28 % in sebum [3,8,12]. The area of the $^{1}$H NMR resonances near 5.14 ppm has been used to quantify SQ [3,8]. The resonances around 5.14 ppm resonances are due to protons on carbons #3,#7,#11,#14,#18 and #22 (Fig. C-1). Confirmation of the 5.14 ppm resonance assignment is clinically important because the relative intensity of this resonance in the NMR spectra of human meibum inversely correlated with and unstable tear film and signs and symptoms of dry eye [5,7]. When the intensity of the resonance is restored with azithromycin or doxycycline treatment, tear film stability is restored and patients no longer are afflicted by symptoms of dry eye [7].

We used an inverse heteronuclear NMR 2D technique called heteronuclear single quantum correlation spectroscopy (HSQC) to confirm the NMR resonance assignments of the NMR spectra of human sebum and confirmed that other NMR resonances do not interfere with the 5.14 ppm resonance [8]. HSQC may be used to determine the proton

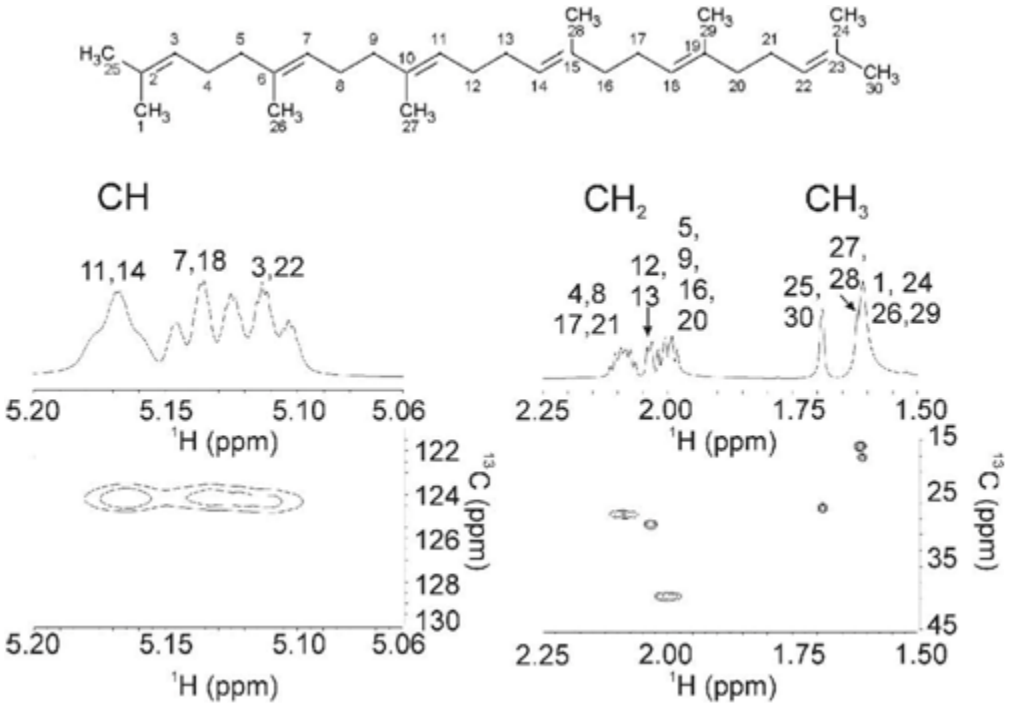


**Figure C-1**. (Top) Formula of squalene. (bottom) $^{1}$H NMR spectrum of squalene atop the heteronuclear single quantum correlation (HSQC) spectrum. Numbers above the $^{1}$H NMR resonances indicate the carbon number of squalene associated with the resonance. Quantification of the protoncarbon ppm associations from HSQC are provided in Tables 1 and 2. Figure 2. $^{1}$H NMR spectra of: a and c) Human lid meibum extracted from Sebutape®. b and d) Squalene.

resonances that are associated with specific carbon resonances [15]. The technique involves the transfer of magnetization from the proton to the heteronucleus (in this case carbon 13) and then back to proton, the more sensitive nucleus. The technique can discern between $CH_3$ and CH moieties and $CH_2$ moieties. In this study we used HSQC to confirm the resonance assignments of SQ [16], and the SQ resonance assignments for the NMR spectra of EML.

## Materials and Methods

### Materials

Cyclohexaned12, SQ and tetramethylsilane, and deuterated chloroform were obtained from SigmaAldrich (St. Louis, MO). HPLC grade chloroform was obtained from ThermoFisher Scientific Inc. (Waltham, MA). Sebutape® was purchased from CuDerm Corporation, Dallas Texas.

### Clinical Diagnosis

The subjects for NMR spectroscopic analysis were recruited from the Kentucky Lion's Eye Center (Louisville KY). Normal status was assigned when the subject's meibomian gland orifices showed no evidence of keratinization or plugging with turbid or thickened secretions, and no dilated blood vessels were observed on the eyelid margin.

### Collection and Processing of Human Meibum and EML for NMR Spectroscopic Analysis

Written, informed consent was obtained from all donors. Protocols and procedures performed at the University of Louisville were reviewed by the University of Louisville Institutional Review Board. All procedures were in accord with the Declaration of Helsinki. Meibomian glands were expressed by pressing the eyelid

between cottontipped applicators with strict attention to avoid touching the eyelid margin during expression. All four eyelids were expressed, and approximately 1 mg of meibum was collected per individual for direct spectroscopic study. For the NMR studies, the expressate was collected with a platinum spatula and immediately dissolved into 0.5 mL of deuterated cyclohexane in a 9mm microvial with a Teflon cap (Microliter Analytical Supplies Ind., Suwanee, GA). Argon gas was bubbled onto the samples to prevent oxidation. The samples in the vials were capped and frozen under argon gas until analysis. Analyses were performed within 3 weeks of collection of the sample. Storage of the sample under argon did not affect the sample [17].

EML was collected from a 59 year old Caucasian donor once in the morning and once at night for a period of a week using Sebutape® [18]. Lipid absorbent Sebutape® is a micro porous film that was designed to collect sebum from the skin [3,18] and EML from the eyelids [18]. The Sebutape® and backing was folded to collect meibum on the lid margins. The eyelid was retracted to evert the eyelid margin but care was taken to apply minimal pressure to avoid stretching of the eyelid which could inadvertently squeeze out meibum. For the collection of meibum, the cardboard was folded upon itself to allow contact with just the eyelid. Sebutape® was pressed for about 45 seconds onto each eyelid. Fiftysix Sebutape® samples were removed from the cardboard backing and placed directly onto a 15 mL glass scintillation vial containing 5 mL of a choloroform. The samples were sonicated under an atmosphere of argon gas in an ultrasonic bath (Branson 1510, Branson Ultrasonics, Danbury, CT) for 10 minutes. The tape was removed from the vial and placed into another vial containing 5 mL choloroform which was again sonicated. The tape was removed and the choloroform from the two extractions were mixed and the chloroform was evaporated under a stream of nitrogen gas. $CDCl_3$

(500 μL) was added to 17.4 mg of extracted EML. The sample was sonicated under an atmosphere of argon gas in an ultrasonic bath (Branson 1510, Branson Ultrasonics, Danbury, CT) for 10 minutes and placed into an NMR tube for spectral measurement.

**NMR Spectral Measurements**

Spectral data were acquired using a Varian VNMRS 700 MHz NMR spectrometer (Varian, Lexington, MA) equipped with a 5 mm H{C/N} C enhanced PFG cold probe (Palo Alto, CA). Spectra were acquired with a minimum of 250 scans, 45˚ pulse width, and a relaxation delay of 1.000 second. All spectra were obtained at 25˚C. HSQC was performed using 512 increments with 16 scans per increment, 45˚ pulse width, and a relaxation delay of 1.000 second, mixing time of 0.080 second, and a onebond coupling constant of 140 Hz and analyzed using MestReNova software, version 7.1.210008 (Mestrelab Research S.L., Santiago de Compostela, Spain). The TMS resonance was set to 0.00 ppm. Commercial software (GRAMS 386; Galactic Industries Corp., Salem, NH) was used for spectral deconvolution and fitting. The area of each band was used for the quantification of lipid composition.

**Purification and Characterization of Squalene from Human Meibum**

Three lipid standards found in meibum were used to test if thin layer chromatography could separate them. About 0.3 mg of each of the wax ester arachidyl dodecanoate, the cholesteryl ester cholesteryl stearate, and SQ were dissolved in 0.3 ml of chloroform. ELM extracted from sebutape® was spotted on a Whatman® thin layer chromatography plate (K6, silica gel 250 im, Piscataway, NJ). Standards were spotted on a separate plate. The plates were eluted with Hexane/Ether (59:1, v/v) at the same time in

the same container. The plates were dried and the standards plate was visualized using iodine vapor. The region where squalene was potentially present was scrapped into a vial with 5ml chloroform and was sonicated for ten minutes in bath sonicator (Branson 1510, Branson Ultrasonics, Danbury, CT), and centrifuged on a bench top centrifuge. The top layer was removed and evaporated in a stream argon. The sample was lyophilized for one hour. Finally, the sample was dissolved in 500 µl $CDCl_3$ for NMR analysis.

**Results**

The molecular structure and $^1H$ NMR spectra of the 3 regions associated with SQ protons are shown in Figure 1. The CH region of the NMR spectrum of SQ is characterized by two clusters of proton resonances, one centered at 5.17 ppm and the other near 5.12 ppm (Fig. C-1). The $CH_2$ region is characterized by three clusters of proton resonances, centered near 2, 2.03 and 2.09 ppm (Fig. C-1). Three resonances are resolved in the $CH_3$ region, one at 1.69 ppm, one at 1.61 ppm containing a shoulder at 1.62 ppm (Fig. C-1). The relative areas of the $^1H$ NMR resonances matched the calculated areas based on the primary structure of SQ (Table C-1). HSQC was used to confirm previous assignments for the $^1H$ and $^{13}C$ NMR spectra of SQ (Table C-2) [16].

The CH resonance region, 5.2 to 5.06 ppm of the $^1H$ NMR spectrum of EML (Fig. 2a) directly corresponds with that of SQ (Fig. C-2b). This region accounts for 6 of the 50 protons of SQ. The close correspondence between the $^1H$ NMR spectra of EML and SQ indicates that the resonances in this region for the NMR spectrum of EML are due to terpenoids. The HSQC spectra confirm the resonance assignments for this region of the $^1H$ and $^{13}C$ spectra of EML (Fig. C-3a, Table C-3). The $^1H$ resonances near 5.15 ppm and the corresponding $^{13}C$ resonances near 124 ppm are from the =CH groups of terpenoids,

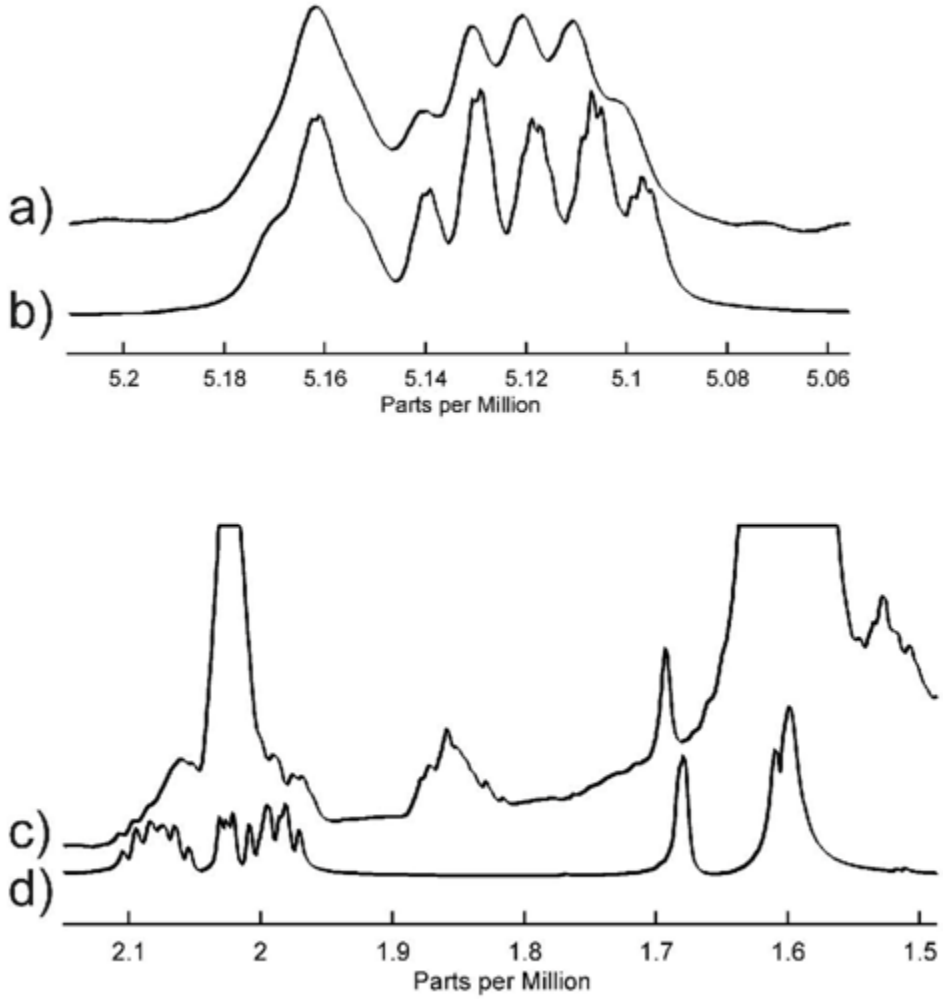


**Figure C-2.** $^{1}$H NMR spectra of: a and c) Human lid meibum extracted from Sebutape®. b and d) Squalene.

| Squalene Moieties | Carbon Number | $^{1}H$ (ppm) | Experimental Relative Area* | Calculated Relative Area* |
|---|---|---|---|---|
| $CH_3$ | 1, 24 | 1.61 | 0.11 | 0.12 |
| | 25, 30 | 1.69 | 0.12 | 0.12 |
| | 26, 29 | 1.61 | 0.11 | 0.12 |
| | 27, 28 | 1.62 | 0.11 | 0.12 |
| $CH_2$ | 4, 21 | 2.09 | 0.084 | 0.08 |
| | 5, 20 | 2.00 | 0.087 | 0.08 |
| | 8, 17 | 2.09 | 0.084 | 0.08 |
| | 9, 16 | 2.00 | 0.087 | 0.08 |
| | 12, 13 | 2.03 | 0.074 | 0.08 |
| CH | 3, 22 | 5.11 | 0.043 | 0.04 |
| | 7, 18 | 5.13 | 0.041 | 0.04 |
| | 11, 14 | 5.17 | 0.040 | 0.04 |

**Table C- 1**. Resonance Areas of $^{1}H$ NMR spectrum of squalene

*The experimental relative area was determined by dividing the area of the proton resonances in the NMR spectrum of squalene by the total areas of all the proton resonances. Curve fitting was used for overlapping resonances. The calculated relative area was determined by dividing the number of protons by the total number of protons from the structure of squalene given in Figure 1.

| | Carbon Number | $^{1}H$ (ppm) | $^{1}H$ (ppm) Literature[18] | $^{13}C$ (ppm) | $^{13}C$ (ppm) Literature[18] | HSQC Confirmation |
|---|---|---|---|---|---|---|
| $CH_3$ Moieties | 1, 24 | 1.61 | 1.61 | 17.67 | 17.60 | $CH_3$ or CH |
| | 25, 30 | 1.69 | 1.69 | 25.77 | 25.63 | $CH_3$ or CH |
| | 26, 29 | 1.61 | 1.61 | 17.67 | 15.93 | $CH_3$ or CH |
| | 27, 28 | 1.62 | 1.62 | 15.97 | 15.98 | $CH_3$ or CH |
| $CH_2$ Moieties | 4, 21 | 2.09 | 2.08 | 26.79 | 26.77 | $CH_2$ |
| | 5, 20 | 2.00 | 1.99 | 39.74 | 39.75 | $CH_2$ |
| | 8, 17 | 2.09 | 2.10 | 26.79 | 26.66 | $CH_2$ |
| | 9, 16 | 2.00 | 2.00 | 39.74 | 39.76 | $CH_2$ |
| | 12, 13 | 2.03 | 2.03 | 28.37 | 28.28 | $CH_2$ |
| CH Moieties | 3, 22 | 5.11 | 5.11 | 124.31 | 125.45 | $CH_3$ or CH |
| | 7, 18 | 5.13 | 5.13 | 124.15 | 124.30 | $CH_3$ or CH |
| | 11, 14 | 5.17 | 5.17 | 124.19 | 124.34 | $CH_3$ or CH |
| No H | 2, 23 | | | | 131.16 | |
| | 10, 15 | | | | 135.11 | |
| | 6, 19 | | | | 135.05 | |

*Eyelid meibum lipid extracted from Sebutape®.

**Table C-2**. HSQC confirmation of $^{1}H$ and $^{13}C$ NMR resonance assignments for squalene.

| | Carbon Number | 1H (ppm) squalene | 1H (ppm) EML* | 13C (ppm) squalene | 13C (ppm) EML* | HSQC of ELM Confirmation |
|---|---|---|---|---|---|---|
| CH3 Moieties | 1, 24 | 1.61 | | 17.67 | | unconfirmed |
| | 25, 30 | 1.69 | 1.69 | 25.77 | 25.80 | CH3 or CH |
| | 26, 29 | 1.61 | | 17.67 | | unconfirmed |
| | 27, 28 | 1.62 | 1.62 | 15.97 | 15.6 | CH3 or CH |
| CH2 Moieties | 4, 21 | 2.09 | 2.10 | 26.79 | 26.94 | CH2 |
| | 5, 20 | 2.00 | 1.99 | 39.74 | 39.74 | CH2 |
| | 8, 17 | 2.09 | 2.10 | 26.79 | 26.94 | CH2 |
| | 9, 16 | 2.00 | 2.00 | 39.74 | 39.74 | CH2 |
| | 12, 13 | 2.03 | 2.04 | 28.37 | 28.41 | CH2 |
| CH Moieties | 3, 22 | 5.11 | 5.11 | 124.31 | 124.27 | CH3 or CH |
| | 7, 18 | 5.13 | 5.13 | 124.15 | 124.27 | CH3 or CH |
| | 11, 14 | 5.17 | 5.17 | 124.19 | 124.24 | CH3 or CH |

**Table C-3**. HSQC confirmation of $^{1}$H and $^{13}$C NMR resonance assignments for EML.

presumably SQ (Fig. C-3a, Table C-3).

In the NMR spectrum of EML (Fig. C-2c), the $^{1}H$ resonances from $CH_3$ and $CH_2$ moieties of SQ (Fig. C-2d) are overwhelmed by resonances from other moieties. However, the resonance at 1.69 ppm assigned to the $CH_3$ moieties from SQ protons on carbons 25 and 30 (Table C-1) are well resolved. Some of the resonances in the NMR spectrum of EML such as the one at 1.69 ppm are shifted slightly when compared to the corresponding resonance of SQ (Fig. C-2). The small shifts are due to the different environments of the moieties. SQ was not diluted with $CDCl_3$ and EML was. The relative area of this resonance is 0.97 times as intense as resonances near 5.15 ppm assigned to the =CH moieties of SQ which is close to the calculated value of 1 confirming the assignment of this resonance (Table C-3) and lack of interference from other resonances. The HSQC spectrum of EML confirms the resonance assignments of the 1.69 $^{1}H$ and 25.77 ppm $^{13}C$ resonance (Table C-3). In the $^{1}H$ NMR spectrum of EML (Fig. C-2c), the SQ $CH_3$ resonances near 1.6 ppm and $CH_2$ resonances near 2.0 ppm are overwhelmed by much larger resonances assigned to the $COOCH_2\underline{CH_2}CH_2$and $\underline{CH_2}CH{=}CH$ from wax and cholesteryl ester moieties. Nevertheless, the $CH_3$ and $CH_2$ resonances from SQ are resolved in the HSQC spectrum (Fig. C-3b). For instance, note that the $^{1}H$ and $^{13}C$ resonances at 2.03 and 39.74 ppm, respectively, assigned to SQ $CH_2$ carbons #5,#9,#16 and #20 (Table C-3) are well resolved (Fig. C-3b).

The $^{1}H$ NMR spectra of a pool of adults and children (Table C-4) in the region of the SQ =C**H** resonances between 5 and 5.2 ppm are shown in Figure C-4B and 5. The largest resonance in this region at 5.32 ppm and shoulder at 5.35 ppm are assigned to the =CH moieties from hydrocarbon chains and carbon #6 of cholesterol esters, respectively. HSQC spectra of the region confirmed that the large proton resonances at

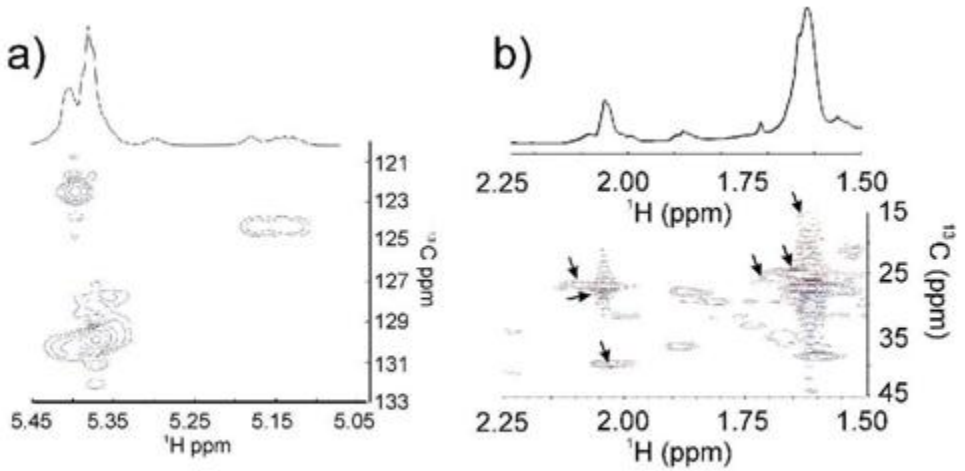


**Figure C-3.** Heteronuclear single quantum correlation spectra of human lid meibum extracted from Sebutape® a) =CHregion of the NMR spectrum. B) CH2 and CH3 region of the spectrum. Arrows point to resonances that are potentially from squalene. Resonance assignments are provided in Table 3.

| Pool | Sample* |
|---|---|
| Infant/child | 01MC, 01MB, 04MC, 04FC, 05FC, 06FC, 08MC |
| Adult | 37MC, 56FC, 58MC, 67MC |

*first two numbers are the age of the donor (y), M= male, F=female, C=Caucasian, B=black

**Table C-4.** Human meibum samples pooled.

5.32 and 5.35 ppm were associated with carbons at 129.3 and 122.0 ppm, respectively, assigned to trans double bonds (Fig. C-4). Vicinal coupling constants ($^{3}J_{HH}$), the distance between the split peaks, are larger for trans– (range: 12– 18 Hz; typical: 15 Hz) than for cis– (range: 0–12 Hz; typical: 8 Hz) isomers [17]. The vicinal coupling constants for the peaks near 5.15 ppm range from 14.7 to 15.4 Hz, typical of and confirming our trans isomer assignment. HSQC could not resolve the protoncarbon associations in the region between 5 and 5.2 ppm. For EML and human meibum samples, the molar ratios of SQ:cholesterol ester:triglyceride:wax ester were calculated from the relative intensities of the 5.11, 4.6, 4.28 to 4.15 and 4.04 ppm $^{1}H$ NMR resonances due to SQ, cholesterol esters, triglycerides and wax esters, respectively [3,4]. The mole percentage of SQ in EML was about 6% and only 1% for pools of human meibum (Table C-5). Thin layer chromatography was used to separate SQ from wax and cholesteryl esters with an Rf of 0.89, 0.29 and 0.22, respectively. The $CH_2$ and $CH_3$ resonance regions of the $^{1}H$ NMR spectrum of the thin layer chromatography band from ELM (Fig. C-6b) that comigrates with SQ standard corresponds with that of SQ (Fig. C-6c). A large resonance near 1.61 ppm in the NMR spectra of extracts from an unloaded thin layer chromatography plate interfered with the resolution of the 1.61 ppm bands.

**Discussion**

Using HSQC and the coupling constants, we confirmed that the $^{1}H$ resonances near 5.2 ppm in the NMR spectrum of SQ, and EML, are from the protons on carbons 11 and 14, and the resonances near 5.1 ppm are from the protons on carbons 3, 7, 22 and 18 (Fig. C-1, Tables C-1-3). The resonance near 5.2 ppm was tentatively assigned to SQ in the NMR spectra of EML [3]. In our EML sample the molar percentage of SQ was 6 %

| Component | EML Mole % | EML Mole % from literature[3] | EML Mole % calculated | Infant Meibum | Adult Meibum | Sebum Mole %[3] |
|---|---|---|---|---|---|---|
| Squalene | 6 | 4 | 4 | 1 | 1 | 28 |
| Cholesteyl esters | 37 | 32 | 31 | 35 | 34 | 3 |
| Triglycerides | 5 | 4 | 5 | 1 | 1 | 38 |
| Wax esters | 52 | 60 | 61 | 63 | 64 | 29 |

Experimental error is less than 5% of the value. EML is a pool of eyelid meibum lipid from a 59 year old Caucasian male. Calculated EML is based on mixing 10% sebum and 90 % meibum and using the literature values for sebum[3] content and our values for adult meibum are in the last column.

**Table C-5.** Mole fractions of components of human sebum from a 59 year old Caucasian male and literature.

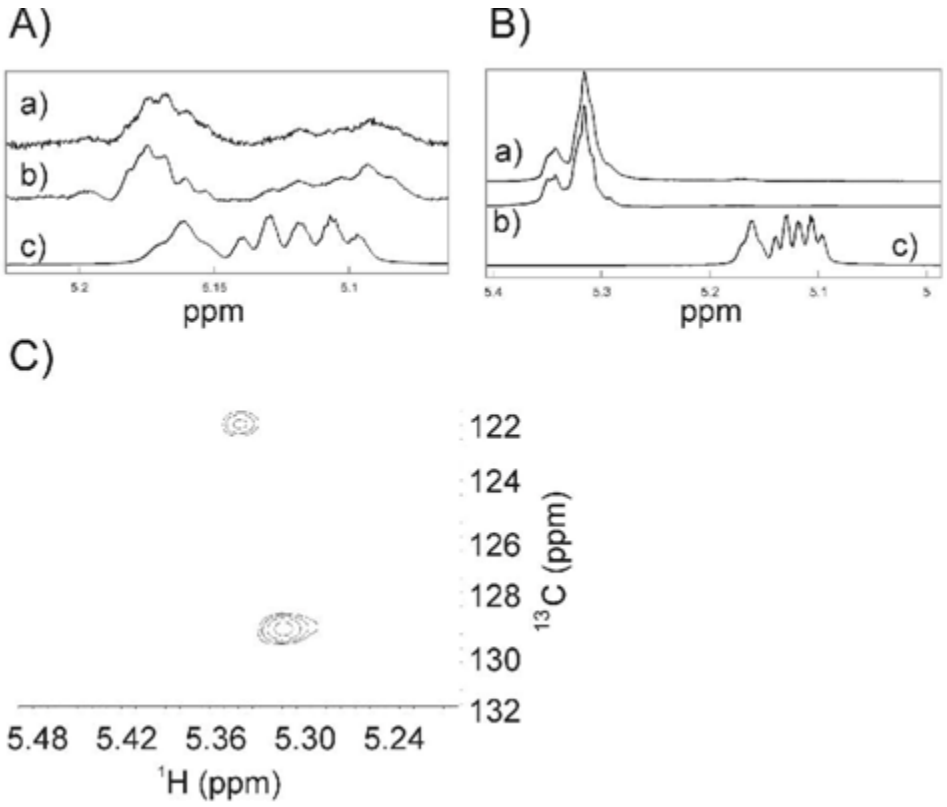


**Figure C-4.** A and B) $^{1}$H NMR spectra of the =CH stretching regions of (a) meibum pooled from adults (Table 4); (b) meibum pooled from infants and children (Table 4); (c) squalene. C) Heteronuclear single quantum correlation (HSQC) spectra of meibum from pooled from infants and children.

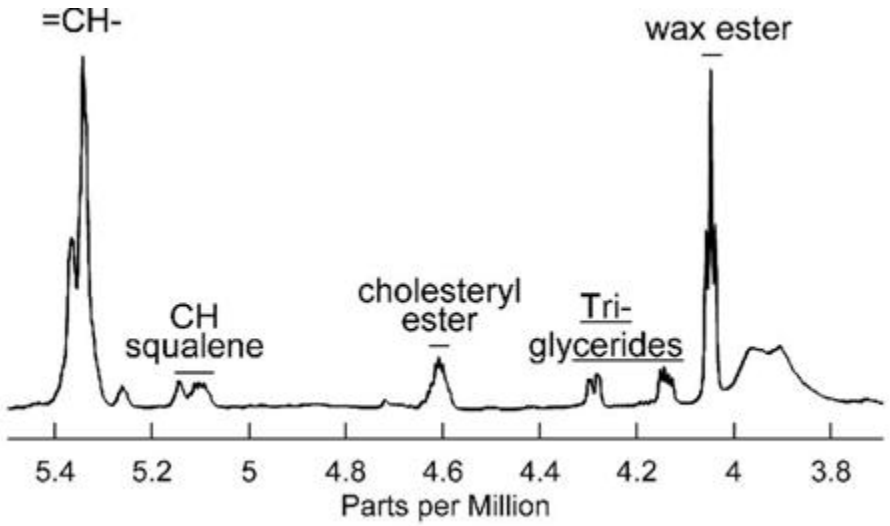


**Figure C-5.** $^{1}$H NMR spectrum of the ester resonance region of a pool of eyelid lipid from a 59 year old male Caucasian.

(Table 5) close to the value reported [3]. Both the relative resonance intensities, position and pairing of $^{1}H$ and $^{13}C$ resonances confirm the NMR assignments (Tables C-1-3).

Based on the intensities of the $^{1}H$ NMR resonances assigned to SQ and those assigned to wax and cholesteryl esters, the relative amount of SQ was about 6 times higher in EML than meibum expressed directly from the meibomian glands. This observation agrees with a mass spectrometry study confirming that SQ is present in tears but because of the lower amount of SQ in meibum it was not detected in meibum by mass spectrometry [19]. SQ was identified in human meibum with the use of highpressure liquid chromatography/mass spectrometry (HPLC/MS) [20], and the level of SQ in human meibum has been reported to be between 0 to 7 % using thin layer chromatography [23-25]. The paucity in the amount of SQ in human meibum contributed to our inability to confirm the NMR resonance assignments using HSQC. Using Raman spectroscopy we estimated only 90 ig of terpenoids per g of meibum [17]. This is a lower limit of terpenoids in meibum because we observed the decrease of the Raman bands possibly due to photochemical decomposition of the sample. The Raman study [17] reported the loss of carotenoids, a class of terpenoids similar to SQ. Based the current NMR study and the lack of color from carotenoids, it is likely that the SQ rather than carotene, is the terpenoid lost in human meibum.

What is the source of the elevated levels of SQ in EML compared with meibum? One possibility is the sebaceous glands in the eyelids. The amount of SQ from sebaceous glands may reach 28 % [3,8]. The glands of Zeis, located on the eyelids and Caruncula lacrimalis, are sebaceous, pilosebaceous glands (associated with hair follicles) [9]. They were discovered almost 200 years ago [9,24]. Jannin noted in 1772 that when the

caruncula was gently compressed, it expelled sebaceous material [9,25]. There are over 400 sebaceous ciliary glands per eye [9], but the meibomian glands are much larger. Sebum contains much more SQ and triglycerides and less cholesteryl esters than meibum (Table C-5). Our NMR data [8] confirmed the levels of SQ reported previously [3]. We calculate that if only 10 % sebum, perhaps from the glands of Zeis, was mixed on the eyelid with meibum, the composition would match that of EML (Table C-5). This is possible since it is known that the tear film lipid layer is in contact with the eyelid skin acting as a barrier to the aqueous layer [26]. A "hydrophobic line" has been observed between the periocular skin and lid margin [27]. Lipophilic substances at the skin of the lower eyelid (such as squalene) may be able to reach the inferior tear meniscus supracutaneously and mix with the tear film lipid layer [27-30]. The large variability in the composition of human meibum may be due to the variable mixing of sebum with meibum [31].

SQ may be beneficial to tear stability. Using Langmuir trough technology we showed in vitro that when meibum was mixed with SQ at low surface pressures, SQ filled thinner regions of meibum films [8]. It is this property of SQ that could potentially stabilize the tear film during break up by migrating to the areas without a tear film lipid layer offering protection to the cornea. SQ is also an antioxidant, scavenging radicals on the skin surface produced by ultraviolet radiation [10,11,13,14]. Nonhuman primates do not have SQ in their sebum [32-34]. Perhaps because humans do not have fur to protect the skin from ultraviolet radiation, we have adapted to have SQ produced in our sebum as a source of protection. It is noteworthy that sebum from most animals do not contain SQ except the otter, beaver, mole and kinkajou which contain up to 94 % SQ in their sebum

[32-35]. All of these species inhabit wet environments suggesting a water repellant function for SQ.

Based on the above studies, loss of SQ could be detrimental. Indeed, loss of SQ with meibomian gland dysfunction and dry eye symptoms have been reported [5,7,17]. Raman studies on human meibum [17] concur with NMR studies showing the loss of terpenoids, most likely SQ, in human meibum from donors with MGD [57].

We confirmed the presence of SQ in EML but not in meibum. We speculate that the source of SQ in EML could be the sebaceous glands. The characteristics of SQ including its antiinflammatory, antioxidant, and antibacterial qualities suggest that a film containing SQ could contribute beneficially to the biophysical and biological functions on the surface of the eye. Its loss in human meibum from patients with dry eye symptoms could be detrimental.

**Acknowledgements**

Supported the Kentucky Lions Eye Foundation, and an unrestricted grant
from Research to Prevent Blindness Inc.

**Conflict of Interest**

There are no conflicts of interests

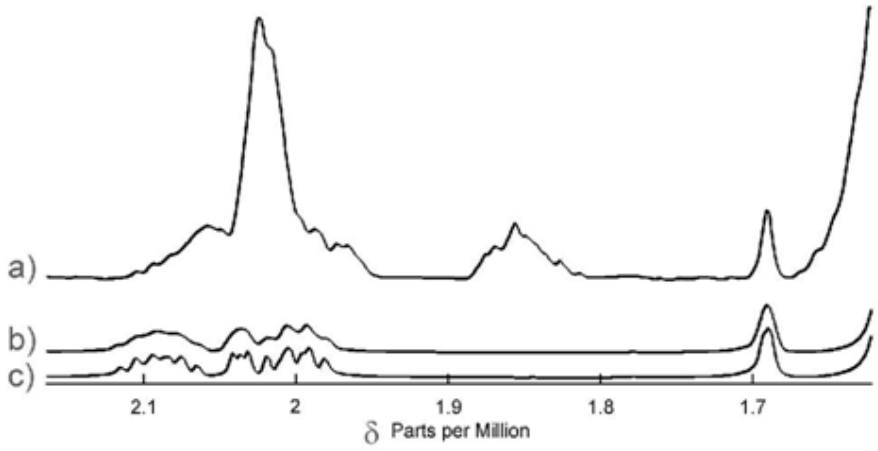


**Figure C-6.** $^{1}$H NMR spectra of: a) ELM, b) ELM thin layer chromatography band extracted from the squalene region, c) squalene. a and c were obtained using a 700 mHz NMR. b was obtained using a 400 mHz instrument.

## REFERENCES


1. Yappert MC, Borchman D (2004) Sphingolipids in human lens membranes: an update on their composition and possible biological implications. Chem Phys Lipids 129:1-20.

2. Borchman D, Yappert MC (2010) Lipids and the Ocular Lens. J Lipid Res 51:2473--88.

3. Robosky LC, Wade K, Woolson D, Baker JD, Manning ML, Gage DA, Reily MD (2008) Quantitative evaluation of sebum lipid components with nuclear magnetic resonance. J Lipid Res 49:686-692.

4. Shrestha RK, Borchman D, Foulks GN, Yappert MC (2011) Analysis of the Composition of Lipid in Human Meibum from Normal Infants, Children, Adolescents, Adults and Adults with Meibomian Gland Dysfunction using $^{1}$HNMR Spectroscopy. Invest Ophthalmol Vis Sci 52:7350-7358.

5. Borchman D, Foulks GN, Yappert MC, Milliner SE (2012) Differences in Human Meibum Lipid Composition with Meibomian Gland Dysfunction using NMR and Principal Component Analysis. Invest Ophthalmol Vis Sci 53:337-47.

6. Borchman D, Foulks GN, Yappert MC, Milliner SE (2012) Changes in Human Meibum Lipid Composition with Age Using NMR Spectroscopy. Invest Ophthalmol Vis Sci 53:475-482.

7. Foulks GN, Borchman D, Yappert MC, Kakar S (2013) Topical Azithromycin and Oral Doxycycline Therapy of Meibomian Gland Dysfunction: A Comparative

Clinical and Spectroscopic Pilot Study. Cornea. . 32:44-53.

8. Georgieva G, Borchman D, Yappert MC, Milliner SE, Yokoi N (2013) Relationships between squalene and film characteristics; an NMR spectroscopy, Brewster angle microscopy and Langmuir trough study. Colloids and Interface Surfaces B. submitted.

9. Murube J (2012) The Origin of Tears. III. The Lipid Component in the XIX and XX Centuries. Ocul Surf 10:200-209.

10. Smith KR, Thiboutot DM (2008) Thematic review series: skin lipids. Sebaceous gland lipids: friend or foe? J Lipid Res 49:271-281.
11. Picardo M, Ottaviani M, Camera E, Mastrofrancesco A (2009) Sebaceous gland lipids. Dermatoendocrinol 1:68–71.
12. Camera E, Ludovici M, Galante M, Sinagra JL, Picardo M (2010) Comprehensive analysis of the major lipid classes in sebum by rapid resolution highperformance liquid chromatography and electrospray mass spectrometry. J Lipid Res 51:3377--3388.
13. Kelly GS (1999) Squalene and its potential clinical uses. Alternative Med 4:29-36.
14. De Luca C, Valacchi G (2010) Surface Lipids as Multifunctional Mediators of Skin Responses to Environmental Stimuli. Mediators of Inflammation 2010:111 article number 321-494.

15. Jacobsen NE (2007) NMR Spectroscopy Explained: Simplified theory, Applications and Examples for Organic Chemistry and Structural Biology; 1st ed.; WileyInterscience. Pogliani L, Ceruti M, Ricchiardi G, Viterbo D (1994) An NMR and molecular mechanics study of squalene and squalene derivatives. Chem Phys Lipids 70:21–34. Oshima Y, Sato H, Zaghloul A, Foulks GN, Yappert MC, Borchman D (2009) Characterization of Human Meibum Lipid using Raman Spectroscopy. Curr Eye Res 34:824–835.

16. Ashraf Z, Pasha U, Greenstone V, Akbar J, Apenbrinck E, Foulks GN, Borchman D (2011) Quantification of Human Sebum on Skin and Human Meibum on the Eye Lid margin using Sebum Tape, Spectroscopy and Chemical Analysis. Curr Eye Res 36:553-562.

17. Butovich IA, Wojtowicz JC, Molai M (2009) Human tear film and meibum. Very long chain wax esters and (Oacyl)omegahydroxy fatty acids of meibum. J Lipid Res 50:2471-85.

18. Krenzer KL, Dana MR, Ullman MD, Cermak JM, Tolls DB, Evans JE, Sullivan DA (2000) Effect of androgen deficiency on the human meibomian gland and ocular surface. J Clin Endocrinol Metab 85:4874-4882.

19. Ehlers N (1965) The precorneal film. Biomicroscopical, histological and chemical investigations. Acta Ophthalmol Suppl 81:11-34.

20. Keith GC (1967) Seborrhoeic blepharokeratoconjunctivitis. Trans Ophthalmol Soc U.K. 87:85-103.

21. Tiffany JM (1978) Individual variations in human meibomian lipid composition. Exp Eye Res 27:289300.

22. Zeis E (1835) In: von Ammon F. Zeitschrift für Ophthalmologie 4:231

23. Janin J (1772) [Anatomic, physiologic and physic recollection and observations of the eye and the diseases of this organ]. Lyon & Paris pp. 85, 90, 92. French

24. Khanal S, Millar TJ (2010) Nanoscale phase dynamics of the normal tear film. Nanomedicine 6:707-13.

25. Tsubota K, Monden Y, Yagi Y, Goto E, Shimmura S (1999) New treatment of dry eye: the effect of calcium ointment through eyelid skin delivery. Br J Ophthalmol 83:767-70.

26. Norn MS (1980) Natural fat in external eye. Vitalstained by Sudan III powder. Acta Ophthalmol (Copenh) 58:331-6.

27. MacKeen DL, Roth HW, Doane MG, MacKeen PD (1998) Supracutaneous treatment of dry eye patients with calcium carbonate Adv Exp Med Biol 438:985-90.

28. Goto E, Dogru M, Fukagawa K, Uchino M, Matsumoto Y, Saiki M, Tsubota K (2006) Successful tear lipid layer treatment for refractory dry eye in office workers by lowdose lipid application on the fulllength eyelid margin Am J Ophthalmol 142:264-70.

29. Pucker AD, Nichols JJ (2012) Analysis of meibum and tear lipids. Ocul. Surf. 10: 23050.

30. De Luca C, Fanfoni GB, Picardo M, NazzaroPorro M, Passi S (1989) The skin surface lipids of man compared with those of other different primates. J Invest Dermatol 92:473-473.

31. De Luca C, Fanfoni GB, Stancato A, Passi S (1997) Significant differences in skin surface lipids between man and other primates. Chem Phy Lipids 88:125-125.

32. Nicolaides N, Fu HC, Rice GR (1968) The skin surface lipids of man compared with those of eighteen species of animals. J Invest Dermatol 81:83-89.

33. Stewart ME, Downing DT (1991) Chemistry and Function of mammalian sebaceous lipids. Advances Lipid Res 24:263-301.

CURRICULUM VITAE

## EDUCATION

University of Louisville (2008-Present)
Louisville, KY
**Ph. D. Anticipated Graduation Date: May 2013**
Dissertation: Spectral Investigation of the Conformation of Primary and Secondary Micelles of Sodium Cholate and the Impact of pH and Ionic Strength.

University of Louisville (2008-2011)
Louisville, KY
**M.S. in Analytical Chemistry**
Thesis: Investigation of Sodium Cholate Primary and Secondary Micelles as Potential Drug Delivery Vehicles

Eastern Kentucky University (2004-2008)
Richmond, KY
**B.S. in Forensic Science**
**Cum Laude and University Honors Scholar**
Areas of Concentration: Chemistry and Biology
Honors Thesis: Carriage of Methicillin-Resistant *Staphylococcus aureus* in University Student Population

## AWARDS AND HONORS

- Five-year Graduate Teaching Assistantship at University of Louisville
- Groundwork Education in Mathematics and Science (GEMS) fellowship (2009 - 2011)
- Poster presentation award recipient (third place), Institute of Molecular Diversity & Drug Design ($IMD^3$), March 8, 2011
- $IMD^3$ Travel Award for the American Chemical Society National Conference, Fall 2012.

## RESEARCH AND PROFESSIONAL EXPERIENCE

**Graduate Researcher** (Fall 2008- Present)
Department of Chemistry, University of Louisville, Louisville KY

- Re-evaluation of previously acquired spectral data and correction of mis-assigned NMR resonances obtained for primary and secondary micelles of sodium cholate (NaCho) micelles.

- NMR spectral studies of sodium cholate micelles to understand the forces and interactions that lead to the formation of these nanostructures. This information is essential for future development of drug delivery nanoconstructs using bile salts.

- One and two-dimensional NMR studies ($^{1}$H, HSQC, HMBC and ROESY) with a 700 MHz NMR spectrometer equipped with a cryogenic probe for:

    - Validation of conformational/structural models proposed previously for primary and secondary micelles of NaCho

    - Investigation of the impact of pH, salt concentration, cation size, and charge on the molecular arrangement of NaCho primary and secondary micelles

- Supervision of undergraduate researchers as well as training them in the operation and troubleshooting of NMR instrumentation. Acted as a liaison between the researchers and the advisor.

**Instructor- CHEM 201 General Chemistry I** (Fall 2012)
Department of Chemistry, University of Louisville, Louisville KY

- Taught students the various aspects in Chemistry including compounds, reactions, stoichiometry, gases, thermodynamics, atomic structure, and periodicity, and molecular structure.
- Responsible for all aspects of teaching: preparing a syllabus, lesson preparation and delivery, and grading.
- Supervised graduate and undergraduate teaching assistants who were responsible for teaching recitation.

**Graduate Research Assistant** (2011 to present)
Department of Chemistry, University of Louisville, Louisville KY

- Study of compositional differences in meibum lipids from normal donors and donors with meibomiam gland dysfunction using NMR spectroscopy.
- Choice and application of appropriate analytical methods, specifically NMR experiments which include: one-dimensional $^{1}$H and $^{13}$C as well as two-dimensional approaches (HSQC, HMBC and ROESY) for identification and quantification of waxes, cholesteryl esters, triglycerides, squalene and saturation in meibum lipids.

**Teaching Assistant- CHEM 201 General Chemistry I** (Spring 2012)
Department of Chemistry, University of Louisville, Louisville KY

- Development of course syllabus for each recitation section. Responsibilities included knowledge of course content, preparing quizzes, and administering grades.
- For each recitation, a presentation was prepared to reinforce content taught by the senior instructor. The overall goal of recitation is to engage student learning through discussion, problem solving, and group work.

**Teaching Assistant- CHEM 527 Separations and Spectroscopy** (Fall 2011)
Department of Chemistry, University of Louisville, Louisville KY

- Teaching the hands-on operation of contemporary chemical instrumentation including gas chromatography, atomic and molecular absorption spectroscopy as well as $^{1}H$ and $^{13}C$ nuclear magnetic resonance (NMR) spectroscopy. Procedure and application of synthetic processes.

**GEMS Fellow** (Fall 2010-Spring of 2011)
Jefferson County Public Schools, University of Louisville, Louisville KY

- Groundwork Education in Mathematics and Science (GEMS) was a collaborative project between University of Louisville and Jefferson County Public Schools funded by National Science Foundation (NSF) Graduate Fellows in K-12 education**.**
- Graduate Fellow at Conway Middle School (Fall 2009-Spring 2010) and Farnsley Middle School (Fall 2010-Spring 2011)
- Planning, developing, implementing an inquiry-based learning approach to enhance student learning. GEMS fellows acted as content specialists and assumed active roles in the classroom.
- Collaboration with other GEMS fellow/teacher teams and mentors in monthly seminars to evaluate student growth toward conceptual understanding, discussed core content being taught in the classroom as well as assessing innovative teaching methods to enhance student learning.

**Chemistry Graduate Student Association (CGSA)-Vice President (**Fall 2009-Spring 2011)
Department of Chemistry, University of Louisville, Louisville KY

- Vice President (2009 – 2011). Organization and coordination of the banquets and hospitality events for the distinguished Nobel Laureates that were invited to speak at the University

- Hostess of the Annual Distinguished Lecturer Series.
  2012 Richard R Schrock
  2011 Ei-ichi Negishi
- Liaison for all Chemistry Graduate Students to the University CGSA.

**Teaching Assistant- CHEM 207** (Summer 2009 and Summer 2011)

Department of Chemistry, University of Louisville, Louisville KY

- Teaching of the methodology of analytical chemistry, as well as the fundamental laboratory procedures that were part of the class.
- Supervision of laboratory sessions that included following proper laboratory safety rules. Grading of reports and managing records for all students.

**Teaching Assistant- CHEM 201 General Chemistry I** (Fall 2008 – Spring 2009)
Department of Chemistry, University of Louisville, Louisville KY

- Development of course syllabus for each recitation section. Responsibilities included knowledge of course content, preparing quizzes, and administering grades.
- For each recitation, a presentation was prepared to reinforce content taught by the senior instructor. The overall goal of recitation is to engage student learning through discussion, problem solving, and group work.

**Undergraduate Research Thesis** (Spring 2008)
Department of Chemistry, Eastern Kentucky University, Richmond KY

- Conducted Research for the Carriage of Methicillin-Resistant *Staphylococcus aureus* in University Student Population.

**Undergraduate Intern: Researcher** (Summer 2007)
United States Department of Agriculture, ARS Forage Animal Production Research Unit (FAPRU), University of Kentucky Campus, Lexington KY

- Fescue Toxicosis has been linked to ergot alkaloids produced by tall fescue and have shown to produce direct narrowing of the blood vessels resulting in reduced blood flow to the animal's extremities.
- Conducted research on the presence of ergot alkaloids in bovine feces using GC-MS analysis.

## PUBLICATIONS AND PAPERS

Differences in human meibum lipid composition with meibomian gland dysfunction using NMR and principal component analysis. Rashmi K. Shrestha, Douglas Borchman, Gary N. Foulks, Marta C. Yappert, and **Sarah E. Milliner** Investigative Ophthalmology & Visual Science **2012**, 53(1), 337-47

Changes in human meibum lipid composition with age using nuclear magnetic resonance spectroscopy. Douglas Borchman, Gary N. Foulks, M.C. Yappert, and **Sarah E. Milliner** Investigative Ophthalmology & Visual Science **2012,** 53 (1), 475-482.

Analysis of the Composition of Lipid in Human Meibum from Normal Infants, Children, Adolescents, Adults, and Adults with Meibomian Gland Dysfunction Using $^{1}$H-NMR Spectroscopy. Rashmi K. Shrestha, Douglas Borchman, Gary N. Foulks, M.C. Yappert, and **Sarah E. Milliner** Investigative Ophthalmology & Visual Science **2011** 52:7350-7358.

$^{13}$C and $^{1}$H NMR Ester Region Resonance Assignments and the Composition of Human Infant and Child Meibum. Exp Eye Res, In Press, **2013**. Douglas Borchman, M. C. Yappert, **Sarah E. Milliner**, D. Duran, G. W. Cox, Ryan. J. Smith, and Rahul Bhola.

Relationships between SQ and film characteristics; an NMR spectroscopy, Brewster angle microscopy and Langmuir trough study. Submitted Colloids and Surfaces B: Biointerfaces. **2013**. Georgiev, G., D. Borchman, M. C. Yappert, **Sarah E. Milliner**, and N. Yokoi.

Confirmation of SQ in human eye lid lipid by heteronuclear single quantum correlation spectroscopy. Lipids. **Submitted, 2013**. Douglas Borchman, M. C. Yappert, **Sarah E. Milliner**, and Rahul Bhola. .

$^{13}$C and $^{1}$H NMR Assignments for Human Infant Meibum Using Inverse Heteronuclear 2D Experiments. **In Preparation for Spectroscopy. 2013**. **Sarah E. Milliner**, Douglas Borchman, Marta C. Yappert, Gray N. Foulks, Ryan J Smith, and Rahul Bhola

## POSTERS AND PRESENTATIONS

**Poster Presentation** (March 2013)
The Institute for Molecular Diversity and Drug Design Symposium, Jewish Hospital and St. Mary's HealthCare, Louisville KY

- "Investigation of the Molecular Arrangement of Primary Micelles of Sodium Cholate" **Sarah E. Milliner** and M.C Yappert.

**Poster Presentation** (August 2012)
American Chemical Society Fall National Meeting, Philadelphia, PA

- "Investigation of sodium cholate primary and secondary micelles as potential drug delivery vehicles" **Sarah E. Milliner** and M.C Yappert.

**Poster Presentation** (March 2012)
The Institute for Molecular Diversity and Drug Design Symposium, Jewish Hospital and St. Mary's HealthCare, Louisville KY

- "Investigation of sodium cholate primary and secondary micelles as potential drug delivery vehicles" **Sarah E. Milliner** and M.C Yappert.

- 3rd place poster award

**Oral Presentation** (April 2011)

- **"**Formative Assessment Strategies Designed to Scaffold Student Learning in K-12 Science." Christine Rich, Lee Ann Nickerson, Thomas Tretter, **Sarah E. Milliner**, Kristen Magness, Katherine Sellers, Amy Strite, Lacey Eckels, and Beth Sanders 2nd Annual STEM Symposium. UK/Partnership Institute for Mathematics and Science Education Reform STEM Education Symposium, Lexington, KY, April 29, 2011. Roundtable presentation.

**Poster Presentation** (March 2010)
NSF Graduate Stem Fellows in K-12 Education, Washington, DC

- "Building Communication Skills: GEMS Strategies Facilitate Science Discourse in the K-12 Classroom." **Sarah E. Milliner**, Kristen Magness, Katherine Sellers, and Christine Rich. American Association for the Advancement of Science/National Science Foundation. Annual GK-12 Conference, Washington D C., March 12, 2011.

**Poster Presentation** (November 2007)
Kentucky Academy of Science 93rd Annual Meeting, Bellarmine University & University of Louisville, Louisville KY

- "Carriage of Methicillin-Resistant *Staphylococcus aureus* in University Student Population."

## MEMBERSHIPS

American Chemical Society (December 2011- present)